2008

STRUCTURE AND FUNCTION OF A NEURONAL GLUTAMATE TRANSPORTER

Gregory Patrick Leary
The University of Montana

STRUCTURE AND FUNCTION OF A NEURONAL GLUTAMATE TRANSPORTER

By

Gregory Patrick Leary

BS in Neuroscience, Regis University, Denver, CO, 2003
BS in Chemistry, Regis University, Denver, CO, 2003

Dissertation

presented in partial fulfillment of the requirements
for the degree of

Doctor of Philosophy
in Neuroscience

The University of Montana
Missoula, MT

Fall 2008

Approved by:

Perry Brown
Associate Provost for Graduate Education

Dr. Michael P. Kavanaugh, Chair
Department of Biomedical and Pharmaceutical Sciences

Dr. Richard J. Bridges
Department of Biomedical and Pharmaceutical Sciences

Dr. John M. Gerdes
Department of Biomedical and Pharmaceutical Sciences

Dr. J.B. Alexander Ross
Department of Chemistry

Dr. J. Stephen Lodmell
Division of Biological Science

Leary, Greg, Ph.D., December 2008 Major
Neuroscience

STRUCTURE AND FUNCTION OF A NEURONAL GLUTAMATE TRANSPORTER

Chairperson: Michael P. Kavanaugh, Ph.D.

Glutamate transporters have a homotrimeric subunit structure with a large central water-filled cavity that extends partially into the plane of the lipid bilayer (Yernool et al., 2004). In addition to uptake of glutamate, the transporters also mediate a chloride conductance that is gated by Na^+ and glutamate. Our data indicate that glutamate binding sites, transport pathways, and chloride channels reside in individual subunits in the trimer and function independently and that the anion channel is gated by alkali cations binding from either side of the membrane. We also investigated conformational changes during glutamate binding by incorporating a fluorescent probe into a site near the postulated external gate (HP2) of a mutant transporter that can bind but not transport L-Glu. Fluorescence changes were observed upon ligand binding that strongly depended on the number of subunits labeled; this suggests quenched fluorophore dimers form at the center of the trimer that are subject to HP2 loop closure upon substrate binding. This supports a model of gate motion that is also consistent with recent x-ray structural data (Boudker et al., 2007). Finally, we propose that the large aqueous central cavity in the trimeric complex (Yernool et al., 2004) may function to restrict the diffusion of molecules near the three ligand binding sites, resulting in an increase in the probability of rebinding.

ACKNOWLEDGMENTS

I have been humbled in this pursuit of science, and now in its completion, I wish to recognize and thank individuals whose time, conversation, and support have allowed me to pursue and finish this degree: my committee-Dr. Sandy Ross, Dr. Stephen Lodmell, Dr. John Gerdes, and Dr. Richard Bridges; my friends and coworkers-Dave Holley, Reuben Darlington, Ben Seaver, Shailesh Agarwal, Dave Bonislawski, Alicia Angell, Loretta Bolyard, Katie Hoffman, Weinan Sun, Todd Seib, Fred Rhoderick, Sarj Patel, Ran Ye, Brent Lyda, Sean Esslinger, Dr. Emily Stone, Dr. Keith Parker, and Laurie Franklin; a special thank you to my mentor and friend, Dr. Mike Kavanaugh, for providing me with opportunities, challenges, and a fair, rigorous critique of my scientific thoughts and experiments. I want to acknowledge the individuals who have been my continual support through this degree and who, in large, are my greatest teachers in life, my family- Gail and Dean Leary, Angie, Jake and Logan Hornby, Amy Leary, Pat Scavarda, Bill and Josephine Leary, Mickey Scavarda, and Cindy Leary. I have grown as an individual and a community member in the past five years, and I want to sincerely thank each person who has shared in this experience. I have learned of failure and the intense environment of science, observed many actions of selflessness, and come to appreciate the importance of detail and accurate expression.

TABLE OF CONTENTS

LIST OF FIGURES

CHAPTER 1: BACKGROUND AND SIGNIFICANCE

Introduction

Excitatory amino acid transporters 1-5 (hEAATs) are membrane proteins fundamental in regulating (Veruki et al., 2006) and clearing synaptically-released glutamate within the central nervous system (CNS) (Diamond and Jahr, 1997). The hEAATs are secondary active transporters that harness energy from the existing Na^+, H^+, and K^+ gradients under physiological cellular conditions. This is in contrast to primary active transporters that metabolize ATP. Knockout mutant mice for Glt-1 (hEAAT2) in combination with GLAST (hEAAT1) result in perinatal mortality with multiple developmental deficits (Matsugami et al., 2006). Unexpectedly, knockout mice for these transporters (Glt-1 and GLAST) individually reveal relatively normal development demonstrating the effectiveness of redundancy and compensatory mechanism in the glutamatergic system. However, despite normal development, Glt-$1^{-/-}$ mice have spontaneous seizures that usually cause death within the first 6 weeks (Tanaka et al., 1997); $GLAST^{-/-}$ mice have difficulties in challenging motor tasks and are more susceptible to brain injury (Watase et al., 1998); and $EAAC1^{-/-}$ mice (hEAAT3) at age 11 months have a decrease in learning on the Morris water maze, and hippocampal neurons taken from these mice have reduced glutathione levels with increased susceptibility to oxidants (Aoyama et al., 2006). Dysfunction of the hEAATs has widely been documented in amyotrophic lateral sclerosis, epilepsy, Huntington's disease, Alzheimer's disease, and ischemic stroke (Beart and O'Shea, 2007).

The transport of L-Glu across the membrane was initially described in brain slice and synaptosomes (Balcar and Johnston, 1972; Logan and Snyder, 1971). Biophysical characterizations of L-Glu transport revealed an electrogenic process that required extracellular-based Na^+ solutions and intracellular based K^+ solutions (Kanner and Sharon, 1978). Within the CNS, Brew and Attwell (1987) documented some of the first glutamate transporter currents in retinal glial cells, pharmacologically distinct from currents associated with ionotropic or metabotropic glutamate receptors. At this same time period, pharmacology had suggested there were distinct and multiple forms of glutamate transport (Ferkany and Coyle, 1986; Fletcher and Johnston, 1991; Robinson et al., 1993). In the early 1990's GLAST (from rat brain), Glt1 (from rat brain), and

EAAC1 (from rabbit intestine) were cloned, allowing the isolation and, thus, fundamental description of these unique glutamate transporters (Kanai and Hediger, 1992; Pines et al., 1992; Shafqat et al., 1993). Soon following, the five human glutamate transporters (hEAATs 1-5) were cloned, each revealing a protein of about 60 kD (Arriza et al., 1997; Arriza et al., 1994; Fairman et al., 1995). Isolated expression of the clones confirmed an electrogenic protein with three unique currents directly associated with the transporter 1) an L-Glu coupled current (Wadiche et al., 1995a); 2) a L-Glu gated anion current thermodynamically uncoupled from L-Glu transport (Wadiche et al., 1995a); and 3) leak currents in the absence of L-Glu, one conductance carried by cations (Kanai et al., 1995; Vandenberg et al., 1995) and the other carried by anions and gated by extracellular Na^+ (Otis et al., 1997; Wadiche and Kavanaugh, 1998). By studying the L-Glu coupled current of the hEAAT3 transporter expressed in *Xenopus laevis* oocytes, Zerangue and Kavanaugh (1996) determined the exact stoichiometry of the L-Glu coupled current as the forward movement across the membrane of three Na^+, one H^+ and one L-Glu coupled to the countertransport of one K^+. Hydrophobicity plots in combination with cysteine scanning mutagenesis studies identified an 8 TMD protein with 2 Hairpin loops (HP1 and HP2) with both N and C-termini intracellular (Grunewald and Kanner, 2000). This membrane topology was confirmed by Yernool et al. (2004) with the crystallization of Glt_{Ph} from *Pyrococcus horikoshii*, an archaeal homolog of the hEAATs, that defined the multimeric structure as a trimer of three identical subunits with a density thought to be a substrate cradled between the two hairpin loops (Figure 1).

My dissertation project has attempted to address fundamental questions posed by this structural architecture. 1) Can the archaeal protein Glt_{ph}, with only 20-30% identity, be a valid model for the mammalian glutamate transporters? 2) How do the coupled or uncoupled currents permeate this multimeric complex? 3) What cations are sufficient or required for the leak conductance? 4) What is the function of the large aqueous basin, which dips halfway through the membrane bilayer, created by the clustering of three identical subunits? And finally, 5) can the HP2 loop be the physical external gate for L-Glu transport, confirming a long-described alternating access model that distinguishes a membrane transporter from a channel (Jardetzky, 1966)?

A. B. C.

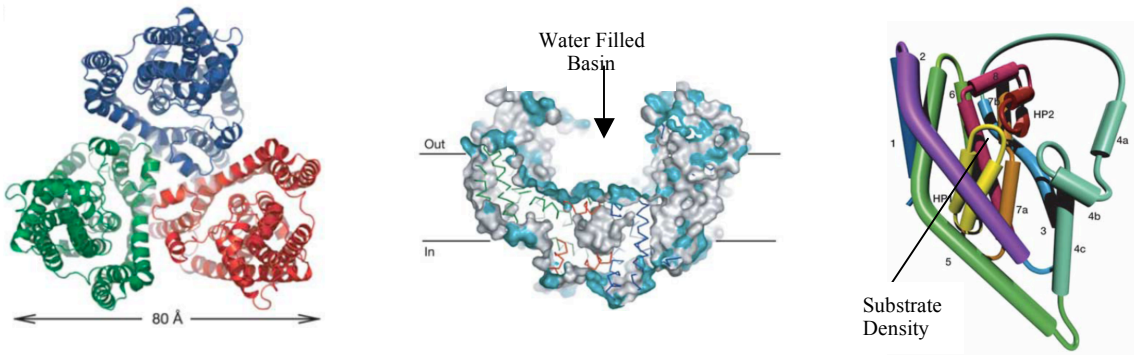

Figure 1: A. A ribbon diagram of Glt_{ph} viewed from the extracellular side, parallel to the membrane. **B.** A surface rendering of Glt_{ph} with a slice through the central basin of the trimeric complex, viewed perpendicular to the membrane. **C.** An individual subunit of Glt_{ph} viewed perpendicular to the membrane and revealing the proposed extracellular gate (HP2) and intracellular ate (HP1) (Yernool et al., 2004).

Distinguishing a Channel from a Transporter

Ions and hydrophilic molecules permeate through the plasma membrane either by diffusion through a water filled channel or by facilitated movement across the membrane by a carrier or transporter. Functionally, both need to discriminate between chemically similar molecules. Channels have been described as proteins that allow diffusion of atoms or small molecules down their electrochemical gradients, usually with high flux rates (up to 10^8/sec). In contrast, transporters are proteins that physically can move molecules across the membrane, from single atoms to polypeptides, against an electrochemical gradient by harnessing energy from ATP (primary active transporter) or from the existing electrochemical gradients for Na^+, K^+, H^+, or Cl^- (secondary active transporter). The flux of molecules through transporters seems to be much slower with rates up to 10^5/sec and as slow as 1/sec. This flux is often associated with larger conformational changes of the protein, which likely accounts for why the Q_{10}, a ratio relating the flux rate before and following a 10 °C change in temperature (rate + 10 °C / Q_{10} rate before temp change), is much higher for transport opposed to diffusion of ions through a channel. Lauger (1980) cautioned that as the energy barrier for a channel increases, the distinction between a channel and transporter is very little. We continue with this in mind because the hEAATs appear, at times, to function as both channel and

transporter; 1) a glutamate or Na^+ gated anion channel (hEAAT5 and hEAAT4) or 2) as a high affinity L-Glu transporter (hEAAT1-3).

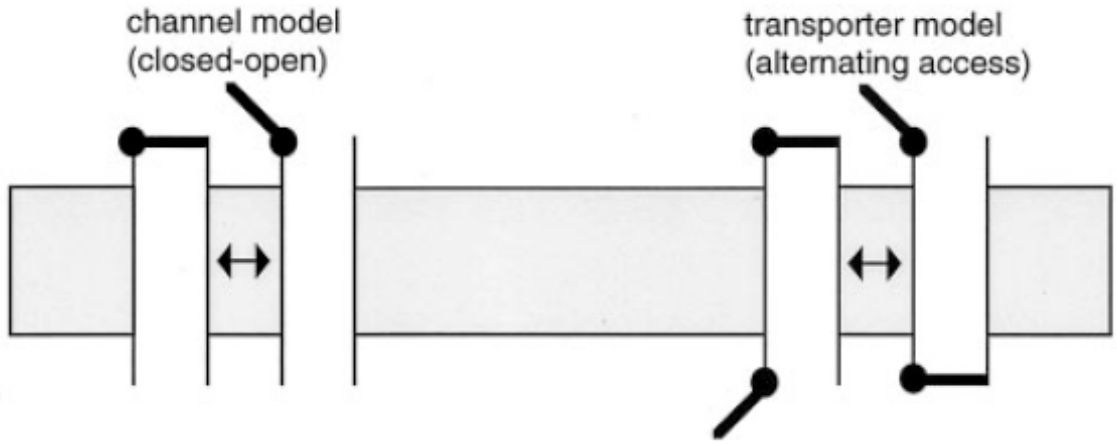

Figure 2: A. A simple illustration depicting the distinction between a channel and transporter based on the number of gates: channel (1 gate) and transporter (2 gates) (Kavanaugh, 1998).

In theory, a channel would have binding sites accessible from both sides of the membrane and a transporter would have a binding site alternately exposed to each side of the membrane, but not both sides simultaneously like the channel (Lauger, 1980). Physiologists have made this distinction between a channel and transporter by the gating mechanism, where a channel would have a single barrier or gate that would act as a switch to allow ion diffusion through a water-filled pore and a transporter would have two gates that function in sequence allowing an alternate access of the permeation pathway to either the cytoplasmic or extracellular side, but not both simultaneously (Figure 2) (Kavanaugh, 1998). Support for a one gate switch model for channels is seen in the flickering quantal nature of conductance from single channels recorded in patches (Neher and Sakmann, 1976) as well as from the relatively recent crystal structure of the K^+ channel, revealing a water filled pathway that extends through the protein (Doyle et al., 1998). Evidence for this long standing two gate, alternating access model for transport has gained strong support in crystallization of multiple membrane transporters that, in general, reveal no water filled permeation pathway (Dutzler et al., 2002; Faham et al., 2008; Yamashita et al., 2005; Yernool et al., 2004). In the crystal structure of the prokaryote chloride channel (CLC), single amino acids seems to be the external and

internal gates revealing a proton/chloride transport exchanger, from what was initially thought to be a chloride channel, reemphasizing the small distinction between channels and transporters (Miller, 2006). In the recent crystal structures of Glt_{ph}, the hEAAT homolog, two obvious hairpin loops, HP1 and HP2, physically appear to be the defining gates regulating the alternating access transport (Figure 1C) (Boudker et al., 2007).

Solute Carrier Family 1 (SLC1)

The hEAATs 1-5 are members of the solute carrier family 1 (SLC1) of membrane proteins that includes the neutral amino acid transporters, ASCT1 and ASCT2 (Kanner and Zomot, 2008). The hEAATs have a 50-60% identity with each other, a 30-40% identity to the neutral amino acid transporters, and a 20-30% identity to dicarboxlate/cation transporters found in bacteria (Slotboom et al., 1999). This SLC1 family is quite distinct in sequence and structure from those of the solute carrier family 6 (SLC6), which includes Na^+ dependent, neurotransmitter transporters for GABA, glycine, dopamine, serotonin, noradrenalin, proline, and taurine (Kanner and Zomot, 2008; Yamashita et al., 2005). Members of the SLC1 family have very conserved motifs in the carboxy-terminal end of the protein, specifically TMD7 and TMD8 (Figure 3, yellow and orange, respectively). Charged residues in the center of these alpha helices tend to function in amino acid selectivity, binding, and transport, and point mutations in these domains often render the protein non-functional or drastically alter the function for glutamate transport. Deviation of the backbone structure for a alpha helics of TMD7, HP1 (Figure 3, green), and HP2 (Figure 3, green) are evolutionally conserved in sequence and seem to be in line with flexible regions of the protein that have the potential of coordinating cations as well as possibly acting as gates for transport. A fairly conserved sequence for TMD2 has been shown to affect the uncoupled anion conductance in the hEAATs as well as for Glt_{ph} (Figure 3, red). Finally, there are 50 residues in the hEAATs between residues Gln 161 and Asn 211 that are not present in the archaeal homolog Glt_{Ph}. This loop is an extracellular domain, whose function is not completely known (Koch et al., 2007b).

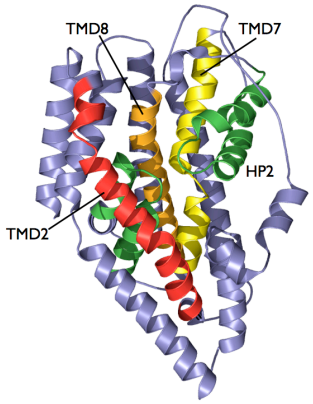

Figure 3: A single subunit of Glt_{Ph} with the hEAAT3 amino acid sequence threaded through the PDB file highlighting helical domains shown to be important for both coupled and uncoupled conductances: TMD2 (red), TMD7 (yellow), TMD8 (orange), and HP2 & HP1 (green).

Apart from individual motifs, the relative similarity in sequence across the family likely suggests a similar trimeric nature even with distant members of this family. The creation of a large aqueous basin caused by the interface of the three identical subunits is definitely a unique feature for a membrane bound protein that as of yet has not been demonstrated to have a purpose (Figure 1 B). The basin is about 60,000 $Å^3$ in volume, and it dips through the outer leaflet of the bilayer. Yernool et al. (2004) suggested this clustering structure may decrease the energy barrier for moving a charged molecule across the plasma membrane by increasing the water filled pathway and decreasing the distance the molecule must transverse the lipid membrane. Other speculations consider the bowl an aqueous 'waiting area' for solutes like Na^+ or L-Glu (Kavanaugh, 2004). In chapter 4 of this dissertation, we find evidence that the water filled basin may act as a possible 'holding area' that constrains the diffusion of inhibitors upon unbinding and increases the probability that they will bind in a subunit across the trimer. For L-Glu within the CNS, the transporters have actually been suggested to initially only buffer L-Glu from the extracellular space through binding, in which there is still a very high probability of L-Glu unbinding at the extracellular face as opposed to being transported (Diamond and Jahr, 1997; Otis and Kavanaugh, 2000; Wadiche and Kavanaugh, 1998). In this instance, the trimeric structure may help increase the capture efficiency of L-Glu

by similarly restricting the diffusion of the L-Glu molecule from the water filled basin and increasing the chances of transport.

Excitatory amino acid transport is a multi-step process

L-Glu transport can be portrayed in discrete states with a simple classical-chemical kinetic model based on the law of mass action. The transitions between each state can be viewed as equilibrium constants, offering physical information about the rates of interaction and dissociation at each step (Colquhoun and Hawkes, 1995). A cyclical alternating access scheme of transport requires a four state model which includes four sets of equilibrium constants (Figure 4): T is the empty transporter with its extracellular gate open to the extracellular milieu, TS is the transporter in the extracellular conformation bound with substrate, T'S is the transporter bound with substrate after translocation to the cytoplasmic face, T' is the empty transporter with its intracellular gate exposed to the cytoplasm. In the hEAATs L-Glu, three Na^+, and one H^+ are shuttled into the cell followed by the coupled outward movement of one K^+ (Levy et al., 1998; Zerangue and Kavanaugh, 1996). The model in Figure 4 can be expanded to include these discrete steps for each binding event (Bergles et al., 2002; Larsson et al., 2004) (Figure 5).

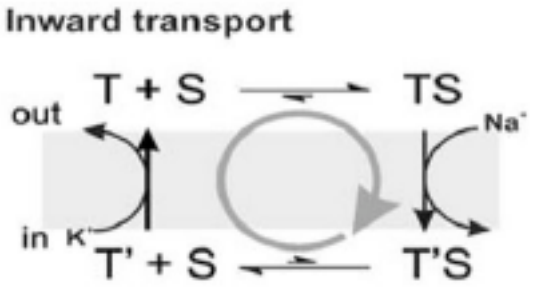

Figure 4: A. A simple four state reaction scheme to describe the transport of L-Glu (Grewer and Rauen, 2005).

Fast application of L-Glu to an outside-out patch of membrane pulled from a cell expressing Glt-1 (rat homolog of hEAAT2) (Figure 7) reveals a rapid inward current that decays to a steady state; this can be explained by the electrogenic transport of glutamate

with a net flux of +2. This transport rate is increased at negative membrane potentials demonstrating that there are voltage dependent transitions between states in the cycle proposed to be at 1, 7, 9, and 15 (Figure 5). Surprisingly, L-Glu binding as well as that of inhibitors is thought to be voltage independent (Bergles et al., 2002; Grewer et al., 2000; Wadiche and Kavanaugh, 1998). In the model, anion conducting states are considered to be at ToNa1, ToNa2, ToNa2G, ToNa2H, ToNa2GH, ToNa3GH, TiNa2, and TiK. At steady state the transport cycling depends on the rate-limiting step, which has been shown by multiple groups to be in the K^+ relocation half of the cycle (15). L-Glu has been shown to transport into the cell when intracellular Na^+ plus L-Glu replaces K^+ based intracellular solutions which can be explained by the transporter entering conditions of homoexchange that occupy only the right half of the model, which entails a futile shuttling of L-Glu back and forth across the membrane (Kanner and Bendahan, 1982). The rates between each step have been either determined experimentally or ones not measured yet have been estimated by fitting experimental data to the model (Bergles et al., 2002). Since the publication of this model in 2002, Larsson et al. (2004) have shown that low pH increases the binding of Na^+ demonstrating H^+ likely binds before L-Glu; however, it is not certain whether a proton is bound before or after Na^+ (Grewer and Rauen, 2005). Two Na^+ ions are depicted in this model as being bound before L-Glu, but there is still much uncertainty as to whether two Na^+ bind before or after L-Glu.

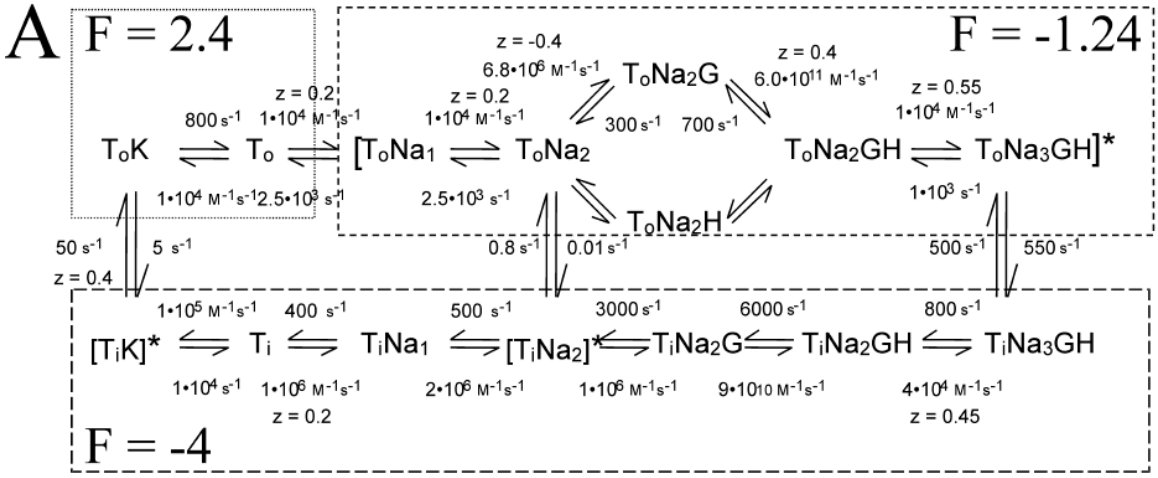

Figure 5: A. A 15 state kinetic model describing glutamate transport separated into steps based on binding and unbinding events or transporter reorientation events (Larsson et al., 2004).

Substrate binding

Early on, the Na^+-dependent, radiolabeled glutamate uptake within the brain was known to be stereoselective because it would not support D-Glu transport; however, it would allow both D and L-Asp to transport with low micromolar affinity (Bridges et al., 1999). Cloning and expression of each of hEAAT (1-5) allowed for both a detailed kinetics analysis for the transporters as well as separation of a unique pharmacological profile that could not be demonstrated in preparations containing multiple transporters (synaptosomes from brain, tissue slices, and cell culture). The transporter cycling rate varies across the hEAAT family where the fastest is hEAAT2 > hEAAT3 > hEAAT1 > hEAAT4 ≈ hEAAT5. In many respects, hEAAT4 and hEAAT5 are thought almost more as glutamate gated anion channels than as glutamate transporters. In terms of substrates, L-Glu seems to bind and transport faster than either L or D-Asp (Bergles and Jahr, 1997; Bergles et al., 2002; Wadiche and Kavanaugh, 1998). In general, good inhibitors seem to look like either the α-amino acid aspartate or glutamate with groups extended from any of the 2-4 carbon atoms. It seems the addition of substantial hydrophobic groups off the β-carboxylic group of aspartate have created some of the most potent inhibitors like the TBOA (threo-β-benzyloxyaspartate) derivatives. Small differences of the specific orientation of atoms off the carbon backbone confer unique selectivity and thus a unique pharmacophore between the hEAATs, revealing the slight differences in each hEAAT (1-5) binding pocket (for review see (Bridges et al., 1999).

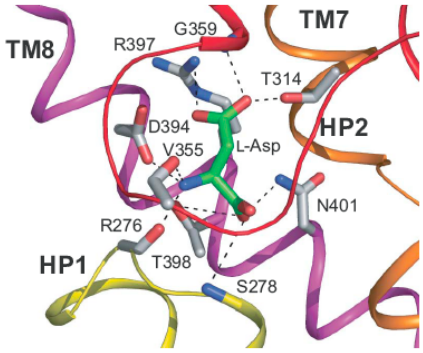

Figure 6: A. Aspartate-binding site in Glt_{Ph} showing HP1 (yellow), TM7 (orange), HP2 (red) and TM8 (magenta). A remarkable number of polar contacts solvate the highly charged substrate and include interactions with D394, main-chain carbonyls of R276 (HP1) and V355 (HP2), the amide nitrogen of N401 (TM8), the hydroxyl of T398 (TM8), the hydroxyl of T314 (TM7), and the main-chain nitrogen of G359 (HP2) (Boudker et al., 2007).

Figure 6 shows L-Asp bound to Glt_{Ph} from a crystal structure by Boudker et al. (2007). The substrate is nestled between HP1 and HP2 located in the exact position of the density seen in the first Glt_{Ph} crystal structure (Figure 1 and (Yernool et al., 2004). The substrate appears to be coordinated by polar atoms from both the main-chain peptide backbone as well as from amino acid side chains. The charged residues D394 and R397 align in sequence with conserved aspartate and arginine residues in the hEAATs. A single point mutation in hEAAT3 of this R447 to cysteine, the residue in the SLC1 neutral amino acid transporter ASCT2, changes the protein into a neutral amino acid transporter that is completely insensitive to glutamate or aspartate binding (Bendahan et al., 2000). Modifications of the residue in the hEAATs that aligns with D394 from Glt_{Ph} also prevents substrate transport, if modified to a neutral amino acid as in the dicarboxlate/cation transporters found in bacteria (Pines et al., 1995; Teichman and Kanner, 2007). This direct overlap of critical residues identified in Glt_{Ph} to coordinate substrate binding with those functionally observed in the hEAATs gives great credibility to the Glt_{Ph} structure as a model for the hEAATs.

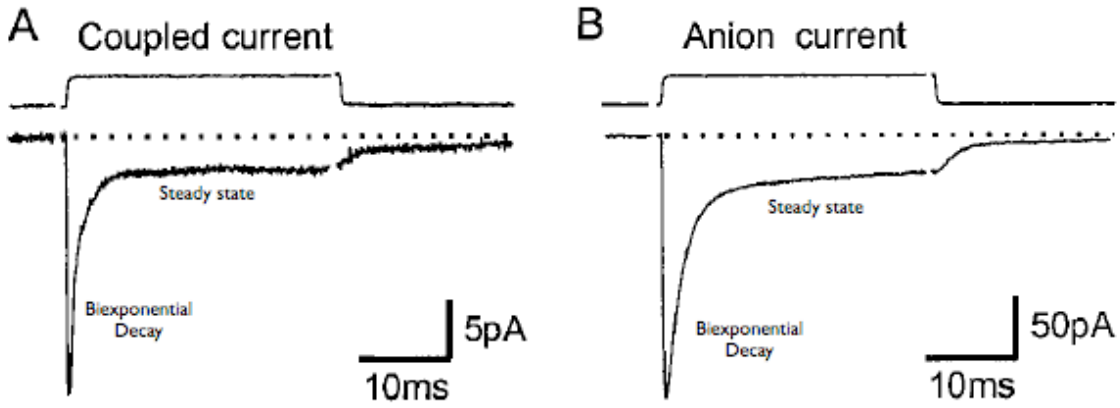

Figure 7: Comparison of coupled and uncoupled responses elicited by L-glutamate. A. L-Glutamate evoked (10mM) transporter current from an outside-out patch recorded in the absence of permeate anions (Kgluconante-based internal solution). **B.** L-Glutamate-evoked (10mM) transporter current from an outside-out patch recorded in the presence of permeate anions (KSCN-based internal solution) (Bergles et al., 2002).

The L-Glu activated transporter current in (Figure 7A or 7B) shows a rapid inward current that has a biexponential decay to a steady state current. According to Otis

and Kavanaugh (2000), this is a typical waveform expected for a system entering and leaving a series of conducting and non-conducting states, (referring to states in Figure 5). This current is a sum of a tightly coupled inward flux associated with the transport of Na^+ plus L-Glu (coupled conductance) and the outward flux of Cl^- (uncoupled anion conductance) (note that both are inward currents relative to a ground in the bath, positive charge moving into the cell or negative charge moving out of the cell). The inward current is not instantaneous, suggesting it is preceded by an electroneutral state thought to be substrate binding (Watzke et al., 2001). Isolating just the L-Glu coupled current by using gluconante-based solutions (Figure 7A), an anion that does not permeate the anion channel, reveals that the coupled current activates slightly faster than the uncoupled current, but the waveform looks very similar to that when anions are present (Figure 7B) (Grewer et al., 2000; Otis and Kavanaugh, 2000). The large inward current likely represents two conducting states revealed by the biexponential decay. Watske et al. (2001) suggest the fast electrogenic component (fast time constant) describes Na^+ binding to the transporter following the binding of L-Glu and the slow electrogenic component (slow time constant) is the translocation of the loaded transporter across the membrane electric field. These two components are insensitive to the presence of internal K^+, demonstrating these two steps are in the first half of the cycle (Figure 5).

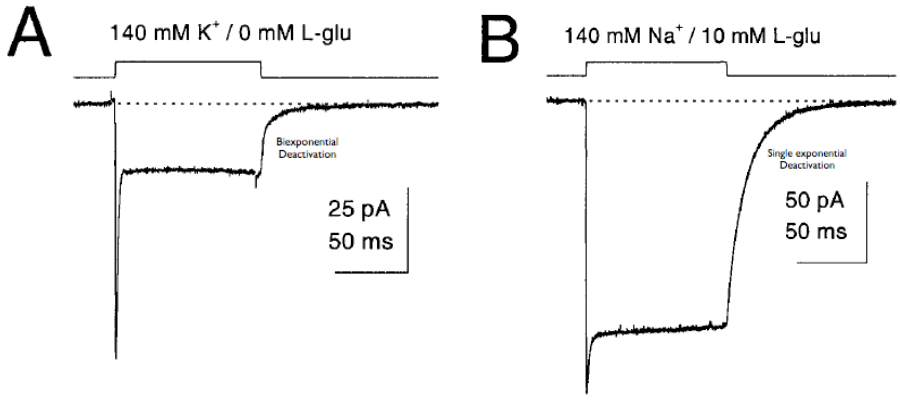

Figure 8: Comparison of deactivation kinetics in forward transport vs. homoexchange. A. L-Glutamate evoked (10mM) forward transporter current from an outside-out patch recorded with 140mM K^+ based internal solution. **B.** L-Glutamate-evoked (10mM) transporter current from an outside-out patch with 140mM Na^+ plus L-Glu (10mM) based internal solution forcing the transporter to function a homoexchange mode (Otis and Kavanaugh, 2000).

At steady state, the transporters are desynchronized entering both conducting and non-conducting states, and the rate of cycling depends on the slowest step in the cycle. The washout of L-Glu shows a double exponential deactivation (Figure 8), thought to represent two different fates for the bound glutamate: 1) forward transport or 2) L-Glu reverse transport and unbinding (Otis and Kavanaugh, 2000). In support of this, replacement of K^+ based solutions with Na^+ plus L-Glu forces the transporter to function as a homoexchanger. Under these conditions, the deactivation kinetics following the washout of L-Glu become a single exponential showing one path for bound glutamate, reverse transport then unbinding (Figure 8B). Considering these two fates for bound L-Glu, *in vivo*, the probability of unbinding is quite significant up to 35% for EAAT2 and up to about 50% in hEAAT1 (Otis and Kavanaugh, 2000; Wadiche and Kavanaugh, 1998). The physiological role for this high probability of unbinding has lead to the conclusion the transporter initially only buffers L-Glu at synapses through binding (Diamond and Jahr, 1997).

Na^+ Binding

One defining characteristic of high affinity L-Glu transport in the brain is its dependence on extracellular Na^+ (Kanner and Sharon, 1978). The ability of the hEAATs to couple 3 Na^+ to L-Glu transport supplies enough energy to maintain a sub-micromolar extracellular glutamate concentration; this has been demonstrated within brain tissue as well as in isolated *Xenopus laevis* oocytes (Herman and Jahr, 2007; Zerangue and Kavanaugh, 1996). The exact position of these Na^+ binding sites are suggested to be close to the substrate binding site in Glt_{Ph}, based on thallium replacement experiments (Figure 9) (Boudker et al., 2007). In Glt_{Ph}, at least two Na^+ seem to occupy the transporter. The first is deep within the protein structure coordinated by an aspartate (D405) on TMD8 and a serine (S278) of HP1, the proposed intracellular gate; a D405N point mutation in Glt_{ph} had significant effects on both Na^+ and substrate binding and this corresponds to a block of uptake in rat homolog Glt-1 (hEAAT2) (Pines et al., 1995). However, controversially this is not supported by the same mutation made in EAAC1 (rat homolog of hEAAT3) where D454N had no effect on Na^+ or substrate binding affinity (Tao et al., 2006). The second Na^+ bound site is positioned below HP2 and seems to be

coordinated by the dipole moment from HP2 and TMD7 (Boudker et al., 2007; Huang and Tajkhorshid, 2008). The expected third Na^+ binding site is not present in the Glt_{Ph} crystal structure, and it is worth considering the stoichiometry of substrate transport may not be the same as for the hEAATs or that thallium cannot sufficiently bind in the position of the third Na^+.

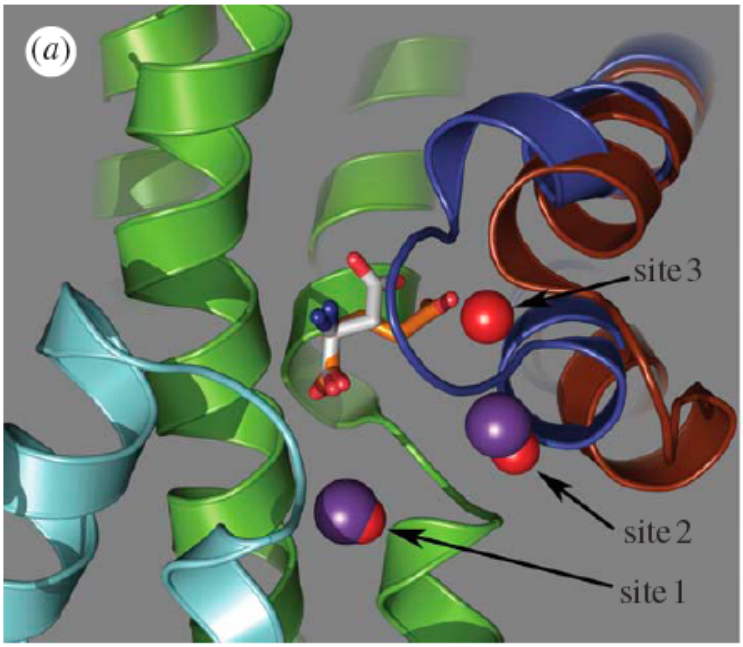

Figure 9: Sodium sites 1-3 (red spheres) are depicted, showing the proximity of sites 1 and 3 to the crystal structure thallium sites (purple spheres identified by Boudker et al. (2007). The site 2-bound ion interacts with the HP2 helix dipole and the γ-carboxyl group of docked glutamate (orange sticks). Overlaid with the docked glutamate molecule is the aspartate (white sticks) that was resolved in the crystal structure. The HP1 loop is depicted in cyan, with occluding HP2 loop in dark blue (Holley & Kavanaugh, 2008).

The first evidence that suggested Na^+ was bound before L-Glu came from the observation that exchange of L-Glu in rat brain synaptosomes was independent of external Na^+, which could be explained, if upon efflux and then unbinding of L-Glu, a Na^+ was still bound and not released before a L-Glu molecule could rebind. With isolated expression of hEAAT2 in oocytes and in the absence of L-Glu, Wadiche and Kavanaugh (1995) demonstrated capacitive Na^+ transient currents blocked by the specific non-tranportable inhibitor DHK, accounting for either one Na^+ binding experiencing 40% of the electric field or two Na^+ binding experiencing an average of 20% of the electric field. This binding of Na^+ could account for about 1/5 of the total net flux of +2. Adding

further support for Na^+ binding before L-Glu, an anion leak gated by Na^+ was measured in the absence of L-Glu that is blocked by inhibitors (Otis et al., 1997; Wadiche and Kavanaugh, 1998). How the two Na^+ defined in the crystal structure of Glt_{ph} correspond to the Na^+ transient currents or the Na^+ gating the anion leak is currently not known. Potential evidence of a link comes from: 1) the fact that both currents are blocked by competitive inhibitors, localizing the Na^+ atoms to the binding sites, and 2) the direct correlation seen between these currents and conformational changes detected with voltage clamp fluorometry (VCF) when transitioning from choline, a cation that does not interact with the hEAATs, to Na^+ (Larsson et al., 2004). Recently, it has been suggested that one Na^+ bound before L-Glu may be voltage independent. In support of this idea, inhibitor binding and unbinding is known to require Na^+ and yet be voltage independent (Wadiche et al., 1995b). It is important to emphasize that strong evidence demonstrates the presence and requirement of at least one bound Na^+ before L-Glu can interact with the transporter; what remains unknown is whether a second Na^+ binds before L-Glu?

Na^+ binding following L-Glu has been suggested from studies on the presteady state kinetics associated with the forward transport of L-Glu (Watzke et al., 2001). A direct coupling interaction of the γ-carboxylate of L-Glu to a third Na^+ has been suggested in the hEAATs (Holley and Kavanaugh, 2008). A similar direct coupling of leucine to Na^+ was captured in a crystal structure of LeuT, a homolog of the mammalian SLC6 family, which could correspond with a general strategy by evolution in these secondary active transporters to prevent any type of substrate leak (Kanner, 2005; Yamashita et al., 2005).

K^+ Binding

Intracellular K^+ is required for the hEAATs to concentrate L-Glu. The K^+ binding and reset of the extracellular binding site is considered by multiple groups to be the rate-limiting step in the transport cycle (Bergles et al., 2002; Grewer et al., 2000; Kanner and Sharon, 1978). When intracellular L-Glu and Na^+ increase, they compete with K^+ for the empty cytoplasmic binding site, turning the transporter into an exchanger (homoexchange). In a similar competition, increased K^+ extracellular can compete with L-Glu and cause reverse transport of L-Glu. This efflux of L-Glu could be a pathway of

brain injury following ischemic stroke, in which extracellular K^+ is increased resulting in L-Glu excitotoxicity, a pathological condition resulting in cell death from overstimulation of ionotropic glutamate receptors, NMDA, AMPA, or kainite (Alix, 2006; Hertz, 2008).

The detection of a K^+ binding site has recently been suggested in hEAAT3 located near the bound substrate and distinct from the Na^+ binding sites (Figure 10) (Holley & Kavanaugh, 2008). This overlap could explain the competition seen between L-Glu and K^+ for binding. This type of model also corresponds well with point mutations studies that have localized residues critical for K^+ coordination near the binding pocket for the substrate, like R447 of TMD8 and Y373 and E374 (TMD7), that if mutated can render the transporter insensitive to K^+ (Bendahan et al., 2000; Kavanaugh et al., 1997; Zhang et al., 1998). Also, the Y373C mutant is the only residue in the protein that has been identified to be accessible from both sides of the membrane, localizing water filled pathways from both cytoplasmic and extracellular sides that converge near this residue (Bendahan et al., 2000).

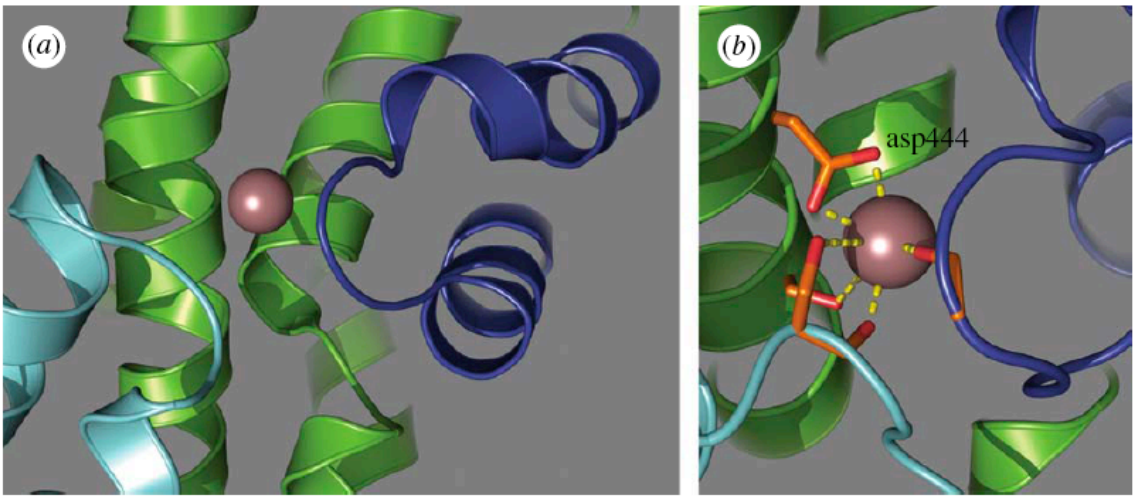

Figure 10: Interactions of K^+ with hEAAT3. A. The K^+ site overlaps with the aspartate-binding site in the Glt_{Ph} crystal structure. B. Bound K^+ is predicted to interact directly with D444, a residue also involved in glutamate binding (mentioned above) (Holley & Kavanaugh, 2008).

Intracellular replacement of K^+ with only Na^+ does not allow a steady-state transport current, though the presteady state inward current associated with substrate and Na^+ binding are still observed (Figure 7). Giving paired-pulses of L-Glu to a cell expressing the transporter and measuring the recovery of the peak amplitude of the

presteady state waveform is a method to measure cycling rate for transport. With Na^+ as the only intracellular cation, the paired pulse recovery is much slower than that with K^+ (Bergles et al., 2002). These two pieces of evidence demonstrate: 1) Na^+ can replace K^+ as an intracellular cation in the transport cycle but is much less effective, resulting in a transport cycling rate where no steady state transport can be detected or 2) Na^+ cannot replace K^+ and the transporter has a way of returning the extracellular binding site independent of an internal cation bound. Larger monovalent cations like Cs^+ and Rb^+ have been shown to replace K^+ in countertransport (Bergles et al., 2002; Kanner and Schuldiner, 1987).

The uncoupled anion conductance

Most mammalian cells maintain an intracellular Cl^- concentration of 5-10 mM and an extracellular Cl^- concentration of 110-150 mM. Following its electrochemical gradient, chloride at depolarized potentials (more positive) would flow out of the cell and at hyperpolarized potentials (more negative) flows into the cell. The hEAATs (1-5) have a substrate gated anion conductance. Functionally, speculations suggest the chloride conductance could offset the accumulating intracellular positive charge during L-Glu transport (net flux +2) as well as dampen the excitability of the membrane (Wadiche et al., 1995a). Only recently has direct evidence for the latter been observed in bipolar neurons where L-Glu binding to hEAAT5 opens an anion channel, hyperpolarizing the membrane and decreasing vesicle fusion (Veruki et al., 2006). Across the family, the rate of uptake for L-Glu is inversely proportional to the size of the anion current in which the rate of uptake is fastest for hEAAT2 > hEAAT3 > hEAAT1 > hEAAT4 ≈ hEAAT5 (Wadiche and Kavanaugh, 1998). This suggests that size of the anion current is coupled to a conducting state during the process of substrate translocation that has a different open probability for each transporter. In support of this idea, the transport of D-Asp in hEAAT1 has been shown to have a larger anion conductance than with L-Glu which directly correlated with slower kinetics for D-Asp at the transporter (Wadiche and Kavanaugh, 1998). Surprisingly, the flux of anions through the protein has little to no effect on the cycling rate of transport or the translocation of L-Glu (Eliasof and Jahr, 1996; Fairman et al., 1995; Picaud et al., 1995; Wadiche et al., 1995a).

Initially, the pathway of anions through the protein was suggested to be through a central pore at the interface of subunits forming the multimeric complex (Eskandari et al., 2000; Torres-Salazar and Fahlke, 2006). More recently, kinetic evidence has demonstrated that both the glutamate and anion permeability pathways are colocalized within individual subunits (Grewer et al., 2005; Koch et al., 2007a; Leary et al., 2007). The Q_{10} for activation of the uncoupled current is near 1 consistent with a channel-like diffusion path for anions void of large conformational changes in the protein. The anion pore has a fairly typical chaotropic selectivity sequence as is seen in other anion preamble channels ($SCN^- > ClO_4^- > NO_3^- > I^- > Br^- > Cl^-$) which confers a minimum 5 Å diameter of the pore (size of ClO_4^-) (Eliasof and Jahr, 1996; Wadiche and Kavanaugh, 1998). The unitary conductance of anions through the transporter has been too small to individually resolve, but noise analysis from photoreceptors estimated a conductance of about 0.5 to 0.7 pS (Larsson et al., 1996; Picaud et al., 1995) and about 0.012 fS for hEAAT1 expressed on *Xenopus laevis* oocytes (Wadiche and Kavanaugh, 1998). This results in single channel currents of about 0.012 to 0.7 pA, equivalent to roughly 7×10^4 to 4×10^6 anions/s, definitely within the gray area of distinguishing a channel from a transporter. The conductance with either NO_3^- or Cl^- exhibit a saturation kinetics in hEAAT1 consistent with interaction of the anion within the pore as opposed to freely diffusing ions through a water path. The monotonically changing relationship when comparing solution with different mole fractions of NO_3^- or Cl^- shows no evidence for multiple anion occupancy within the pore (Wadiche and Kavanaugh, 1998). Glt_{Ph} has recently been shown to support an anion conductance(Ryan and Mindell, 2007), but in the crystal structure of Glt_{Ph}, there is no obvious water filled anion permeation path. Hints of the anion channel location follow a deep water filled pathway down TMD2 identified by cysteine scanning mutagenesis using the thiol-reactive, negative charged MTSES or an even smaller thiol-reactive HgCl. Residues with altered anion conductance followed by cysteine modification are colored in black (Figure 11).

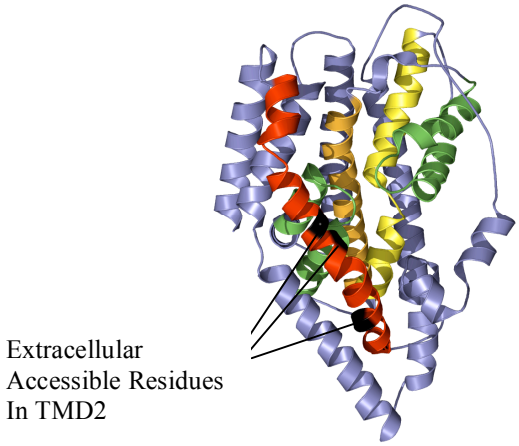

Figure 11: A single subunit of Glt_{Ph} with the hEAAT3 amino acid sequence threaded through the PDB file, highlighting residues, colored black, on TMD2 (red) that are extracellularly accessible by thiol-reactive probes and alter the uncoupled anion conductance, revealing a deep water filled pore in the protein not detected in the crystal structure. TMD2 (red), TMD7 (yellow), TMD8 (orange), and HP2 & HP1 (green).

An anion leak current gated by extracellular Na^+ is tonically active in the resting cell (Bergles and Jahr, 1997; Grewer et al., 2000; Otis et al., 1997; Wadiche and Kavanaugh, 1998). This current can be isolated by a block with a nontransportable, competitive inhibitor for the hEAATs, such as DHK or TBOA, revealing an anion conductance of 10-15% the anion current activated by L-Glu (discussed above), and with the same permeability for anions, shown with the same reversal potential. Slight differences exist between the selectivity sequence for the anion leak and that of the L-Glu activated conductance, posing slight conformation difference in the anion pore under two different conditions (Ryan et al., 2004). The model of Bergels et al. (2002) (Figure 5) proposes cations bound on either side of the membrane resulting in an anion conducting state (ToNa1, ToNa2, TiNa2, and TiK). Of these states, only the ToNa1, ToNa2 and TiNa2 have been shown experimentally to conduct anions (Bergles et al., 2002). In chapter 3, in support of these conducting states, we show evidence that Na^+ or K^+ bound on either side of the membrane is enough to support an anion conductance. Finally, work on Glt_{Ph} in proteoliposomes suggested that there is an anion leak insensitive to inhibitors resulting in a larger anion conductance within the resting cell than was initially thought. Our work in chapter 3 on cation gating the anion channel supports a larger resting anion current independent of the competitive nontransportable inhibitor TBOA.

Summary

The biophysical and biochemical properties of the mammalian glutamate transporters have been intensely studied for over thirty years, and the recent advance of a crystal structure of Glt_{Ph}, an archaeal analog of the EAATs, has only created more questions. The homotrimeric structure of Glt_{Ph} seems to be also conserved in the EAATs. The large aqueous basin created by the interface of the three identical subunits, a water filled vestibule, appears to be a general theme among plasma membrane transporters that allows an aqueous pathway to extracellular binding sites (Gouaux and Mackinnon, 2005). The exact permeation pathways for glutamate, cations, and anions through the protein remains unknown, though all are thought to pass through individual subunits. In addition, it is not known how these proteins almost mechanically couple glutamate to Na^+, H^+, and K^+ to maintain an impressive low nanomolar extracellular glutamate concentration within the CNS. A chemical kinetic reaction mechanism with discrete states for the individual binding or unbinding of 3 Na^+, H^+, Glu, and K^+ replicates experimental electrophysiology data well providing a reversible, stepwise, progression model of glutamate transport. The location of these energy minimum binding sites for each ion or molecule within the crystal structure has been approximately localized by mutagenesis experiments targeting conserved residues within the protein. However, there is much speculation about how these mutagenesis experiments map directly or indirectly to function. In the future, the help of molecular dynamics modeling as well as new crystal structures revealing higher resolution and unique conformations of the protein will help elucidate our understanding of glutamate transporter below a resolution of 10 Å.

References

Alix JJ (2006) Recent biochemical advances in white matter ischaemia. *Eur Neurol* **56**(2):74-77.

Aoyama K, Suh SW, Hamby AM, Liu J, Chan WY, Chen Y and Swanson RA (2006) Neuronal glutathione deficiency and age-dependent neurodegeneration in the EAAC1 deficient mouse. *Nat Neurosci* **9**(1):119-126.

Arriza JL, Eliasof S, Kavanaugh MP and Amara SG (1997) Excitatory amino acid transporter 5, a retinal glutamate transporter coupled to a chloride conductance. *Proc Natl Acad Sci U S A* **94**(8):4155-4160.

Arriza JL, Fairman WA, Wadiche JI, Murdoch GH, Kavanaugh MP and Amara SG (1994) Functional comparisons of three glutamate transporter subtypes cloned from human motor cortex. *J Neurosci* **14**(9):5559-5569.

Balcar VJ and Johnston GA (1972) The structural specificity of the high affinity uptake of L-glutamate and L-aspartate by rat brain slices. *J Neurochem* **19**(11):2657-2666.

Beart PM and O'Shea RD (2007) Transporters for L-glutamate: an update on their molecular pharmacology and pathological involvement. *Br J Pharmacol* **150**(1):5-17.

Bendahan A, Armon A, Madani N, Kavanaugh MP and Kanner BI (2000) Arginine 447 plays a pivotal role in substrate interactions in a neuronal glutamate transporter. *J Biol Chem* **275**(48):37436-37442.

Bergles DE and Jahr CE (1997) Synaptic activation of glutamate transporters in hippocampal astrocytes. *Neuron* **19**(6):1297-1308.

Bergles DE, Tzingounis AV and Jahr CE (2002) Comparison of coupled and uncoupled currents during glutamate uptake by GLT-1 transporters. *J Neurosci* **22**(23):10153-10162.

Boudker O, Ryan RM, Yernool D, Shimamoto K and Gouaux E (2007) Coupling substrate and ion binding to extracellular gate of a sodium-dependent aspartate transporter. *Nature* **445**(7126):387-393.

Bridges RJ, Kavanaugh MP and Chamberlin AR (1999) A pharmacological review of competitive inhibitors and substrates of high-affinity, sodium-dependent glutamate transport in the central nervous system. *Curr Pharm Des* **5**(5):363-379.

Diamond JS and Jahr CE (1997) Transporters buffer synaptically released glutamate on a submillisecond time scale. *J Neurosci* **17**(12):4672-4687.

Doyle DA, Morais Cabral J, Pfuetzner RA, Kuo A, Gulbis JM, Cohen SL, Chait BT and MacKinnon R (1998) The structure of the potassium channel: molecular basis of K+ conduction and selectivity. *Science* **280**(5360):69-77.

Dutzler R, Campbell EB, Cadene M, Chait BT and MacKinnon R (2002) X-ray structure of a ClC chloride channel at 3.0 A reveals the molecular basis of anion selectivity. *Nature* **415**(6869):287-294.

Eliasof S and Jahr CE (1996) Retinal glial cell glutamate transporter is coupled to an anionic conductance. *Proc Natl Acad Sci U S A* **93**(9):4153-4158.

Eskandari S, Kreman M, Kavanaugh MP, Wright EM and Zampighi GA (2000) Pentameric assembly of a neuronal glutamate transporter. *Proc Natl Acad Sci U S A* **97**(15):8641-8646.

Faham S, Watanabe A, Besserer GM, Cascio D, Specht A, Hirayama BA, Wright EM and Abramson J (2008) The crystal structure of a sodium galactose transporter reveals mechanistic insights into Na+/sugar symport. *Science* **321**(5890):810-814.

Fairman WA, Vandenberg RJ, Arriza JL, Kavanaugh MP and Amara SG (1995) An excitatory amino-acid transporter with properties of a ligand-gated chloride channel. *Nature* **375**(6532):599-603.

Ferkany J and Coyle JT (1986) Heterogeneity of sodium-dependent excitatory amino acid uptake mechanisms in rat brain. *J Neurosci Res* **16**(3):491-503.

Fletcher EJ and Johnston GA (1991) Regional heterogeneity of L-glutamate and L-aspartate high-affinity uptake systems in the rat CNS. *J Neurochem* **57**(3):911-914.

Gouaux E and Mackinnon R (2005) Principles of selective ion transport in channels and pumps. *Science* **310**(5753):1461-1465.

Grewer C, Balani P, Weidenfeller C, Bartusel T, Tao Z and Rauen T (2005) Individual subunits of the glutamate transporter EAAC1 homotrimer function independently of each other. *Biochemistry* **44**(35):11913-11923.

Grewer C and Rauen T (2005) Electrogenic glutamate transporters in the CNS: molecular mechanism, pre-steady-state kinetics, and their impact on synaptic signaling. *J Membr Biol* **203**(1):1-20.

Grewer C, Watzke N, Wiessner M and Rauen T (2000) Glutamate translocation of the neuronal glutamate transporter EAAC1 occurs within milliseconds. *Proc Natl Acad Sci U S A* **97**(17):9706-9711.

Grunewald M and Kanner BI (2000) The accessibility of a novel reentrant loop of the glutamate transporter GLT-1 is restricted by its substrate. *J Biol Chem* **275**(13):9684-9689.

Herman MA and Jahr CE (2007) Extracellular glutamate concentration in hippocampal slice. *J Neurosci* **27**(36):9736-9741.

Hertz L (2008) Bioenergetics of cerebral ischemia: a cellular perspective. *Neuropharmacology* **55**(3):289-309.

Huang Z and Tajkhorshid E (2008) Dynamics of the extracellular gate and ion-substrate coupling in the glutamate transporter. *Biophys J* **95**(5):2292-2300.

Jardetzky O (1966) Simple allosteric model for membrane pumps. *Nature* **211**(5052):969-970.

Kanai Y and Hediger MA (1992) Primary structure and functional characterization of a high-affinity glutamate transporter. *Nature* **360**(6403):467-471.

Kanai Y, Nussberger S, Romero MF, Boron WF, Hebert SC and Hediger MA (1995) Electrogenic properties of the epithelial and neuronal high affinity glutamate transporter. *J Biol Chem* **270**(28):16561-16568.

Kanner BI (2005) Molecular physiology: intimate contact enables transport. *Nature* **437**(7056):203-205.

Kanner BI and Bendahan A (1982) Binding order of substrates to the sodium and potassium ion coupled L-glutamic acid transporter from rat brain. *Biochemistry* **21**(24):6327-6330.

Kanner BI and Schuldiner S (1987) Mechanism of transport and storage of neurotransmitters. *CRC Crit Rev Biochem* **22**(1):1-38.

Kanner BI and Sharon I (1978) Active transport of L-glutamate by membrane vesicles isolated from rat brain. *Biochemistry* **17**(19):3949-3953.
Kanner BI and Zomot E (2008) Sodium-coupled neurotransmitter transporters. *Chem Rev* **108**(5):1654-1668.
Kavanaugh MP (1998) Neurotransmitter transport: models in flux. *Proc Natl Acad Sci U S A* **95**(22):12737-12738.
Kavanaugh MP (2004) Accessing a transporter structure. *Nature* **431**(7010):752-753.
Kavanaugh MP, Bendahan A, Zerangue N, Zhang Y and Kanner BI (1997) Mutation of an amino acid residue influencing potassium coupling in the glutamate transporter GLT-1 induces obligate exchange. *J Biol Chem* **272**(3):1703-1708.
Koch HP, Brown RL and Larsson HP (2007a) The glutamate-activated anion conductance in excitatory amino acid transporters is gated independently by the individual subunits. *J Neurosci* **27**(11):2943-2947.
Koch HP, Hubbard JM and Larsson HP (2007b) Voltage-independent sodium-binding events reported by the 4B-4C loop in the human glutamate transporter excitatory amino acid transporter 3. *J Biol Chem* **282**(34):24547-24553.
Larsson HP, Picaud SA, Werblin FS and Lecar H (1996) Noise analysis of the glutamate-activated current in photoreceptors. *Biophys J* **70**(2):733-742.
Larsson HP, Tzingounis AV, Koch HP and Kavanaugh MP (2004) Fluorometric measurements of conformational changes in glutamate transporters. *Proc Natl Acad Sci U S A* **101**(11):3951-3956.
Lauger P (1980) Kinetic properties of ion carriers and channels. *J Membr Biol* **57**(3):163-178(-RETURN-).
Leary GP, Stone EF, Holley DC and Kavanaugh MP (2007) The glutamate and chloride permeation pathways are colocalized in individual neuronal glutamate transporter subunits. *J Neurosci* **27**(11):2938-2942.
Levy LM, Warr O and Attwell D (1998) Stoichiometry of the glial glutamate transporter GLT-1 expressed inducibly in a Chinese hamster ovary cell line selected for low endogenous Na+-dependent glutamate uptake. *J Neurosci* **18**(23):9620-9628.
Logan WJ and Snyder SH (1971) Unique high affinity uptake systems for glycine, glutamic and aspartic acids in central nervous tissue of the rat. *Nature* **234**(5327):297-299.
Matsugami TR, Tanemura K, Mieda M, Nakatomi R, Yamada K, Kondo T, Ogawa M, Obata K, Watanabe M, Hashikawa T and Tanaka K (2006) From the Cover: Indispensability of the glutamate transporters GLAST and GLT1 to brain development. *Proc Natl Acad Sci U S A* **103**(32):12161-12166.
Miller C (2006) ClC chloride channels viewed through a transporter lens. *Nature* **440**(7083):484-489.
Neher E and Sakmann B (1976) Single-channel currents recorded from membrane of denervated frog muscle fibres. *Nature* **260**(5554):799-802.
Otis TS and Kavanaugh MP (2000) Isolation of current components and partial reaction cycles in the glial glutamate transporter EAAT2. *J Neurosci* **20**(8):2749-2757.
Otis TS, Kavanaugh MP and Jahr CE (1997) Postsynaptic glutamate transport at the climbing fiber-Purkinje cell synapse. *Science* **277**(5331):1515-1518.

Picaud SA, Larsson HP, Grant GB, Lecar H and Werblin FS (1995) Glutamate-gated chloride channel with glutamate-transporter-like properties in cone photoreceptors of the tiger salamander. *J Neurophysiol* **74**(4):1760-1771.

Pines G, Danbolt NC, Bjoras M, Zhang Y, Bendahan A, Eide L, Koepsell H, Storm-Mathisen J, Seeberg E and Kanner BI (1992) Cloning and expression of a rat brain L-glutamate transporter. *Nature* **360**(6403):464-467.

Pines G, Zhang Y and Kanner BI (1995) Glutamate 404 is involved in the substrate discrimination of GLT-1, a (Na+ + K+)-coupled glutamate transporter from rat brain. *J Biol Chem* **270**(29):17093-17097.

Robinson MB, Sinor JD, Dowd LA and Kerwin JF, Jr. (1993) Subtypes of sodium-dependent high-affinity L-[3H]glutamate transport activity: pharmacologic specificity and regulation by sodium and potassium. *J Neurochem* **60**(1):167-179.

Ryan RM and Mindell JA (2007) The uncoupled chloride conductance of a bacterial glutamate transporter homolog. *Nat Struct Mol Biol* **14**(5):365-371.

Ryan RM, Mitrovic AD and Vandenberg RJ (2004) The chloride permeation pathway of a glutamate transporter and its proximity to the glutamate translocation pathway. *J Biol Chem* **279**(20):20742-20751.

Shafqat S, Tamarappoo BK, Kilberg MS, Puranam RS, McNamara JO, Guadano-Ferraz A and Fremeau RT, Jr. (1993) Cloning and expression of a novel Na(+)-dependent neutral amino acid transporter structurally related to mammalian Na+/glutamate cotransporters. *J Biol Chem* **268**(21):15351-15355.

Slotboom DJ, Konings WN and Lolkema JS (1999) Structural features of the glutamate transporter family. *Microbiol Mol Biol Rev* **63**(2):293-307.

Tanaka K, Watase K, Manabe T, Yamada K, Watanabe M, Takahashi K, Iwama H, Nishikawa T, Ichihara N, Kikuchi T, Okuyama S, Kawashima N, Hori S, Takimoto M and Wada K (1997) Epilepsy and exacerbation of brain injury in mice lacking the glutamate transporter GLT-1. *Science* **276**(5319):1699-1702.

Tao Z, Zhang Z and Grewer C (2006) Neutralization of the aspartic acid residue Asp-367, but not Asp-454, inhibits binding of Na+ to the glutamate-free form and cycling of the glutamate transporter EAAC1. *J Biol Chem* **281**(15):10263-10272.

Teichman S and Kanner BI (2007) Aspartate-444 is essential for productive substrate interactions in a neuronal glutamate transporter. *J Gen Physiol* **129**(6):527-539.

Torres-Salazar D and Fahlke C (2006) Intersubunit interactions in EAAT4 glutamate transporters. *J Neurosci* **26**(28):7513-7522.

Vandenberg RJ, Arriza JL, Amara SG and Kavanaugh MP (1995) Constitutive ion fluxes and substrate binding domains of human glutamate transporters. *J Biol Chem* **270**(30):17668-17671.

Veruki ML, Morkve SH and Hartveit E (2006) Activation of a presynaptic glutamate transporter regulates synaptic transmission through electrical signaling. *Nat Neurosci* **9**(11):1388-1396.

Wadiche JI, Amara SG and Kavanaugh MP (1995a) Ion fluxes associated with excitatory amino acid transport. *Neuron* **15**(3):721-728.

Wadiche JI, Arriza JL, Amara SG and Kavanaugh MP (1995b) Kinetics of a human glutamate transporter. *Neuron* **14**(5):1019-1027.

Wadiche JI and Kavanaugh MP (1998) Macroscopic and microscopic properties of a cloned glutamate transporter/chloride channel. *J Neurosci* **18**(19):7650-7661.

Watase K, Hashimoto K, Kano M, Yamada K, Watanabe M, Inoue Y, Okuyama S, Sakagawa T, Ogawa S, Kawashima N, Hori S, Takimoto M, Wada K and Tanaka K (1998) Motor discoordination and increased susceptibility to cerebellar injury in GLAST mutant mice. *Eur J Neurosci* **10**(3):976-988.

Watzke N, Bamberg E and Grewer C (2001) Early intermediates in the transport cycle of the neuronal excitatory amino acid carrier EAAC1. *J Gen Physiol* **117**(6):547-562.

Yamashita A, Singh SK, Kawate T, Jin Y and Gouaux E (2005) Crystal structure of a bacterial homologue of Na+/Cl--dependent neurotransmitter transporters. *Nature* **437**(7056):215-223.

Yernool D, Boudker O, Jin Y and Gouaux E (2004) Structure of a glutamate transporter homologue from Pyrococcus horikoshii. *Nature* **431**(7010):811-818.

Zerangue N and Kavanaugh MP (1996) Flux coupling in a neuronal glutamate transporter. *Nature* **383**(6601):634-637.

Zhang Y, Bendahan A, Zarbiv R, Kavanaugh MP and Kanner BI (1998) Molecular determinant of ion selectivity of a (Na+ + K+)-coupled rat brain glutamate transporter. *Proc Natl Acad Sci U S A* **95**(2):751-755.

CHAPTER 2: THE GLUTAMATE AND CHLORIDE PERMEATION PATHWAYS ARE COLOCALIZED IN INDIVIDUAL NEURONAL GLUTAMATE TRANSPORTER SUBUNITS

G.P. Leary, E.F. Stone, D.C. Holley, A.N. Tzingounis, and M.P. Kavanaugh

Introduction

In mammals including humans, high affinity glutamate transporters are encoded by a group of five genes (EAAT 1-5; SLC1A1-A5) that are members of the dicarboxylate/amino acid:cation symporter family that also includes the neutral amino acid transporters, ASCT1 and ASCT2. This gene family is distinct from the family of genes encoding the transporters for neurotransmitters such as GABA, serotonin, dopamine, norepinephrine, glycine, and others. The excitatory amino acid transporters are found throughout the central nervous system and peripheral tissues; they are the major routes for cellular uptake of glutamate (Danbolt, 2001).

EAAT function is well-described by a cyclical alternating access transport model in which L-glutamate is co-transported with 3 Na^+ ions and 1 H^+, followed by countertransport of 1 K^+ ion, restoring the initial state (Zerangue and Kavanaugh, 1996; Levy et al., 1998). In addition to mediating coupled glutamate transport, EAATs also exhibit a thermodynamically uncoupled chloride conductance that is increased in the presence of glutamate (Fairman et al., 1995; Picaud et al., 1995; Wadiche et al. 1995; Billups et al., 1996). The chloride conductance varies relative to the glutamate transport rate among different EAAT subtypes (EAAT5 ≈ EAAT4 > EAAT1 > EAAT3 > EAAT2). Whether the channel activity plays a physiological role in each of them is presently unclear, but the chloride conductance of the glutamate transporters on presynaptic terminals of retinal bipolar cells has recently been shown to modulate synaptic release by hyperpolarizing the terminal (Veruki et al., 2006, Wersinger et al. 2006). The channel conductance has a chaotropic selectivity sequence, $SCN^- > NO_3^- > I^- > Cl^- > F^-$ (Wadiche et al., 1995; Eliasof and Jahr, 1996). The gating of this anion conductance has been proposed to be linked to state transitions in the glutamate transport cycle, but the small predicted unitary conductance for the channel and the transporter has not allowed a direct test of this hypothesis (Picaud et al., 1995; Larsson et al., 1996; Wadiche and Kavanaugh, 1998). The structure of a homologous archael transporter from *Pyrococcus horikoshii* was recently solved at 3.5Å (Yernool et al., 2004), but the

structural nature of the chloride channel pore remains unclear. The transporter is a trimer of identical subunits (figure 2.1A), and each subunit appears to be able to independently transport glutamate (Koch and Larrson, 2005; Grewer et al., 2005**).** In contrast, it is less clear whether chloride permeation occurs independently in each subunit or whether channel function involves interacting subunits (Torres-Salazar & Fahlke, 2006) in analogy to ligand-gated channels such as ionotropic glutamate receptors, which have a pore in the central axis of the multimer. In this work we analyzed and modeled the isolated transport and channel conductance components and show that the channel gating is described by a simple model in which each subunit in a trimer has a channel that is independently gated by glutamate.

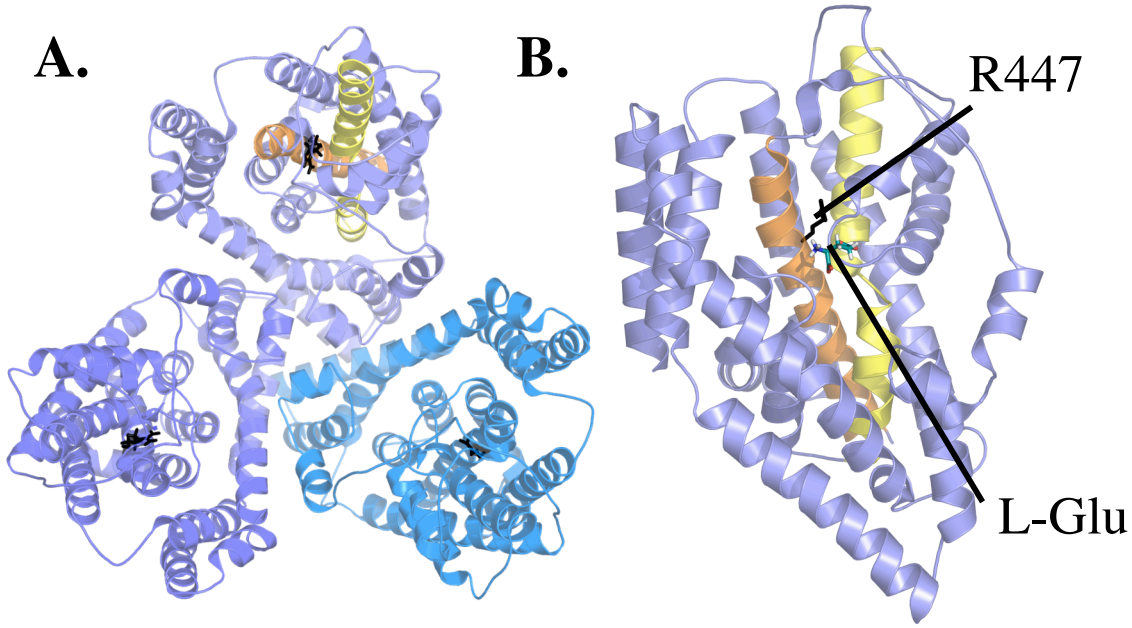

Figure 2.1: The hEAAT3 trimer threaded through a crystal structure from *Pyrococcus horikoshii*, a bacterial glutamate transporter homologue.
A. The structure identifies three identical subunits forming a trimer (Yernool et al., 2004). **B.** A single subunit showing the substrate, L-Glu, bound. The R447 residue for EAAT3 that was mutated in this study is shown in black.

Experimental Procedures

Electrophysiology and flux assays- Human EAAT3 cRNA was microinjected in stage V-VI oocytes, and transport and anion currents and radiolabel fluxes were recorded 3-5 days later as previously described (Wadiche et al., 1995). In co-expression experiments, equal

amounts of wild-type and mutant subunit plasmid DNA were mixed prior to linearization and transcription. Recording solution (Cl-Ringer) contained 96mM NaCl, 2mM KCl, 1mM $MgCl_2$, 1.8mM $CaCl_2$, and 5mM HEPES (pH7.4). In chloride substitution experiments, 90mM $NaNO_3$ was used to replace equimolar NaCl (NO_3-Ringer). Microelectrodes were filled with 3M KCl and had resistances from 1 to 3 MΩ. Two electrode voltage clamp recordings were performed at 22°C with a Geneclamp 500 interfaced to an IBM-compatible PC using a Digidata 1320 A/D controlled with the pCLAMP 6.0 program suite (Molecular Devices). The currents were low-pass filtered at 1 kHz and digitized at 5 kHz. Currents induced by L-glutamate or L-alanine were isolated by subtracting currents recorded in control solution. Data were analyzed offline and modeling and fitting of substrate concentration-dependence of the currents were performed with Kaleidagraph software (v 3.6).

Analytical Modeling of the Anion Channel Gating- Our models proceed from the assumption that one transporter subunit binds and transports glutamate independently of the others (Koch and Larsson 2005; Grewer et al., 2005; and present results). Then, the unidirectional transport of substrate S to release P (when $[S]_{trans} = 0$) by each transporter subunit T is described by:

$$T + S \underset{k_b}{\overset{k_f}{\rightleftharpoons}} C \xrightarrow{k_t} T + P$$

If an independent anion channel is contained in each subunit and its open probability is increased by binding of substrate, then, at steady-state, the normalized current amplitude is given by the Michaelis-Menton relationship:

$$\frac{I}{I_{\max}} = \frac{C}{C+T} = \frac{S}{S+K}$$

where $K = \dfrac{k_b + k_t}{k_f}$

If, in contrast, an anion channel is formed by three subunits in the trimeric complex, then its open probability is increased by binding of glutamate to either 1, 2, or 3 subunits. The set of transporter reaction equations defining the transporter states occupied by 0 (T), 1 (C_1), 2 (C_2), or 3 (C_3) molecules of glutamate is:

$$T + S \underset{k_b}{\overset{3k_f}{\rightleftharpoons}} C_1 \xrightarrow{k_t} T + P$$

$$C_1 + S \underset{2k_b}{\overset{2k_f}{\rightleftharpoons}} C_2 \xrightarrow{2k_t} C_1 + P$$

$$C_2 + S \underset{3k_b}{\overset{k_f}{\rightleftharpoons}} C_3 \xrightarrow{3k_t} C_2 + P$$

If occupancy of only one subunit is required to open the channel, we assume that singly, doubly, and triply occupied trimers are all open; for the case where two are required then doubly or triply occupied trimers are open, for the case where three is required then only triply occupied trimers are open. At steady-state, the normalized current amplitudes for each anion channel gating model are as follows:

single occupancy:

$$\frac{I}{I_{\max}} = \frac{C_1 + C_2 + C_3}{C_1 + C_2 + C_3 + T} = \frac{S^3 + 3S^2K + 3SK^2}{(K^3 + 3SK^2 + 3S^2K + S^3)}$$

double occupancy:

$$\frac{I}{I_{\max}} = \frac{C_2 + C_3}{C_1 + C_2 + C_3 + T} = \frac{S^3 + 3S^2K}{(K^3 + 3SK^2 + 3S^2K + S^3)}$$

triple occupancy:

$$\frac{I}{I_{\max}} = \frac{C_3}{C_1 + C_2 + C_3 + T} = \frac{S^3}{(K^3 + 3SK^2 + 3S^2K + S^3)}$$

Derivations of these equations are given in the accompanying *supplement*.

Results

Each subunit in a trimer transports substrate independently. Wild type hEAAT3 subunits were coexpressed with mutant R447C subunits by injecting RNA transcribed from equal amounts of each cDNA into *Xenopus laevis* oocytes. The R447C mutation has been shown to induce an altered charge selectivity for neutral amino acids such as L-alanine (Bendahan et al, 2000; figure 2.2). L-Alanine (1000 μM) did not activate currents in oocytes expressing wild-type hEAAT3 alone (n=4), nor did L-glutamate (1000 μM) activate currents in oocytes expressing the R447C mutant alone (n=3; figure 2.2 A,B). This selectivity swich was confirmed by radiolabeled uptake assays with either 30μM

[^{3}H]D-Asp or [H^3]L-Ala (figure 2.2C). Co-immunoprecipitation evidence suggests that wild-type and R447 mutants form hetero-multimers when co-expressed in the same cells (Grewer et al., 2005). We therefore examined and compared the L-Ala and L-Glu concentration-dependence of transport currents in oocytes expressing heterotrimeric wild-type hEAAT3 and R447C mutant subunits with the currents activated in homotrimeric populations of each subunit. The concentration-response data were fitted to the Hill equation and the $EC_{50.}$values and Hill coefficients were measured at a series of membrane potentials between -100mV and 60mV. At -20 mV, the reversal potential for Cl^-, the current activated by glutamate predominantly reflects coupled transport (Wadiche et al 1995; figure 2.2 A). At all membrane potentials, the L-Glu and L-Ala concentration-dependence of currents in oocytes expressing heterotrimers was the same as for oocytes expressing homotrimeric wild-type and mutant transporter subunits, respectively (Figure 2A,B; p>0.5). These data are consistent with the conclusion that glutamate transport occurs independently in each subunit within the trimeric complex, since a binding site and translocation pathway formed by multiple subunits would be expected to be altered in the heterotrimers (Awes et al., 2004; Koch and Larsson, 2005; Grewer et al., 2005).

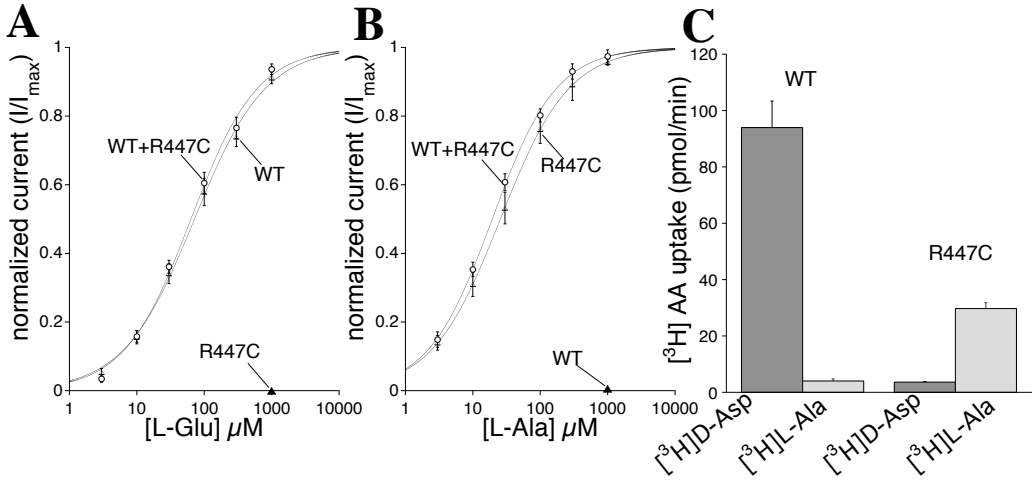

Figure 2.2: Individual subunits in a trimer transport substrate independently: the R447C mutation in hEAAT3 results in a reversed selectivity for neutral and acidic amino acids, and the substrate-dependent transporter currents are unchanged in hetero-multimers comprised of wild-type and mutant subunits.

A. The L-glutamate concentration-response of transporter currents for homo-multimeric WT (open triangle: Km = 85.7 µM +/-19; n_{hill} = 0.84 +/- 0.02; n=7), R447C (solid triangle) (n=3), and the hetero-multimeric R447C+WT subunits (open circle: Km = 70.4 µM +/-12.5; n_{hill} = 0.89 +/-.07; n=6). The extracellular solution contained 96 mM chloride. **B.** L-alanine concentration-response of transporter currents for the homo-multimeric WT (filled triangle) (n=4), R447C (open triangle: Km = 30.8 µM +/-9; n_{hill} = 0.85 +/-.05; n=4), and for the hetero-multimeric R447C coexpressed with WT subunits (open circle: Km = 20.8 µM +/-6; n_{hill} = 0.91 +/-.05; n=6). The extracellular solutions contained 90mM nitrate to amplify the transporter anion current. Steady-state currents were recorded at a membrane potential in of 20 mV for L-ala and -20 mV for L-Glu. The currents were fitted to $I/I_{max}=S^n/(S^n+K^n)$. **C.** Radiolabel uptake (30μM [^{3}H]D-Asp or L-Ala) also demonstrates the selectivity shift.

Analytical modeling of anion channel gating. We considered two general classes of models for anion channel gating in a trimeric molecule: 1) a channel within each subunit that is activated by glutamate binding or 2) a single channel that is gated by glutamate binding to one, two, or three subunits. Using the intrinsic transport kinetic parameter K estimated from measurement of the EC_{50} of glutamate transport in the absence of anion flux (44 μM; see figure 4A), we derived the predicted concentration-dependence conductance of the anion channel for each of the models. This estimated value was in good agreement with previous microscopic rate measurements and modeling; with a glutamate binding rate of 6.8×10^6 M^{-1} s^{-1}, an unbinding rate of 300 s^{-1}, and a transport rate of 14.6 s^{-1} (Wadiche et al., 1995; Larsson et al. 2004), $K = \frac{k_b + k_t}{k_f} = 46 \mu M$ (also see methods and supplemental material). This value was used to derive the predicted glutamate concentration-dependence of the channel conductance for the one channel/one subunit model as well as for the three models in which a central channel is gated by glutamate binding to one, two, or three subunits. For a given transport constant K, which reflects glutamate binding, unbinding, and transport rates, each channel gating model predicts a unique concentration dependence of anion channel activation which can be experimentally tested to identify the gating mechanism of the anion channel (figure 2.3).

The isolated anion current is best fit by the model of one channel within each subunit. The four models represented in figure 2.3 predict distinct differences in anion channel gating as a function of glutamate concentration. The glutamate concentration-dependence of the anion conductance was determined by subtracting the coupled current recorded at the anion reversal potential from the total current at the same potential. Because the presence of the permeant anion NO_3^- does not affect the rate of coupled transport (Wadiche and Kavanaugh, 1998), the anion current was isolated by subtracting the coupled transport current (recorded in Cl-Ringer at -20 mV) from the current recorded in the same cell after switching the external solution to NO_3-Ringer. Figure 2.4A shows the L-Glu dependence of both the anion current and the coupled currents at -20 mV. The concentration-dependence of anion channel activation was compared to each model and quantified by chi square measurement (Figure 2.4B). The data are best fit by the model in

which one anion channel within each subunit is gated independently ($\chi^2 = 8.08$). The next best fit was for the model in which the anion conductance is gated by binding of glutamate to at least two subunits ($\chi^2 = 202$). Similar results were obtained fitting the kinetics of the anion conductance isolated at potentials up to +60mV (data not shown).

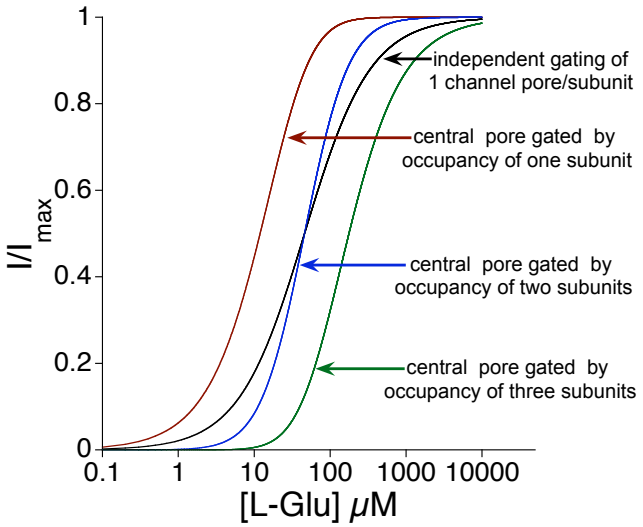

Figure 2.3: Analytical modeling of the trimeric transporter predicts distinct kinetics for anion channel gating. A model depicting 1) An anion channel independently gated within each subunit of the trimer (black line: Km = 45μM; n_{hill} = 1). 2) A central anion pore gated by non-cooperative binding to one or more subunits (red line: Km = 11.90; n_{hill} = 1.48). 3) A central anion pore gated by occupancy of two subunits (blue line: Km = 46.33; n_{hill} = 1.57). 4) A central anion pore gated by occupancy of three subunits (green line: Km = 180.50; n_{hill} = 1.18). The curves were generated from the equations for the respective models shown above, using a transporter kinetic constant, K, of 45 μM (Larsson et al., 2005).

Discussion

Data from several laboratories obtained by co-expression of wild-type and mutant subunits is consistent with the conclusion that glutamate binds and translocates independently through single subunits within a trimeric complex (Grewer et al., 2005; Koch and Larsson, 2005; Awes et al. 2004; Leary et al. 2006). In agreement with Grewer et al., (2005), we found that co-expression of R447C subunits with wild-type subunits results in transporter currents consistent with two populations of transporters translocating substrate independently. Some caveats arise when making quantitative inferences about gating of anion currents using this experimental approach because of untested asumptions of random translation and interaction of wild-type and mutant subunits expressed at the plasma membrane surface as well as uncertainties about the

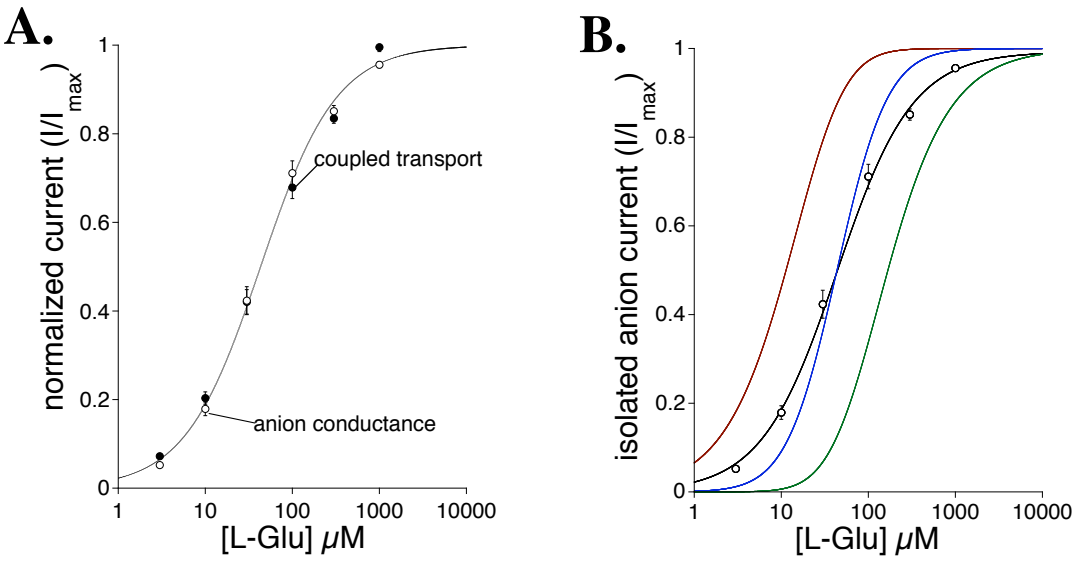

Figure 2.4: The hEAAT3 anion channel conductance is best fit by the model of a single pathway within each subunit. **(A)** The isolated coupled transport current (solid circle: Km = 43.7μM; n=8) was recorded in Cl^- at the anion reversal potential, -20 mV, and the uncoupled anion current (open circle: Km = 42.8; n = 8) was recorded in 90 mM NO_3 at -20 mV. The coupled and anion currents were fitted to (I/I_{max}=[L-Glu]/([L-Glu]+Km). **(B)** The model fits for the experimental anion conductance data are shown for an anion channel within each subunit (black line: chi^2 = 8.08), one central anion pore gated by non-cooperative binding to one or more subunits (red line: chi^2 = 1369), one central anion pore gated by non-cooperative binding to at least two subunits (blue line: chi^2 = 202), or one central anion pore gated by non-cooperative binding of all three subunits (green line: chi^2 = 867). The measured coupled transport constant used for the fitting was 43.7 μM .

microscopic conductance properties of the various homo- and heterotrimers. To circumvent these caveats, we applied Michaelis-Menten analysis to homotrimeric wild-type transporters and derived equations that predict the distribution of singly, doubly, and triply-occupied trimeric complexes as a function of glutamate concentration. These derivations depend only on the assumption that each subunit transports glutamate independently (Grewer et al., 2005; Koch and Larsson, 2005; Awes et al. 2004; Leary et al. 2006).

We find that the glutamate concentration-dependence of the fractional anion conductance is the same as the fraction of total subunits occupied by glutamate, consistent with the presence of a channel in each subunit that is gated by glutamate binding. This is in contrast to the predictions for gating of a central channel controlled by occupancy of one, two, or three subunits. A consequence of the one subunit/one channel gating scheme is that the concentration-dependencies of transport and anion conductance

are expected to be identical, which is indeed observed (figure 2.4A). This result conflicts with that of Torres-Salazar et al. (2006), who found evidence of subunit cooperativity in a recent study of channel gating of the related EAAT4 glutamate transporter. Aside from the difference in subtype, it is presently unclear why these results differ. It is possible that in the recording conditions of Torres-Salazar et al. (2006), some of which involve activation of transient anion currents by voltage jumps, additional conductances could be reflected in the pre steady-state currents which are not monitored in the steady-state conditions studied here. Additionally, the analytical solutions we apply are derived from steady-state assumptions.

The detailed molecular mechanisms controlling the chloride channel functions of glutamate transporters are still unclear. A cluster of residues in TMD2 that affect anion permeation has been identified by Ryan et al., (2004). These residues are in a helix that is adjacent to the likely glutamate binding site (figure 2.1B). TMD8, where R447 lies, and TMD7, where other residues implicated in alkali cation coupling lie (Kavanaugh et al. 1997), are also close to the likely glutamate binding site. The identity of the coupled alkali cation also strongly influences the anion conductance (Borre and Kanner, 2001), suggesting that these helices could potentially be involved in forming a permeation path that could be shared by L-glutamate, the coupled cations, and Cl^- ions. A further unresolved question concerns the reason for the trimeric nature of the transporter given that the subunits function independently. It is unknown whether dissociated monomeric subunits are functional, but it is possible that a multimeric structure has evolved to play a functional role; e.g. a large aqueous bowl projecting partially through the plane of the membrane might facilitate transport of charged substrates. Analysis of the quaternary structure and channel properties of other members of this transporter superfamily may shed further light on these issues.

References

Awes, AN, Hubbard, J, Kanner, BI, Kavanaugh, MP. Structure of the selectivity filter in the glutamate/neutral amino acid transporter family (2004) Program No. 168.13. Washington, DC: Society for Neuroscience, 2004. Online

Bendahan A, Armon A, Madani N, Kavanaugh MP, Kanner BI (2000) Arginine 447 plays a pivotal role in substrate interactions in a neuronal glutamate transporter. J Biol Chem 275:37436-37442.

Billups B, Rossi D, Attwell D (1996) Anion conductance behavior of the glutamate uptake carrier in salamander retinal glial cells. J Neurosci 16:6722-6731.

Borre L, Kanner BI (2001) Coupled, but not uncoupled, fluxes in a neuronal glutamate transporter can be activated by lithium ions. J Biol Chem 276:40396-40401.

Danbolt NC (2001) Glutamate uptake. Prog Neurobiol 65:1-105.

Eliasof S, Jahr CE (1996) Retinal glial cell glutamate transporter is coupled to an anionic conductance. Proc Natl Acad Sci U S A 93:4153-4158.

Eskandari S, Kreman M, Kavanaugh MP, Wright EM, Zampighi GA (2000) Pentameric assembly of a neuronal glutamate transporter. Proc Natl Acad Sci U S A 97:8641-8646.

Fairman WA, Vandenberg RJ, Arriza JL, Kavanaugh MP, Amara SG (1995) An excitatory amino-acid transporter with properties of a ligand-gated chloride channel. Nature 375:599-603.

Grewer C, Balani P, Weidenfeller C, Bartusel T, Tao Z, Rauen T (2005) Individual subunits of the glutamate transporter EAAC1 homotrimer function independently of each other. Biochemistry 44:11913-11923.

Kavanaugh MP, Bendahan A, Zerangue N, Zhang Y, Kanner BI (1997) Mutation of an amino acid residue influencing potassium coupling in the glutamate transporter GLT-1 induces obligate exchange. J Biol Chem 272:1703-1708.

Koch HP, Larsson HP (2005) Small-scale molecular motions accomplish glutamate uptake in human glutamate transporters. J Neurosci 25:1730-1736.

Larsson HP, Picaud SA, Werblin FS, Lecar H (1996) Noise analysis of the glutamate-activated current in photoreceptors. Biophys J 70:733-742.

Larsson HP, Tzingounis AV, Koch HP, Kavanaugh MP (2004) Fluorometric measurements of conformational changes in glutamate transporters. Proc Natl Acad Sci U S A 101:3951-3956.

Levy LM, Warr O, Attwell D (1998) Stoichiometry of the glial glutamate transporter GLT-1 expressed inducibly in a Chinese hamster ovary cell line selected for low endogenous Na+-dependent glutamate uptake. J Neurosci 18:9620-9628.

Liman ER, Tytgat J, Hess P (1992) Subunit stoichiometry of a mammalian K+ channel determined by construction of multimeric cDNAs. Neuron 9:861-871.

Picaud SA, Larsson HP, Grant GB, Lecar H, Werblin FS (1995) Glutamate-gated chloride channel with glutamate-transporter-like properties in cone photoreceptors of the tiger salamander. J Neurophysiol 74:1760-1771.

Ryan RM, Mitrovic AD, Vandenberg RJ (2004) The chloride permeation pathway of a glutamate transporter and its proximity to the glutamate translocation pathway. J Biol Chem 279:20742-20751.

Seal RP, Shigeri Y, Eliasof S, Leighton BH, Amara SG (2001) Sulfhydryl modification of V449C in the glutamate transporter EAAT1 abolishes substrate transport but not the substrate-gated anion conductance. Proc Natl Acad Sci U S A 98:15324-15329.

Torres-Salazar D, Fahlke C (2006) Intersubunit interactions in EAAT4 glutamate transporters. J Neurosci 26:7513-7522.

Veruki, ML, Mørkve, SH, Hartveit, E (2006) Activation of a presynaptic glutamate transporter regulates synaptic transmission through electrical signaling Nature Neurosci. 9:1388-1396

Wadiche JI, Kavanaugh MP (1998) Macroscopic and microscopic properties of a cloned glutamate transporter/chloride channel. J Neurosci 18:7650-7661.

Wadiche JI, Amara SG, Kavanaugh MP (1995) Ion fluxes associated with excitatory amino acid transport. Neuron 15:721-728.

Weiss JN (1997) The Hill equation revisited: uses and misuses. Faseb J 11:835-841.

Wersinger, E. Schwab, Y., Sahe, J.-A., Rendon, A., Pow, DV, Picaud, S., Roux, MJ (2006)

The glutamate transporter EAAT5 works as a presynaptic receptor in mouse rod bipolar cells. J. Physiol. DOI: 10.1113/jphysiol.2006.118281 published online Sep 14, 2006

Yernool D, Boudker O, Jin Y, Gouaux E (2004) Structure of a glutamate transporter homologue from Pyrococcus horikoshii. Nature 431:811-818.

Zerangue N, Kavanaugh MP (1996) Flux coupling in a neuronal glutamate transporter. Nature 383:634-637.

Supplemental material:

To quantitatively distinguish between possible channel gating mechanisms we formed Hill-type equations for the dependence of the measured signal upon the concentration of substrate. These equations were then fit to experimental data to determine which reaction mechanism yielded the best fit. For all the reaction mechanisms considered, the steps in the analysis are the same. First the reaction mechanism was enunciated in terms of the involved components, i.e. for one anion channel per subunit:

$$T + S \underset{k_b}{\overset{k_f}{\rightleftharpoons}} C \xrightarrow{k_t} T + P$$

Then the Law of Mass action was invoked to form ordinary differential equations (ODEs) in the concentrations of the given molecules. For the reaction above this yields the following set of equations, where we have used notation to write [X] = X for a given molecule X.

$$\frac{dT}{dt} = -k_f T\, S + k_b C + k_t C$$

$$\frac{dS}{dt} = -k_f T\, S + k_b C$$

$$\frac{dC}{dt} = k_f T\ S - k_b C - k_t C$$

$$\frac{dP}{dt} = k_t C$$

We assume the uncoupled anion current, since it is gated by the transporter bound with substrate, is directly proportional to the concentration of complex, C. This can be determined in terms of substrate concentration S by making a quasi-steady state assumption that the complex formed is in equilibrium, so that the time derivative of each/any quantity, is zero. The resulting algebraic equations can be solved and simplified to yield a single equation for a concentration ratio of complex to total transporter.

In the case of one channel per sub-unit the result is the familiar Michaelis-Menton approximation to enzyme kinetics, with a saturation curve given by

$$\frac{C}{C+T} = \frac{S}{S + \frac{(k_b + k_t)}{k_f}} = \frac{S}{S+K}$$

where $K = \frac{k_b + k_t}{k_f}$

For the models involving a central pore gated by non-cooperative binding to one or more subunits, the reaction mechanisms considered are:

$$T + S \underset{k_b}{\overset{3k_f}{\rightleftharpoons}} C_1 \xrightarrow{k_t} T + P$$

$$C_1 + S \underset{2k_b}{\overset{2k_f}{\rightleftharpoons}} C_2 \xrightarrow{2k_t} C_1 + P$$

$$C_2 + S \underset{3k_b}{\overset{k_f}{\rightleftharpoons}} C_3 \xrightarrow{3k_t} C_2 + P$$

where C_n is the transporter complex with n molecules of ligand bound. If occupancy of only one subunit is required to open the channel then singly, doubly, and triply occupied trimers are all open. If two are required, then doubly or triply occupied trimers are open to selective anions, and if all all three must be bound to open the anion channel, only the triply occupied trimers are considered to be open. Therefore we need to solve for quasi-steady state concentrations of C_1, C_2 and C_3, and the chloride current will be proportional to the ratios:

$$\frac{C_3}{C_1 + C_2 + C_3 + T}$$

$$\frac{C_2 + C_3}{C_1 + C_2 + C_3 + T}$$

$$\frac{C_1 + C_2 + C_3}{C_1 + C_2 + C_3 + T}$$

For three subunits bound to open, two subunits bound to open and one subunit bound required to open the channel, respectively.

The ODEs for the reactions resulting from the law of mass action are as follows:

$$\frac{dC_1}{dt} = 3k_f TS + 2(k_b + k_t)C_2 - (k_b + k_t + 2k_f S)C_1$$

$$\frac{dC_2}{dt} = -(2k_b + 2k_t + k_f S)C_2 + 2k_f C_1 S + (3k_b + 3k_t)C_3$$

$$\frac{dC_3}{dt} = -(3k_b + 3k_t)C_3 + k_f C_2 S$$

Invoking the quasi-steady state assumption, solving for the equilibrium state of the three complexes and using the fact that the total number of transporters is conserved, yields:

$$C_1 = \frac{3\,S\,K^2 T_0}{(K^3 + 3SK^2 + 3S^2K + S^3\ )}$$

$$C_2 = \frac{3\,S^2 K\,T_0}{(K^3 + 3SK^2 + 3S^2K\ + S^3)}$$

$$C_3 = \frac{S^3 T_0}{(K^3 + 3SK^2 + 3S^2K\ + S^3\ )}$$

Here T_0 is the total number of transporters and is equal to $T + C_1 + C_2 + C_3$ at any time. Therefore:

single occupancy:

$$\frac{I}{I_{\max}} = \frac{C_1 + C_2 + C_3}{C_1 + C_2 + C_3 + T} = \frac{S^3 + 3S^2K\ + 3\,SK^2}{(K^3 + 3SK^2 + 3S^2K + S^3\ )}$$

double occupancy:

$$\frac{I}{I_{\max}} = \frac{C_2 + C_3}{C_1 + C_2 + C_3 + T} = \frac{S^3 + 3S^2K}{(K^3 + 3SK^2 + 3S^2K\ + S^3)}$$

triple occupancy:

$$\frac{I}{I_{\max}} = \frac{C_3}{C_1 + C_2 + C_3 + T} = \frac{S^3}{(K^3 + 3SK^2 + 3S^2K + S^3)}$$

CHAPTER 3: ALKALI CATION GATING OF THE UNCOUPLED ANION CONDUCTANCE IN THE EXCITATORY AMINO ACID TRANSPORTER 1

Introduction

At glutamatergic synapses in the central nervous system, the excitatory amino acid transporters 1-5 (hEAAT 1-5) are fundamental in the regulation and clearance of L-Glu. In addition to this ability to concentrate L-Glu within the cell and keep extracellular L-Glu below micromolar levels (Herman and Jahr, 2007; Zerangue and Kavanaugh, 1996), the glutamate transporters have a thermodynamically uncoupled anion channel gated by Na^+ (anion leak conductance) or Na^+ plus L-Glu (uncoupled anion conductance) (Fairman et al., 1995; Wadiche et al., 1995). Within the homotrimer, described by the crystal structure of an archeal homolog Glt_{Ph} (Yernool et al., 2004), the anion channel is an intrinsic part of each subunit (Grewer et al., 2005; Koch et al., 2007; Leary et al., 2007). These anion channels are conserved in the SLC1 family and even in the distant relative of the archaeal aspartate transporter Glt_{Ph} (Ryan and Mindell, 2007). The anion conductance in the hEAATs is intricately coupled to the binding and translocation of 3 Na^+, $1H^+$, and L-Glu. The amplitude of the anion conductance in the EAATs is inversely proportional to the transport rate, where the anion conductance of hEAAT5 ≈ hEAAT4 > hEAAT1 > hEAAT3 > hEAAT2, likely revealing a conducting state or states accessed during substrate transport (Bergles et al., 2002; Wadiche and Kavanaugh, 1998). Recently, Veruki et al. (2006) and Wersinger et al. (2006) made the first functional description of the anion channel as an inhibitory feedback mechanism, hyperpolarizing the presynaptic membrane of bipolar cells of the eye and reducing L-Glu vesicle fusion.

The gating by only Na^+ of the anion leak conductance in the resting cell has been detected in both cells expressing high levels of glutamate transporters in the brain as well as in cells expressing transporters in isolation (Bergles and Jahr, 1997; Otis et al., 1997; Wadiche and Kavanaugh, 1998). Ryan and Mindell (2008), who recently measured the anion conductance in Glt_{Ph}, suggested that in addition to a Na^+ dependent leak, subject to block by the competitive inhibitor TBOA, there may also be a transporter related anion leak insensitive to the block by inhibitor. In this study, we us outside-out patches from *Xenopus laevis* oocytes expressing hEAAT1 to determine which alkali cations are required to gate the leak conductance. The presence of Na^+ or K^+ on either side of the

membrane supports the anion leak conductance, not seen with $TRIS^+$ based solutions. Further and in agreement with Ryan and Mindell (2008), only a portion of this conductance is associated with the presence of hEAAT1 is blocked by TBOA.

Experimental Methods

Electrophysiology patch clamp recordings- Human EAAT1 cRNA was microinjected in stage V-VI oocytes, and transport and anion currents were recorded 3-5 days later. After removal of the vitelline membrane, outside-out patch recordings were made with fire-polished pipettes (4-5 MΩ) as previously described (Wadiche and Kavanaugh, 1998). Three Cl^- based extracellular solutions were used (Na^+, K^+, or $TRIS^+$ based) containing 100mM NaCl, TRISCl, or KCl, 10mM TRISCl, 1mM $MgCl_2$, 1.8mM $CaCl_2$, and 5mM HEPES (pH7.4 with TRISbase). Three NO_3^- based intracellular solutions were used containing 100mM $NaNO_3$, $TRISNO_3$, or KNO_3, 10mM TRISCl, 1mM $MgCl_2$, 1.8mM $CaCl_2$, and 5mM HEPES (pH7.4 with TRISbase). The more permeable SCN^- anion was used in some experiments to replace $NaNO_3$ and KNO_3 in the intracellular solutions to confirm the presence of an anion conductance associated with hEAAT1. Membrane currents were recorded with a Geneclamp 500 interfaced to an IBM-compatible PC using a Digidata 1200 A/D controlled with the pCLAMP 6.0 program suite (Axon Instruments). Only patches with membrane seal resistances > 10 GΩ were used in experiments from either uninjected or hEAAT1 injected oocytes. Records were lo-pass Bessel filtered at 2-5 kHz and digitized at 2kHz. Currents induced by L-glutamate or L-alanine or blocked by TBOA were isolated by subtracting currents recorded in control solution. Also, chord conductances across voltages associated with the hEAAT1 transporter were obtained by subtracting the chord conductance from patches pulled from uninjected oocytes from those from hEAAT1 injected oocytes, under the same respective ion conditions.

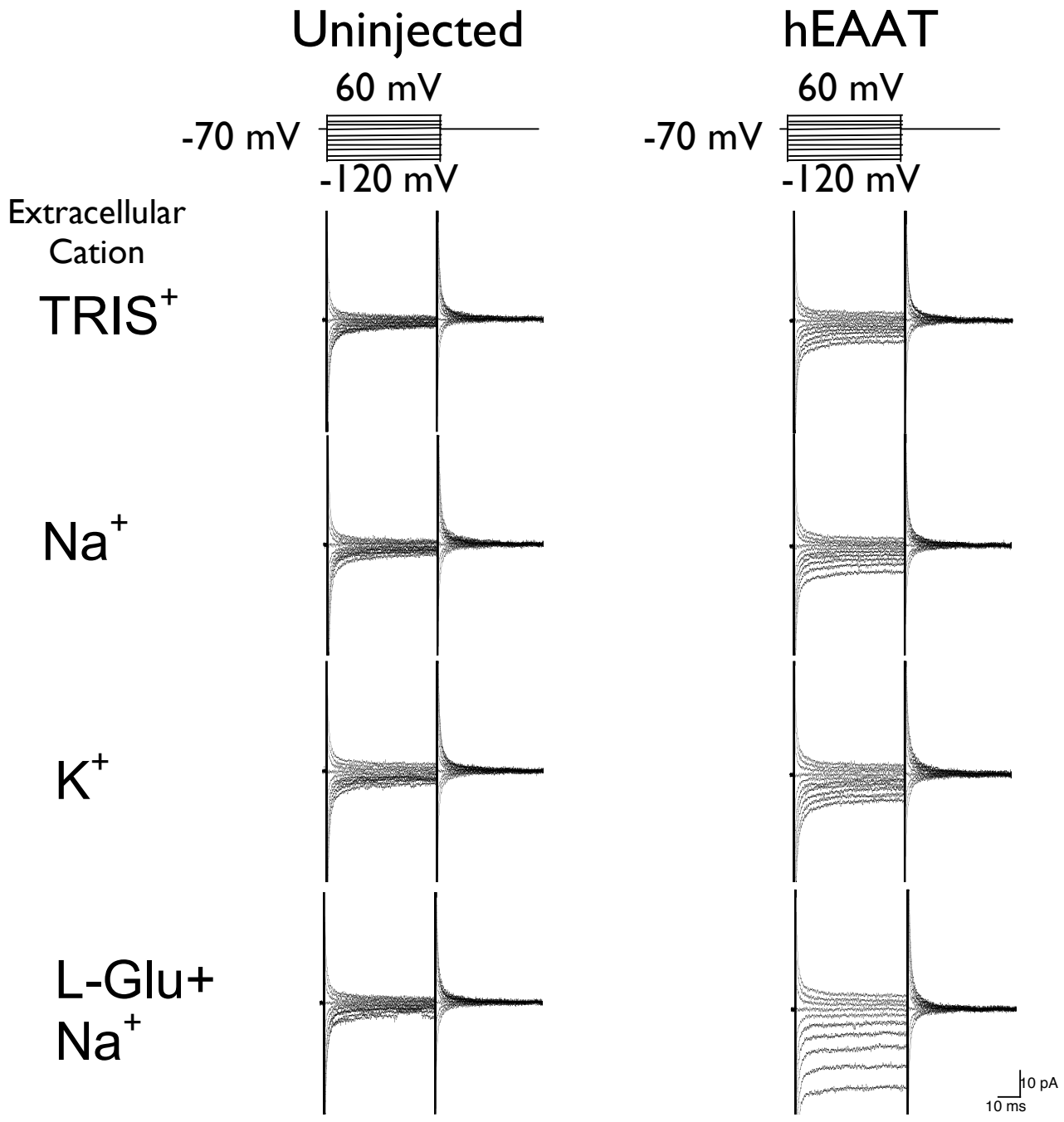

Figure 3.1: Monovalent cation gating of the hEAAT1 anion conductance in outside-out macropatches. Representative experiments of outside-out patches from an uninjected oocyte (left) and an hEAAT1 injected oocyte (right) in response to Na^+, K^+, or $TRIS^+$ as the only extracellular cation. A KNO_3 intracellular solution was used, and L-Glu + Na^+ was a positive control to demonstrate the presence of hEAAT1 transporters.

Results

The anion channel gating is supported with a K^+ based intracellular solution.

In the hEAATs, it is not completely understood which cations, if any, are sufficient to gate the "anion leak" conductance. Outside-out macropatches from *Xenopus laevis* oocytes allowed us to control the concentrations of cations ($TRIS^+$, K^+, or Na^+) on both sides of the membrane. $TRIS^+$ was used as a control cation because it neither supports glutamate transport nor activates the uncoupled anion conductance. We performed experiments only on outside-out (o/o) patches that resealed with a resistance of 10 gigaohm or greater. These patches were voltage clamped at 0 mV, and at steady state for each respective extracellular cation, a current-voltage (I-V) relationship was defined by a series of jumps from -120 mV to 60 mV. To resolve anion currents in the patches, intracellular Cl^- anions were substituted with either NO_3^- or SCN^- because of their greater permeability through the transporter anion channel (Eliasof and Jahr, 1996; Wadiche et al., 1995). The Nernst equation predicted a reversal potential for the hEAAT1 uncoupled anion conductance of 56 mV when 110 mM NO_3^- replaced Cl^- as the intracellular anion and 104 mV when 110 mM SCN^- replaced Cl^-. This assumed the permeability ratio of NO_3^-:Cl^- of 10.8, SCN^-:Cl^- of 67 (Wadiche and Kavanaugh, 1998).

Under physiological conditions, the cytoplasmic face of the hEAATs is exposed to high K^+ (100 mM). With KNO_3 based intracellular solution, voltage jumps in extracellular $TRIS^+$, Na^+, or K^+ revealed currents that were inwardly rectifying at negative potentials, reversed and became outward at positive potentials for patches from either hEAAT1 or uninjected oocytes (Figure 3.1). These I-V relationships were similar with $NaNO_3$ or $TRISNO_3$ based intracellular solutions. L-Glu (1mM) plus Na^+ stimulated the anion conductance in o/o patches with hEAAT1 transporters but had no effect on o/o patches from uninjected oocytes (Figure 3.1 and 3.2A). Comparing the hEAAT1 and uninjected current amplitude at -120 mV showed an obvious and significant increase in the steady state conductance for $TRIS^+$, Na^+, and K^+ extracellular (Figure 3.1 and Figure 3.2A). This corresponds with previous studies suggesting Na^+ binding can gate an hEAAT associated 'anion leak' (Otis et al., 1997; Wadiche and Kavanaugh, 1998), and it appears this extracellular cation binding site can be occupied also by K^+.

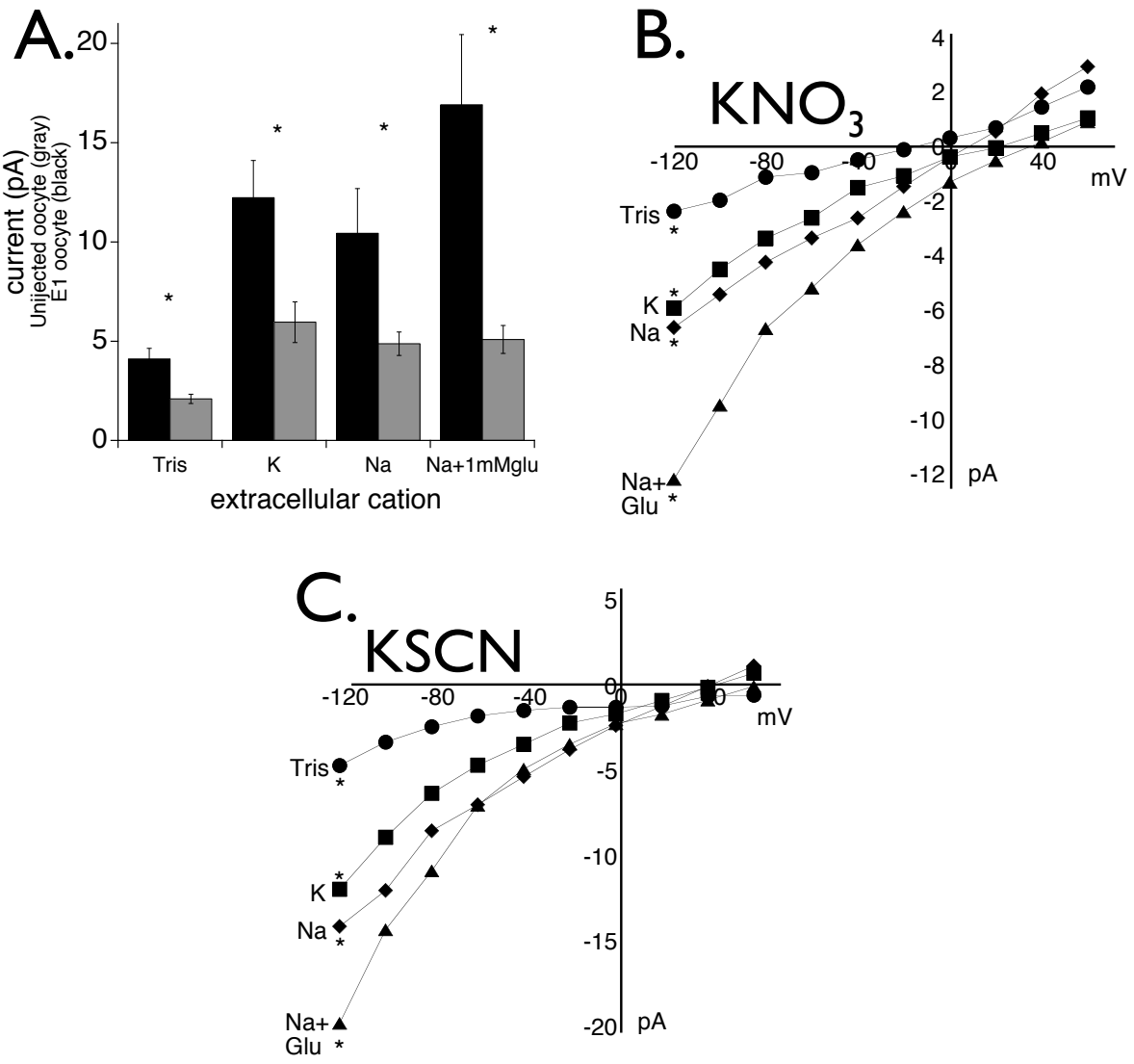

Figure 3.2: The hEAAT1 anion conductance is gated by K^+ from either side of the membrane. A. The average current amplitudes at -120 mV for 7 to 8 outside-out patches from uninjected (gray_$TRIS^+$ = 2.09 +/- 0.23 pA; Na^+ = 4.87 +/- 0.59 pA; K^+ = 5.96 +/- 1.03 pA; L-Glu + Na^+ = 5.09 +/- 0.70 pA) or hEAAT1 (black_ $TRIS^+$ = 4.11 +/- 0.53 pA; Na^+ = 10.44 +/- 2.25 pA; K^+ = 12.23 +/- 1.88 pA; L-Glu + Na^+ = 16.92 +/- 3.53 pA) oocytes with Na^+, K^+, or $TRIS^+$ as the respective extracellular cation (KNO_3 intracellular). **B.** Isolated hEAAT1 I-V relationships for extracellular $TRIS^+$, Na^+, K^+, or L-Glu + Na^+ determined by subtracting currents from patches of uninjected oocytes, same patches as in 2A. The reversal potential for each was E_{TRIS} = -10 mV, E_{Na} = 10 mV; $E_{L\text{-}Glu+Na}$ = > 40 mV; E_K = 20 mV (KNO_3 intracellular). **C.** Isolated hEAAT1 I-V relationships for extracellular $TRIS^+$, Na^+, K^+, or L-Glu + Na^+ with intracellular KSCN. Currents from patches of uninjected oocytes were subtracted from those with hEAAT1. The reversal potential for each condition was > 60 mV (n = 4 to 7 patches).

Because there is a significant increase in conductance with a $TRIS^+$ based extracellular solution when comparing uninjected patches to hEAAT1 patches, it may be suggested that a K^+ atom is bound to the internal face of the protein under physiological conditions that can support an anion conductance in the transporter.

The hEAAT1 transporter current-voltage relationships (I-V) with $TRIS^+$, Na^+, L-Glu plus Na^+, or K^+ were isolated by subtracting the respective currents from patches not expressing the transporter (Figure 3.2B). The reversal potential for each was left-shifted from the expected Nernst prediction for NO_3^- of 56 mV. This left-shift in the I-V for KNO_3 would suggest 1) an additional conductance carried by a separate ion or 2) an error within the experimental system (see discussion). Substitution of KNO_3 with KSCN as the intracellular based solution, expectedly, increased the average current amplitude at negative potentials and shifted the reversal potentials to > 60 mV (Figure 3.2C). Both of these effects demonstrate the current measured is at least, in part, if not all, due to the uncoupled anion conductance associated with the transporter.

The anion channel gating is supported with a Na^+ based intracellular solution.

Intracellular replacement of K^+ with Na^+ based solutions cannot support steady-state L-Glu transport, though it will allow L-Glu binding as well as exchange (Bergles et al., 2002). In our experiments, replacing KNO_3 with $NaNO_3$ or NaSCN also did not support steady state currents gated by L-Glu (Figure 3.3A, 3B ($NaNO_3$), or 3C (NaSCN)). Na^+ or K^+ extracellular appeared to bind and gate a conductance at negative membrane potentials on hEAAT1 o/o patches compared to those from uninjected oocytes (Figure 3.3A). This follows previous observations in a bacterial glutamate transporter (Glt_{ph}) (Ryan and Mindell, 2007).

For hEAAT1, subtracting currents of uninjected o/o patches from hEAAT1 currents revealed currents that had reversal potentials > 60 mV (Figure 3.3B), which supported that these currents were carried by NO_3^-. Even though Na^+ cannot replace K^+ for steady-state transport, it was not known in the hEAATs if Na^+ intracellular can bind and support an anion conductance as was seen for K^+ in figure 3.2C. With a $TRIS^+$ based extracellular solution, there was a trend of a current at negative membrane potentials, which was not significant (Figure 3.3B). When we replaced $NaNO_3$ with NaSCN, this current became very apparent, demonstrating Na^+ could occupy an intracellular binding

site and gate the anion conductance (Figure 3.3C). Again, the increase in current amplitude with SCN^- and the reversal potentials near the expected reversal potential (-56 mV and -110 mV) confirmed that the conductance is carried through the transporter anion selective pore.

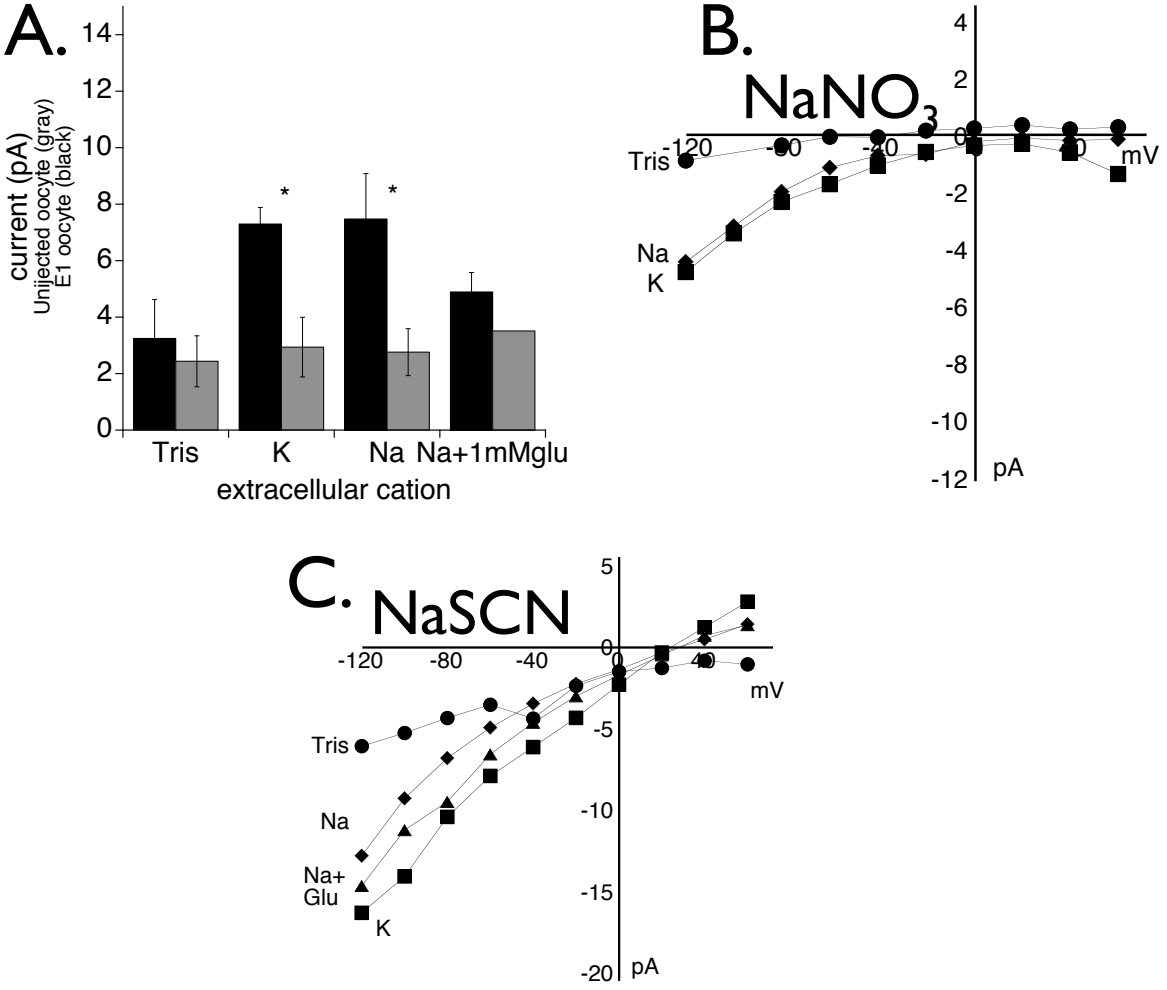

Figure 3.3: The hEAAT1 anion conductance is gated by Na^+ from either side of the membrane. A. The average current amplitudes at -120 mV for 4 to 5 outside-out patches from uninjected (gray_$TRIS^+$ = 2.44 +/- 0.90 pA; Na^+ = 2.76 +/- 0.83 pA; K^+ = 2.94 +/- 1.06 pA; L-Glu + Na^+ = 3.51 pA) or hEAAT1 (black_ $TRIS^+$ = 3.24 +/- 1.38 pA; Na^+ = 7.48 +/- 1.61 pA; K^+ = 7.30 +/- 0.58 pA; L-Glu + Na^+ = 4.98 +/- 0.69 pA) oocytes with Na^+, Na^+ + L-Glu, K^+, or $TRIS^+$ as the respective extracellular cation ($NaNO_3$ intracellular). **B.** Isolated hEAAT1 I-V relationships for extracellular $TRIS^+$, Na^+, or K^+ determined by subtracting currents from patches of uninjected oocytes, same patches as in 3A. The reversal potential for each was > 60 mV ($NaNO_3$ intracellular). **C.** Isolated hEAAT1 I-V relationships for extracellular $TRIS^+$, Na^+, K^+, or L-Glu + Na^+ with intracellular NaSCN. Again, currents from patches of uninjected oocytes were subtracted from those of hEAAT1. The reversal potential for each condition was E_{TRIS} > 60 mV, E_{Na} = 30 mV; $E_{L\text{-}Glu+Na}$ = 30 mV; E_K = 30 mV (n = 3 to 4 patches).

The anion channel gating is supported with a $TRIS^+$ based intracellular solution.

No research has studied gating of the transporter anion channel with no intracellular cation bound. With a $TRISNO_3$ based intracellular solution, bath application of NaCl and KCl did activate conductances in hEAAT1 at -120 mV (Figure 3.4A). This conductance was carried by NO_3^- because the isolated currents (subtraction of uninjected patches from hEAAT1 patches) reversed near 60 mV (Figure 3.4B). The addition of L-Glu plus Na^+ did not increase this conductance (not shown), which further demonstrated the requirement of intracellular K^+ for steady-state transport of substrate.

Whether the hEAATs have an anion leak completely independent of any bound cation is not known. With $TRIS^+$ based intracellular and extracellular solutions, currents of uninjected patches compared to hEAAT1 patches revealed no significant conductance (Figure 3.4B). Though this showed that there was no detectable anion leak in hEAAT1 transporter, it is possible an anion leak could be below the resolution of our technique.

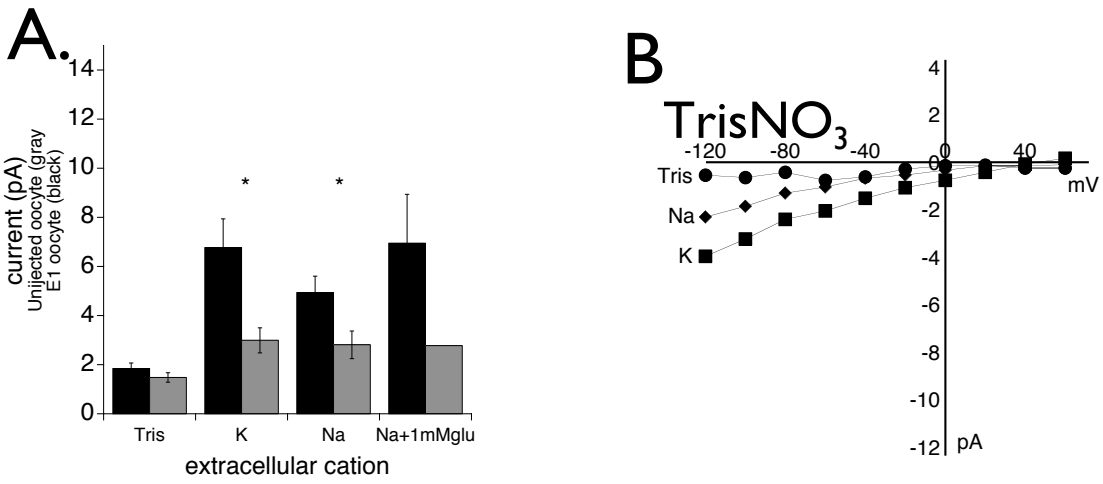

Figure 3.4: There is no measurable hEAAT1 anion conductance in the absence of Na^+ and K^+. **A.** The average current amplitudes at -120 mV for 6 to 15 outside-out patches from uninjected (gray_$TRIS^+$ = 1.48 +/- 0.19 pA; Na^+ = 2.81 +/- 0.56 pA; K^+ = 2.99 +/- 0.51 pA; L-Glu + Na^+ = 2.78 pA) or hEAAT1 (black_ $TRIS^+$ = 1.85 +/- 0.22 pA; Na^+ = 4.94 +/- 0.67 pA; K^+ = 6.78 +/- 1.17 pA; L-Glu + Na^+ = 6.95 +/- 1.99 pA) oocytes with $TRIS^+$, Na^+, Na^+ + L-Glu, or K^+ as the respective extracellular cation ($TRISNO_3$ intracellular). **B.** Isolated hEAAT1 I-V relationships for extracellular $TRIS^+$, Na^+, or K^+ determined by subtracting currents from patches of uninjected oocytes, same patches as in 4A. The reversal potential for each was > 60 mV ($TRISNO_3$ intracellular).

TBOA only partially blocked the anion current gated by alkali cations.

An 'anion leak' gated by Na^+ had been described previously for the hEAATs in which application of inhibitors at negative holding potentials resulted in an outward current (Bergles and Jahr, 1997; Grewer et al., 2000; Otis et al., 1997; Wadiche and Kavanaugh, 1998). Figures 3.2, 3.3, and 3.4 showed that Na^+ or K^+ can bind and gate this current from either side of the membrane. Surprisingly, application of Na^+ plus 200 μM TBOA or Benzyl aspartate (BA) (not shown) blocked only a small fraction of this anion current (Figure 3.5A). TBOA did not affect Na^+ currents in uninjected oocytes (Figure 3.5B). The small current blocked by the inhibitor did not reverse by 60 mV, supporting that it was carried by NO_3^- anions (Figure 3.5C_circle). In addition, the current not blocked by TBOA, also did not reverse by 60 mV, consistent with the idea the two currents have the same ionic basis (Figure 3.5C_squares). Because the anion leak has always been defined by the current blocked by an inhibitor, this may demonstrate a larger baseline anion current associated with the transporter. This helps validates anion currents independent of TBOA as has been suggested in Glt_{ph} (Ryan and Mindell, 2007).

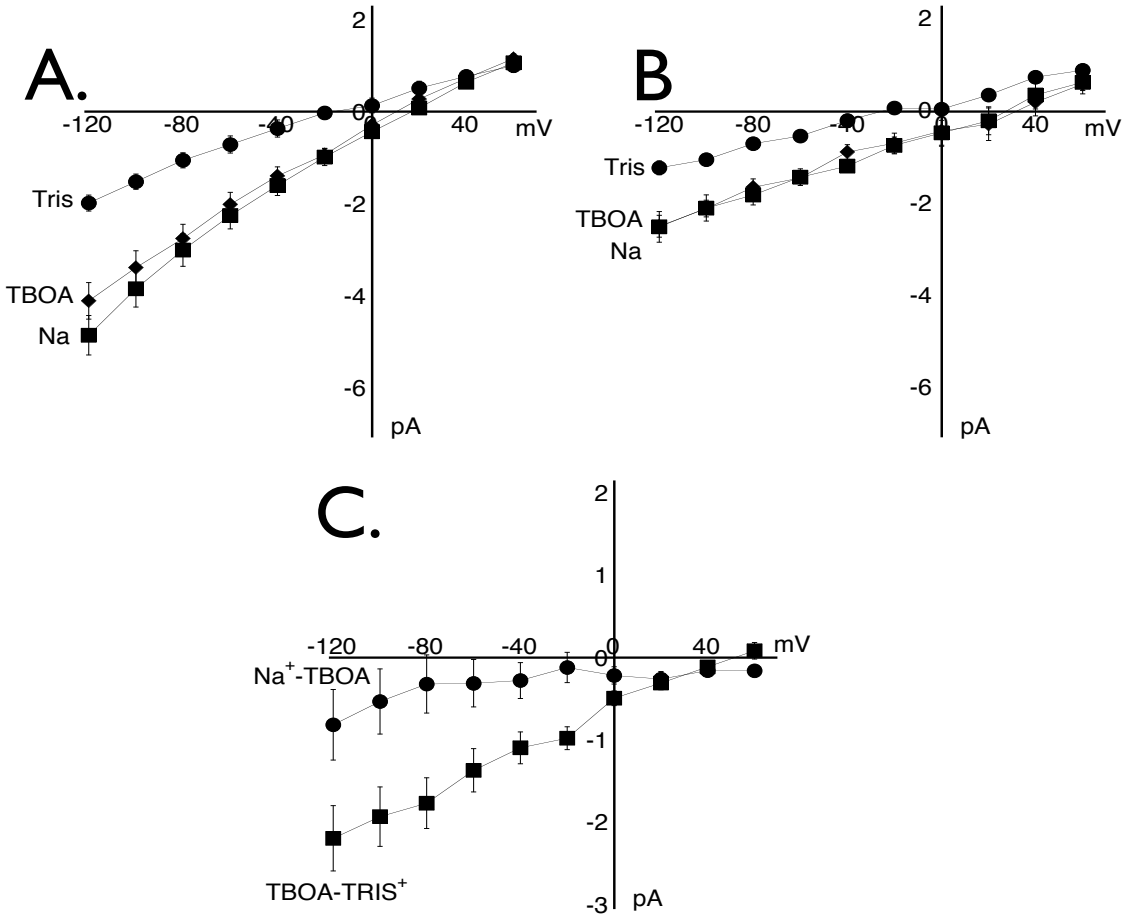

Figure 3.5: TBOA only blocks a fraction of the anion conductance gated by extracellular Na^+ A. Currents from hEAAT1 o/o patches plotted as a function of membrane potential with extracellular $TRIS^+$, Na^+, or Na^+ + TBOA 100µM ($TRISNO_3$ intracellular). **B.** Currents from unijected o/o patches plotted as a function of membrane potential with extracellular $TRIS^+$, Na^+, or Na^+ + TBOA 100µM ($TRISNO_3$ intracellular). **C.** The currents blocked by TBOA in the hEAAT1 o/o patches (Figure 3.5_A) isolated by subtracting Na^+ + TBOA from the currents in just Na^+ at each membrane potential (circles), and the current not blocked by TBOA (Figure 3.5_A) isolated by subtracting currents in $TRIS^+$ from those with Na^+ + TBOA (squares). The reversal potential for both is > 60 mV.

Discussion

In rod bipolar cells, the anion channel of the hEAATs has been shown to hyperpolarize the presynaptic terminal thus reducing vesicular L-Glu release (Veruki et al., 2006; Wersinger et al., 2006). Though this likely describes hEAAT5, each of hEAATs 1-5 has an anion channel gated by L-Glu plus Na^+ (Arriza et al., 1997; Fairman et al., 1995; Wadiche et al., 1995) as well as gated by just extracellular Na^+ (Bergles and Jahr, 1997; Otis et al., 1997; Wadiche and Kavanaugh, 1998). Extracellular binding of Na^+ is apparent in the absence of L-Glu (Wadiche et al., 1995), and a recent crystal structure supports sites thought to be occupied by Na^+ before L-Glu binds (Boudker et al., 2007). Our data suggest that either extracellular Na^+ or K^+ can occupy one of these sites and gate the uncoupled anion conductance (Figure 3.1-3.4). The anion conductance seen with extracellular $TRIS^+$ suggests that an additional cation binding site exists on the intracellular side of the membrane that can be occupied by either K^+ or Na^+. It is not known if this K^+ is related at all to the K^+ that is countertransported during coupled transport of L-Glu (Zerangue and Kavanaugh, 1996). The high concentration of K^+ intracellular and high concentration of Na^+ extracellular under physiological conditions suggests this anion conductance is consistently passing Cl^- within the resting cell.

With KNO_3 or NaSCN based intracellular solutions, we saw a left-shift in the reversal potential from the expected Nernst equation prediction of 56 mV for NO_3^- and 110 mV for SCN^-. This would suggest that 1) K^+ or Na^+ intracellular gates a transporter associated conductance carried by ions different or in addition to the anion conductance, which thus shifts the reversal potentials (Kanai et al., 1995; Vandenberg et al., 1995) or 2) intracellular Na^+ or K^+ can gate the anion conductance, and the left shift in the reversal potential is merely an error arising from subtracting patches of different experiments, with different seal resistances. In support of the latter, we repeated these experiments with either NO_3^- and SCN^- in separate batches of oocytes, and the reversal potential did not appear to shift in the same direction for both experiments. More convincing, if the current was carried by K^+, the left-shift of the reversal should have only occurred with the K^+ based extracellular solution and not for the $TRIS^+$ or Na^+ based extracellular solution (Figure 3.2B). For NaSCN, if Na^+ carried the conductance, an increase in Na^+

extracellular should have shifted the I-V to the right and not to the left as was observed in figure 3.3C.

The amplitude of the anion conductance gated by Na^+ has always been described by the conductance blocked by inhibitors plus Na^+. By defining cations that gate the anion conductance from either side of the membrane, we were able to demonstrate that the inhibitor TBOA (200 μM) only slightly blocked the anion conductance on hEAAT1. This revealed a larger baseline anion current associated with the transporter than was initially thought and may expand on our understanding of the anion channels functional role in the resting cells.

References

Arriza JL, Eliasof S, Kavanaugh MP and Amara SG (1997) Excitatory amino acid transporter 5, a retinal glutamate transporter coupled to a chloride conductance. *Proc Natl Acad Sci U S A* **94**(8):4155-4160.

Bergles DE and Jahr CE (1997) Synaptic activation of glutamate transporters in hippocampal astrocytes. *Neuron* **19**(6):1297-1308.

Bergles DE, Tzingounis AV and Jahr CE (2002) Comparison of coupled and uncoupled currents during glutamate uptake by GLT-1 transporters. *J Neurosci* **22**(23):10153-10162.

Boudker O, Ryan RM, Yernool D, Shimamoto K and Gouaux E (2007) Coupling substrate and ion binding to extracellular gate of a sodium-dependent aspartate transporter. *Nature* **445**(7126):387-393.

Eliasof S and Jahr CE (1996) Retinal glial cell glutamate transporter is coupled to an anionic conductance. *Proc Natl Acad Sci U S A* **93**(9):4153-4158.

Fairman WA, Vandenberg RJ, Arriza JL, Kavanaugh MP and Amara SG (1995) An excitatory amino-acid transporter with properties of a ligand-gated chloride channel. *Nature* **375**(6532):599-603.

Grewer C, Balani P, Weidenfeller C, Bartusel T, Tao Z and Rauen T (2005) Individual subunits of the glutamate transporter EAAC1 homotrimer function independently of each other. *Biochemistry* **44**(35):11913-11923.

Grewer C, Watzke N, Wiessner M and Rauen T (2000) Glutamate translocation of the neuronal glutamate transporter EAAC1 occurs within milliseconds. *Proc Natl Acad Sci U S A* **97**(17):9706-9711.

Herman MA and Jahr CE (2007) Extracellular glutamate concentration in hippocampal slice. *J Neurosci* **27**(36):9736-9741.

Kanai Y, Nussberger S, Romero MF, Boron WF, Hebert SC and Hediger MA (1995) Electrogenic properties of the epithelial and neuronal high affinity glutamate transporter. *J Biol Chem* **270**(28):16561-16568.

Koch HP, Brown RL and Larsson HP (2007) The glutamate-activated anion conductance in excitatory amino acid transporters is gated independently by the individual subunits. *J Neurosci* **27**(11):2943-2947.

Leary GP, Stone EF, Holley DC and Kavanaugh MP (2007) The glutamate and chloride permeation pathways are colocalized in individual neuronal glutamate transporter subunits. *J Neurosci* **27**(11):2938-2942.

Otis TS, Kavanaugh MP and Jahr CE (1997) Postsynaptic glutamate transport at the climbing fiber-Purkinje cell synapse. *Science* **277**(5331):1515-1518.

Ryan RM and Mindell JA (2007) The uncoupled chloride conductance of a bacterial glutamate transporter homolog. *Nat Struct Mol Biol* **14**(5):365-371.

Vandenberg RJ, Arriza JL, Amara SG and Kavanaugh MP (1995) Constitutive ion fluxes and substrate binding domains of human glutamate transporters. *J Biol Chem* **270**(30):17668-17671.

Veruki ML, Morkve SH and Hartveit E (2006) Activation of a presynaptic glutamate transporter regulates synaptic transmission through electrical signaling. *Nat Neurosci* **9**(11):1388-1396.

Wadiche JI, Amara SG and Kavanaugh MP (1995) Ion fluxes associated with excitatory amino acid transport. *Neuron* **15**(3):721-728.

Wadiche JI and Kavanaugh MP (1998) Macroscopic and microscopic properties of a cloned glutamate transporter/chloride channel. *J Neurosci* **18**(19):7650-7661.

Wersinger E, Schwab Y, Sahel JA, Rendon A, Pow DV, Picaud S and Roux MJ (2006) The glutamate transporter EAAT5 works as a presynaptic receptor in mouse rod bipolar cells. *J Physiol* **577**(Pt 1):221-234.

Yernool D, Boudker O, Jin Y and Gouaux E (2004) Structure of a glutamate transporter homologue from Pyrococcus horikoshii. *Nature* **431**(7010):811-818.

Zerangue N and Kavanaugh MP (1996) Flux coupling in a neuronal glutamate transporter. *Nature* **383**(6601):634-637.

CHAPTER 4: MICROSCOPIC RATE ANALYSIS OF THE NOVEL GLUTAMATE TRANSPORTER BLOCKER 2-FAA REVEALS COMPLEX UNBINDING KINETICS

G.P. Leary, D.C. Holley, E.F. Stone, B.R. Lyda, C.S. Esslinger, and M.P. Kavanaugh

Introduction

The excitatory amino acid transporters (hEAAT1, hEAAT2, hEAAT3, hEAAT4, and hEAAT5) are secondary active transporters that are prominently known for terminating excitatory synaptic transmission within the CNS by removing L-Glu from the extracellular space. Functionally, the hEAATs move L-Glu against its concentration by coupling transport to the sodium, potassium, and proton gradients with a stochiometric influx of 3Na, 1H+, and 1 L-Glu coupled to the countertransport of 1 K+ (Levy et al., 1998; Zerangue and Kavanaugh, 1996). A crystal structure of a homologous archael transporter from *Pyrococcus horikoshii* reveals a bowl shaped trimer of three identical subunits with individual binding sites located within each subunit. The three wedge-shaped subunits allow for a deep basin that permeates 30 Å into the membrane bilayer. The basin is lined with hydrophobic residues and thought to be water filled with a volume of 400 $Å^3$ (Yernool et al., 2004). Structurally, the water filled basin has been suggested to decrease the energy barrier of transporting substrates across a lipid bilayer by providing a water filled cavity that expands beyond the 1^{st} leaflet of the bilayer (Gouaux and Mackinnon, 2005). In addition, the basin has been described as a "waiting area" for transported solutes allowing easy access to binding sites located within the bilayer (Kavanaugh, 2004; Yernool et al., 2004). These explanation act to propose testable hypothesize, and emphasize a that deficit exists in our understanding of how the architecture revealed through X-ray crystallography maps to the function of these membrane transporters.

2-β-fluorenyl-aspartylamide ((S)-4-(9H-fluoren-2-ylamino)-2-amino-4-oxobutanoic acid; 2-FAA) (Figure 4.1A) is a novel, low nanomolar, non-transportable substrate for the hEAATs with a reported 5-10 fold selectivity for hEAAT3; it has recently been suggested for the use in treatment for schizophrenia (Dunlop, 2006). The molecule has an asparagine backbone with a fluorinyl ring extended from the amino side chain. The molecular design follows that of L-aspartate-β-hydroxamate (Bridges et al., 1999), and

the addition of the hydrophobic ring drastically increases the potency for all hEAATs but also the selectivity seen at hEAAT3. Measuring microscopic rate constants for an inhibitor offers the advantage of delineating the binding interactions from the dissociation interactions between the molecule and a protein in addition to offering an accurate estimate of the K_i. Previously, studying reaction rates has been used to determine the microscopic rate constants (k_{on} and k_{off}) for many agonists and antagonists and often requires patch clamping in combination with a fast flow perfusion device (Benveniste et al., 1990; Jones et al., 1998; Otis and Kavanaugh, 2000; Wadiche and Kavanaugh, 1998). It is the purpose of this article to demonstrate how two-electrode voltage clamp (TEVC) of *Xenopus laevis* oocytes can be used to determine the K_i of 2-FAA by studying the reaction rates as opposed to the steady states equilibriums. In measuring the blocking rate and recovery from block rate, we conclude that the selectivity of 2-FAA for hEAAT3 is a result of a slower dissociation rate compared to hEAAT2 and hEAAT1, with no differences in binding rates. In addition, the recovery from block of 2-FAA is about 3 times faster in the presence of L-Glu, and this acceleration is also induced by incorporation of non-functional subunits into the trimer. This supports the idea that the quaternary structure of the transporter (the water filled basin) effectively restricts diffusion, thus changing the apparent off-rate of bound blocker.

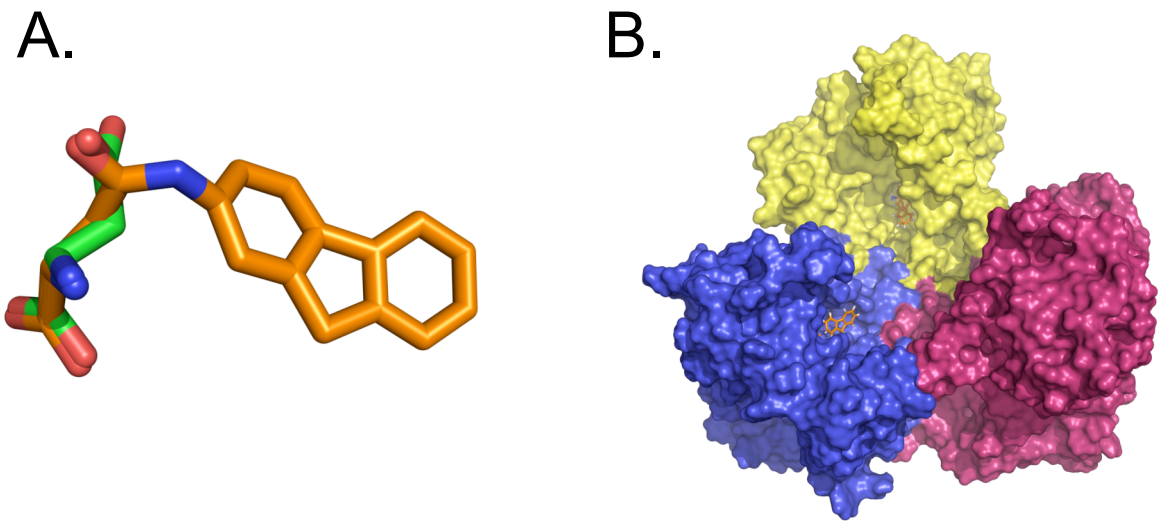

Figure 4.1: **A.** An overlay of 2FAA (orange) with L-aspartate (green). **B.** An hEAAT3 homology model threaded through Gltph (2NWW.pdb) using the SWISS-MODEL homology modeling server. 2FAA is positioned on the backbone of TBOA and optimized using the SYBYL force field (Tripos SYBYL 7.3). The structure was visualized using PyMol version 0.99.

Experimental Methods

Electrophysiology. Human brain glutamate transporter EAAT1, EAAT2, and EAAT3 cRNA were expressed in stage V-VI *Xenopus* oocytes. For mutant transporters coexpressed with wildtype, proportional linearized DNA was combined and then transcribed to RNA. Coexpressed oocytes demonstrated currents upon L-Glu or L-Ala application proportional to the expected dilution ratio. Recording solution (frog Ringer) contained 96mM NaCl, 2mM KCl, 1mM $MgCl_2$, 1.8mM $CaCl_2$, and 5mM HEPES (pH7.4). Microelectrodes were pulled to a resistance between 1 MΩ and 3 MΩ and filled with 3M KCl. Data was recorded with power lab 2/20 (AD instruments) interfaced with a G4 powerbook using Chart v5.0.1 software. Na-dependent charge movements were recorded with a Digidata 1200 (axon instruments) interfaced with Pentium 1 PC,ß and settings for measuring the Na-dependent charge movements were the same as reported in (Wadiche et al., 1995) except for our voltage jump was from -80 mV to 20mV. Data was analyzed offline with Axograph X (v1.0.8) and Kaleidagraph (v3.6).

Solution was perfused over the eggs at rapid rates (16-20 mL/min). Exchange of the bath was estimated by fitting the wash in and wash out of 3 μM L-Glu to single exponentials. Time constants for the bath exchange were between 2-5 seconds. Concentrations for the blocking rate were excluded if the time constant to block was less than 1/10 the bath exchange; this was observed for higher concentrations of 2-FAA. Specialized chambers were designed to decrease the volume and increase the laminar flow over the oocyte. The chamber had dimensions of 3 mM width, 3 mM depth, and 20 mM length.

The structure of 2-FAA was modeled using Tripos SYBYL7.3. Docking in was performed using the Tripos force field using simulated annealing molecular dynamics in SYBYL7.3, (2000 fs, 300 K). The structures were visualized using PyMol0.99.

Anylitical modeling of 2-FAA's competitive inhibition.

Modeling the reactions using the Law of Mass Action, we derived ordinary differential equations (ODEs) that could be solved for the decay constants observed in the experiment in terms of microscopic on/off rates. For the first stage in the reaction, the binding of glutamate, the reaction mechanism is presumed to be

$$T + G \rightleftharpoons C \rightarrow T + G_{in}$$

Where we label the binding rate k_1, the unbinding rate k_{-1}, and the transfer rate k_t. Following standard techniques (see appendix) we derived ODEs for the time dependent concentrations of *T, G, C*. These we denote by *C(t), G(t), T(t)*. If the concentration of glutamate is taken to be a constant, $\bar{G}$, the closed form solution for *C(t)* was found to be

$$C(t) = K(1 - e^{\gamma 1 t})$$

where $K = \frac{k_1 T_0 \bar{G}}{\gamma_1}$, and $\gamma_1 = k_1 \bar{G} - k_{-1} + k_t$. T_0 is the total concentration of transporters and appears only as a scaling factor. The decay constant for this phase of the reaction is clearly γ_1, as expected. The concentration of *C* tends to the equilibrium value *K* over long times.

The second stage of the reaction, in which the blocker molecule 2-FAA is added, can be modeled in the same way. The reaction mechanism is

$$T + B \rightleftharpoons D$$

where now we label the binding rate k_2, and the unbinding rate k_{-2}. For this stage both glutamate and drug concentration are assumed to be fixed at $\bar{G}$ and $\bar{B}$ respectively. The concentrations of the complexes *C(t)*, *D(t)*, evolve over time to another set of equilibrium values with decay rates given by

$$\lambda_+ = -\frac{\gamma_1 + \gamma_2}{2} \pm \frac{\sqrt{(\gamma_1 - \gamma_2)^2 + 4k_1 k_2}}{2}$$

where $\gamma_1 = k_{-1} + k_t + k_1 \bar{G}$, $\gamma_2 = k_{-2} + k_2 \bar{B}$, $\bar{k}_1 = k_1 \bar{G}$, $\bar{k}_2 = k_2 \bar{B}$. We observe that since the rates $\gamma_1 >> \gamma_2$, and that $\gamma_1 >> 4\bar{k}_1 k_2$, the two decay rates are approximately $\lambda_- = -\gamma_1$; $\lambda_+ = -\gamma_2$.

The fast rate γ_1, is determined by the rates at which glutamate is transferred, and the much slower rate γ_2, is what will be observed in the experiment, and follows the first order approximation form of

$$\gamma_2 = k_{-2} + k_2 \bar{B}$$

If the exponent is fit from the experiment as the concentration of the drug is varied, it should follow a linear dependence on that concentration, with slope k_2 and y intercept of k_{-2}.

The third stage of the reaction is the drug wash-off and this is modeled with the same equations as the second stage, except that now the concentration of the free drug is taken to be zero, and unchanging. In this case the resulting ODEs have exact solutions again, and the concentration *C(t)* is found to be

$$C(t) = \bar{C}e^{-\gamma_1 t} + \frac{k_1 \bar{G}\bar{C}}{k_{-2} - \gamma_1}(e^{-k_{-2}t} - e^{-\gamma_1 t}) + K(1 - e^{-\gamma_1 t})$$

where $\bar{C}$ is the equilibrium value from the second stage, and *K* is the equilibrium value for the complex in the absence of drug, computed for the first stage of the reaction. At the start of the reaction *(t=0)* the complex concentration equals $\bar{C}$, and in the long term evolves to *K*. There are again two distinct decay rates, γ_1 and k_{-2}. The off rate of the drug is orders of magnitude slower than γ_1, so it will be the rate observed in this stage of the experiment, and it does not depend upon the concentration of glutamate.

Results

Measuring the microscopic rate constants for 2-FAA with a two-electrode voltage clamp

Application of 10 μM L-Glu to oocytes injected with cRNA for hEAAT3 results in an inward current that rapidly reaches steady state (Figure 4.2A). Co-application of 10 μM L-Glu with 20 nM 2-FAA (Figure 4.2B) produces a rapid inward current followed by a slow block to a new steady state, suggesting L-Glu binds to the transporter and induces a current much faster than the block by 2-FAA. An identical fractional block of the L-

Glu current is observed when the oocyte is first equilibrated with 20 nM 2-FAA (Figure 4.2C).

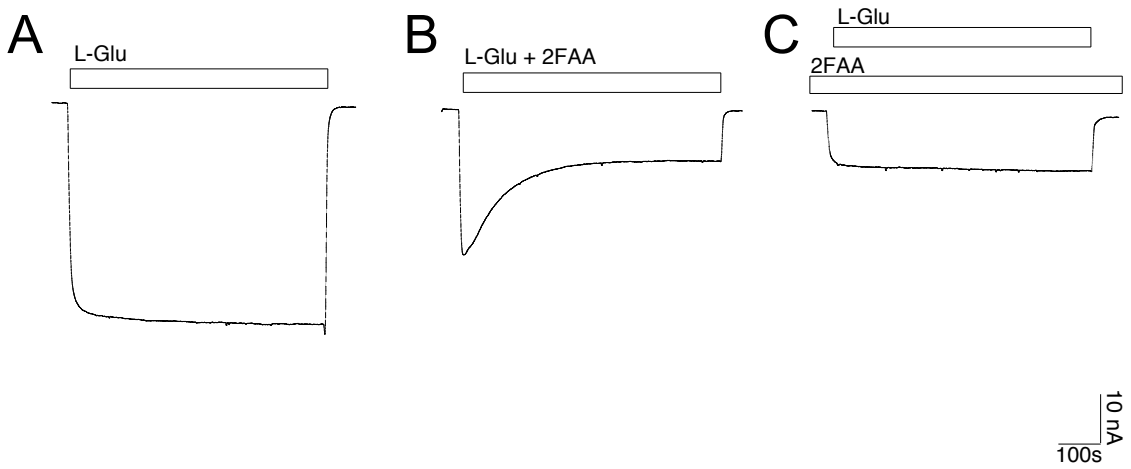

Figure 4.2: The slow blocking kinetics of 2FAA relative to L-Glu in oocytes expressing hEAAT3. A. Application of 10 μM L-Glu causes an inward current with fast wash in and wash out kinetics (-40 mV). **B.** Co-application of 10 μM L-Glu with 20 nM 2FAA (-40 mV) results in a fast inward current with a slow decay to steady state. **C.** Application of 10 μM L-Glu with 20nM 2FAA already at equilibrium (-40 mV) results in a fractional block equal to that seen at steady state in B.

Repeated application of 2-FAA changed V_{max} and prevented us from completing a full Schild analysis. However, increasing L-Glu could recover the V_{max} at different 2-FAA concentrations within the same hour, suggesting that 2-FAA acts as a competitive inhibitor of the EAATs (data not shown). At high concentrations 2-FAA (1-10 μM) induced inward currents in both injected and un-injected oocytes.

We considered an alternative approach to estimating the K_i by studying the rates of block and recovery from block for 2-FAA (Figure 4.3A). The slow kinetics associated with the block by 2-FAA (Figure 4.2B) allowed us to use two-electrode voltage clamp of *Xenopus* oocytes to resolve the microscopic rate constants for 2-FAA with hEAAT3. A competitive inhibitor for the EAATs can be described by the simple reaction mechanism below:

$$T_o + G \underset{k_{off}}{\overset{k_{on}}{\rightleftharpoons}} C \xrightarrow{k_{trans}} T_o + G_i$$

$$T_o + B \underset{k_{off}}{\overset{k_{on}}{\rightleftharpoons}} D$$

Reaction mechanism 1

where T_o is the transporter facing the extracellular milieu, G is L-Glu, C is the transporter bound with L-Glu, G_i is L-Glu after being translocated into the cell, B is the competitive inhibitor 2-FAA, and D is the transporter bound with the inhibitor. For glutamate, the microscopic rates have been measured to be $k_{on} = 6.8 \times 10^6\ M^{-1}s^{-1}$, $k_{off} = 44\ s^{-1}$, and $k_{transport} = 15\ s^{-1}$ (Wadiche et al., 1995; Wadiche and Kavanaugh, 1998). In general, application of a substrate or an inhibitor under voltage clamp will produce a square current waveform if the kinetics of binding and unbinding of the molecule are faster than the solution exchange. This is apparent for application of 3 μM L-Glu (Figure 4.3A and 3B, inverted 3 μM L-Glu current recording) where the current time course represents the limiting rate of the bath exchange. With the substrate in equilibrium, application of an inhibitor will shift the response to a new equilibrium that will depend on the rates for the binding and unbinding of the substrate and inhibitor, transport of the substrate, the concentrations of both substrate and inhibitor, and the solution exchange (Benveniste et al., 1990). It is apparent in figure 4.3B that the time constant for the solution exchange (inverted 3 μM L-Glu current, 4.5 s) is much faster than that for the time constant for block of 10nM 2-FAA (215 s). To limit any error associated with the solution exchange, we only made rate calculations in which the time constant of the solution exchange was less than 1/10 the blocking time constant of 2-FAA. We minimized the bath exchange (τ = 2-5 s) by creating a narrow, shallow chamber (3 x 3 x 20 mM) to increase the linear flow and decrease the volume of solution. A vertical flow oocyte chamber has also been designed with bath exchange rates documented below 100 ms that could increase the resolution of this technique (Baburin et al., 2006).

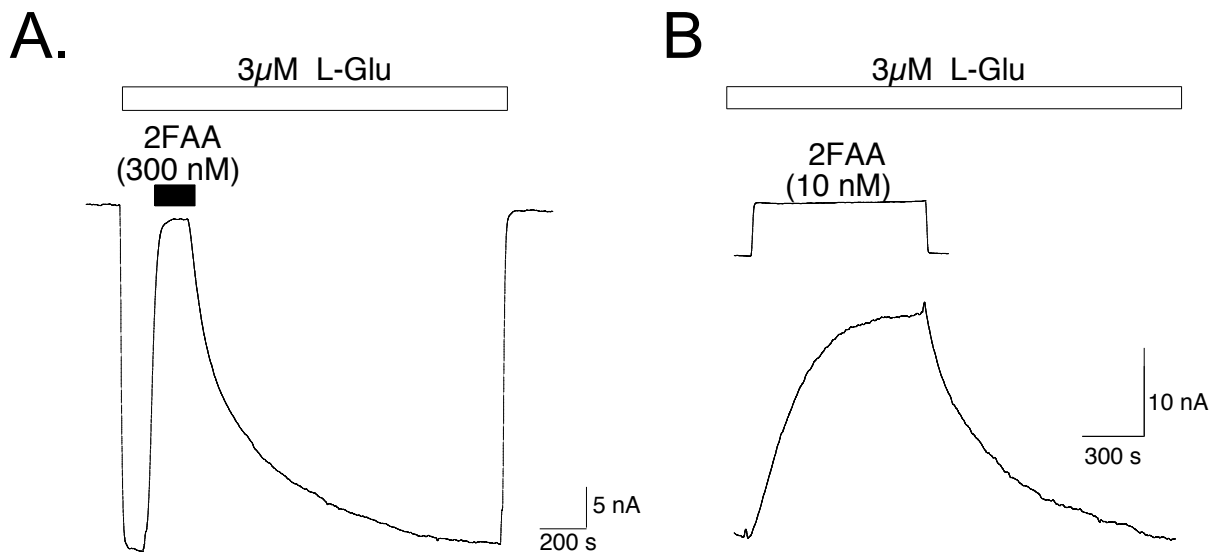

Figure 4.3: Effects of 2FAA on steady-state glutamate transport currents in hEAAT3. A. A representative experiment illustrating the block and the recovery from block of the steady-state 3 μM L-Glu current by 2FAA (300 nM; Vm = -60mV). **B.** Onset and offset of block by 800 sec application of 10 nM 2FAA. Solution exchange kinetics (monitored with a 3 μM L-Glu pulse for 800 sec) shown inverted above.

Assessing the Blocking kinetics of 2-FAA on hEAAT3 in the presence of L-Glu.

Using the law of mass action, we derived ordinary differential equations for each component in *reaction mechanism 1*. Knowing the microscopic rates of binding, unbinding, and transport of L-Glu for the EAATs and the rates of block and dissociation for 2-FAA, we were able to determine by modeling that the binding, unbinding, and transport of L-Glu would be too fast to effect the measured blocking and recovery rate of the drug (see methods). Because the time course almost completely depends on the rate limiting time constant, (2-FAA) binding and unbinding, we can simplify the relationship for the blocking rate as a function of the inhibitor concentration:

$$Y = k_{on}[NBI59159] + k_{off}$$

Equation 1

The blocking rate (Y) has a linear relationship to the concentration of 2-FAA with a slope equal to k_{on} of 2-FAA and the y-intercept equal to the k_{off} of 2-FAA. Figure 4.4A shows a representative experiment measuring the blocking rate of a 3 μM L-Glu current with varying concentrations of 2-FAA. A single exponential relationship (red line) fits the blocking rate data well. At higher concentrations of 2-FAA (300, 1000, and 3000 nM), the blocking rate plateaus around 0.33 s^{-1} (data not shown). As mentioned before, the solution exchange (2-5 s) becomes the limiting factor at higher concentrations of 2-FAA and agrees with the rate at the plateau. A linear regression on the 3, 10, and 30 nM blocking rate measurements (Figure 4.4B) gives an estimate of the k_{on} of 4.39 +/- 0.75 x 10^5 M^{-1} s^{-1} and the k_{off} of 0.0038 +/- 0.0007 s^{-1}. This confirms the assumptions in Figure 4.2 that the kinetics for 2-FAA binding to hEAAT3 are an order of magnitude slower than L-Glu (6.8 x 10^6 M^{-1} s^{-1}). The K_i calculated from the microscopic rate constants for hEAAT3 (k_{off}/k_{on}) is 8.4 +/- .4 nM.

Considering *Reaction mechanism 1*, a rapid washout of drug would remove any chemical energy driving the reaction forward and thus result in an single exponential recovery from the block of 2-FAA that depends only on the k_{off}, a rate that is intrinsic to the drug/protein interaction. This rate will be independent of the initial concentration of drug used to reach the steady state block. Figure 4.4B (squares) shows that the recovery from block rate does not vary with the 10, 30, and 100 nM (not shown) concentration of 2-FAA. As mentioned previously, higher concentrations of drug result in slower dissociation rates of the drug (300 – 10,000 nM). The k_{off} estimates from the y-intercept (0.0038 +/- 0.0007) corresponds well to the average rate of recovery from block (0.004 +/- 0.0002).

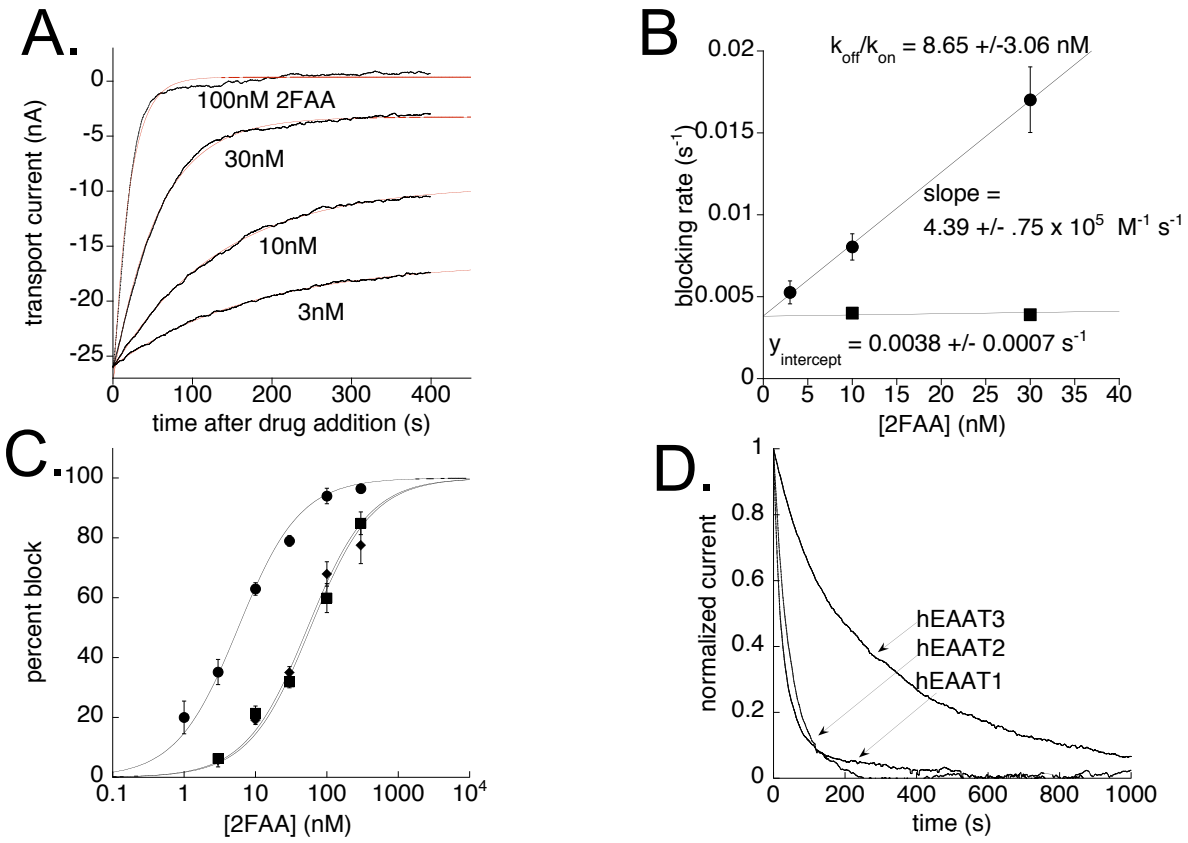

Figure 4.4: The microscopic kinetics of 2FAA on hEAAT3 measured using L-Glu induced transporter currents. A. Representative traces showing the decay of the steady-state transport current induced by 3 µM L-Glu following a jump into 3, 10, 30, and 100 nM 2FAA (-60 mV). **B.** Linear regression of the blocking rates of the 3 µM L-Glu transporter current (like from Fig 4A) reveals a slope of 4.39 +/- .75 x 10^5 $M^{-1}s^{-1}$ (circles) and a y-intercept of 0.0038 +/- 0.0007 s^{-1}. The recovery from block rate (like from 4D) for hEAAT3 is independent of the concentration of 2FAA at 10, 30, and 100 nM (squares_100 nM not shown). **C.** The steady state block of 2FAA for the 3 µM L-Glu current: hEAAT1 (diamonds; IC_{50} = 53.7 +/- 6.1 nM), hEAAT2 (squares; IC_{50} = 59.0 +/- 6.3 nM), and hEAAT3 (circles; IC_{50} = 5.7 +/- .5 nM) (-60 mV). **D.** Representative traces showing the recovery of the steady state transport current from block of 2FAA for hEAAT1 (0.031 s^{-1} +/- 0.002), hEAAT2 (0.028 s^{-1} +/- 0.003), and hEAAT3 (0.0040 s^{-1} +/- 0.0002).

The selectivity of 2-FAA for hEAAT3

2-FAA has been shown to have a higher potency for hEAAT3 than hEAAT2 or hEAAT1 (Dunlop and Butera, 2006). The K_i estimates taken from a Cheng-Prusoff conversion of the IC_{50} (Figure 4.4C) are hEAAT1 (54 +/- 6 nM), hEAAT2 (59 +/- 6 nM),

and hEAAT3 (6 +/- 1 nM). It was possible to measure the rate of recovery from block for hEAAT1 and hEAAT2, but the blocking rate measurements were limited by the solution exchange. Figure 4.4D shows representative traces of the recovery from block of a 3 μM L-Glu current for hEAAT1 (0.031 +/- 0.002 s^{-1}), hEAAT2 (0.028 +/- 0.003 s^{-1}), and hEAAT3 (0.004 +/- 0.0002 s^{-1}). We back calculated the k_{on} using the relationship

$$K_i = k_{off} / k_{on}$$

with K_i estimates from the Cheng-Prusoff conversion of the IC50's and the k_{off} from the recovery from block for hEAAT1 (6 +/- 1 x 10^5 M^{-1} s^{-1}), hEAAT2 (5 +/- 1 x 10^5 M^{-1} s^{-1}), and hEAAT3 (7 +/- 1 x 10^5 M^{-1} s^{-1}). This is in close agreement with those measured from the blocking rate and demonstrates that the selectivity for hEAAT3 is primarily a result of a slower dissociation rate of the drug and not an initial binding discrimination.

Assessing the Blocking kinetics of 2-FAA on hEAAT3 in the absence of L-Glu.

Transient Na^+ charge movements blocked by kainate or TBOA have been described for the EAATs (Larsson et al., 2004; Wadiche et al., 1995; Watzke et al., 2001). To determine the microscopic rate constants for 2-FAA in the absence of L-Glu, we measured the blocking rate and the rate of recovery from block for the Na-dependent charge movements by performing voltage jumps from -80 mV to +20 mV (Figure 4.5A *inset left*). Time integrals of transient currents blocked by the drug at onset (Q_{on}) and offset (Q_{off}) of voltage jumps showed conservation of charge (Figure 4.5A *inset right*). The concentration dependence of the blocking rate (Figure 4.5A) has a linear relationship (Figure 4.5B). The k_{on} from the slope (3.85 +/- 0.59 x 10^5 M^{-1} s^{-1}) was not different from that observed in the presence of L-Glu (Figure 4.4B), but a large difference was observed for the k_{off} at the y-intercept (0.0012 +/- 0.0004 s^{-1}). Analyzing the rate of recovery from block of 100 nM 2-FAA (3 min) produced an identical dissociation rate (0.0013 +/- 0.0002 s^{-1}); for comparison, the average recovery from block in the presence (Figure 4.4D, inverted current_closed circles) and absence of L-Glu (Figure 4.4D, Na^+ transients_open circles) are plotted in Figure 4.5C. This result is inconsistent with pseudo first-order unbinding kinetics and suggests a significant probability of drug rebinding subject to competition with glutamate. Similar experiments in holding the oocyte at -20 mV and jumping to -120 mV revealed similar kinetics to those obtained at -80 mV,

suggesting a voltage independent block between -80 mV and -20 mV; this is consistent with with a voltage independent block of kainate (reference). Application of L-Glu (3 – 100 μM) for 270 s following the block of 100 nM 2-FAA accelerates the return of the Na^+-transient currents in a dose dependent manner to fractions seen in the presence of L-Glu at five minutes following washout (Figure 4.5C *inset*). This supports the notion that L-Glu can occupy sites that may be used to rebind 2-FAA.

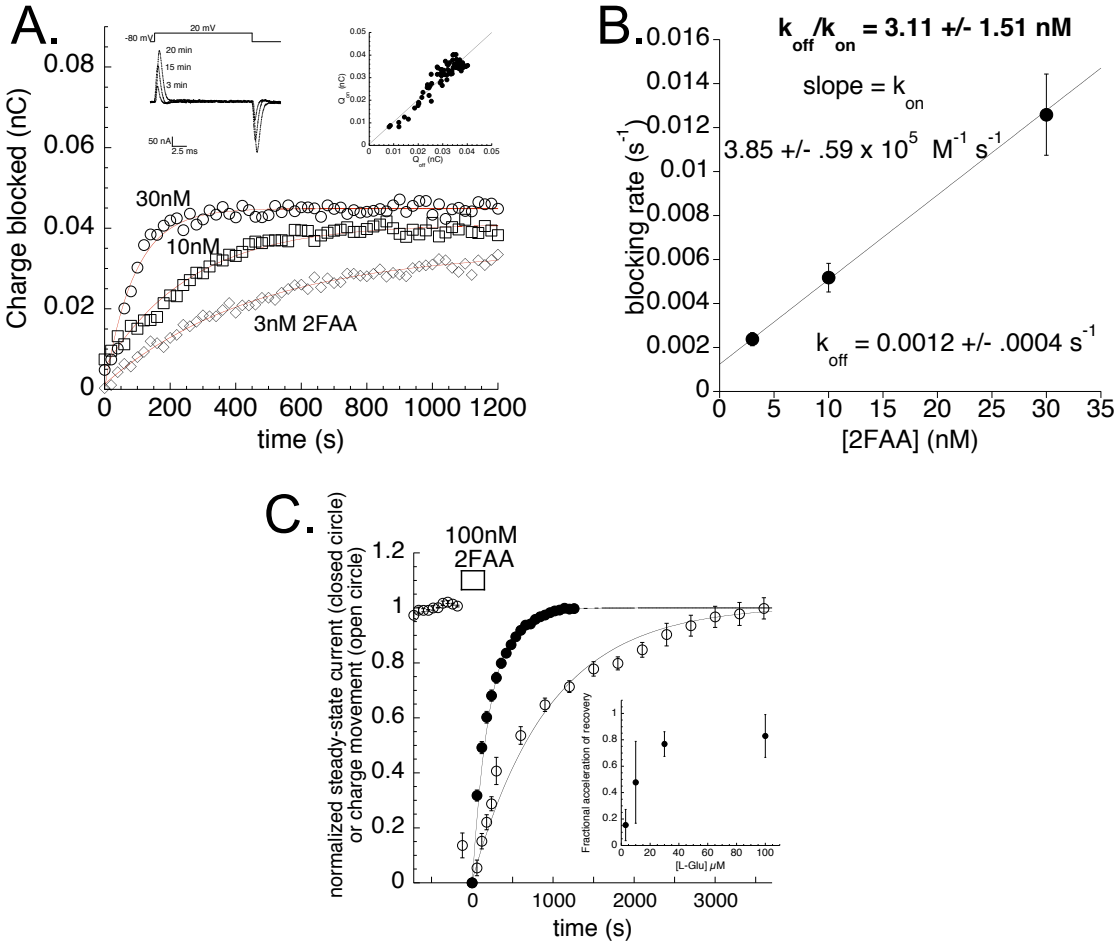

Figure 4.5: The microscopic kinetics of 2FAA measured in the absence of L-Glu using transporter associated Na^+ transient currents. A. The blocking rate of 3, 10, and 30 nM 2FAA on the Na^+-dependent charge movements. *Inset left:* Capacitive transient currents blocked by 10 nM 2FAA at 3, 15, and 20 minutes. *Inset right:* Correlation of the 2FAA sensitive charge movements during on and off pulses demonstrating the conservation of charge movements. **B.** Linear regression of blocking rates of the transient currents in the absence of glutamate by 2FAA yields a slope of 3.85 +/- .59 x 10^5 $M^{-1}s^{-1}$, and reveals a lower apparent k_{off} (0.0012 +/- 0.0004 s^{-1}). **C.** Comparison of the rate of recovery from block by 2FAA in the presence and absence of L-Glu. The Na+-dependent charge movement recovery (open circles (0.0012 s^{-1} +/- 0.0007) is 3.3 times slower than when L-Glu is present (closed circles, inverted average of figure 4D). *Inset:* Application of L-Glu for the first 270 s of the washout of 2FAA speeds the recovery in a concentration-dependent manner (-80 mV).

An alternative approach to prevent the rebinding of 2-FAA within the multimeric complex was to express the hEAAT3 transporter with an excess of hEAAT3 R447C, a mutant that converts the transporter to a neutral amino acid transporter similar to hASCT2 (Grewer et al., 2005; Leary et al., 2007). L-Ala induced currents in hEAAT3 R447C are insensitive to block of 100 nM 2-FAA (Figure 4.6A), and no Na^+-transient currents in this mutant are blocked by 100 nM 2-FAA (Figure 4.6B). We expressed heteromultimers of hEAAT3 and hEAAT3 R447C by injecting cRNA of the respective transporters at a ratio of 1:3. The probability, p(n), of having *n* hEAAT3 subunit within the trimeric complex is:

$$p(3) = .25^3 = 1.5\ \%,\ p(2) = 3*.25^2*.75 = 14.1\ \%,\ p(1) = 3*.25*.75^2 = 42.2\ \%,\ \text{and}\ p(0) = 0.75^3 = 42.2\ \%.$$

The recovery of a 10 μM L-Glu current from 100 nM block of 2-FAA has a recovery rate of 0.0042 +/- 0.0006 (Figure 4.6D), similar to that of hEAAT3 (0.0040 +/- 0.0002; Figure 4.4). However, the recovery rate from 2-FAA block of the Na-charge movements was 0.0033 +/- 0.0006 s^{-1} (Figure 4.6C), which is significantly different from that observed for hEAAT3 (Figure 4.6D). This indicates that the presence of nonfunctional binding sites speeds the apparent dissociation rate of 2-FAA. We propose that the large aqueous central cavity in the trimeric complex (Yernool et al., 2004) may restrict diffusion near the three ligand binding sites, resulting in an effective dissociation rate significantly slower than the true first-order subunit unbinding rate.

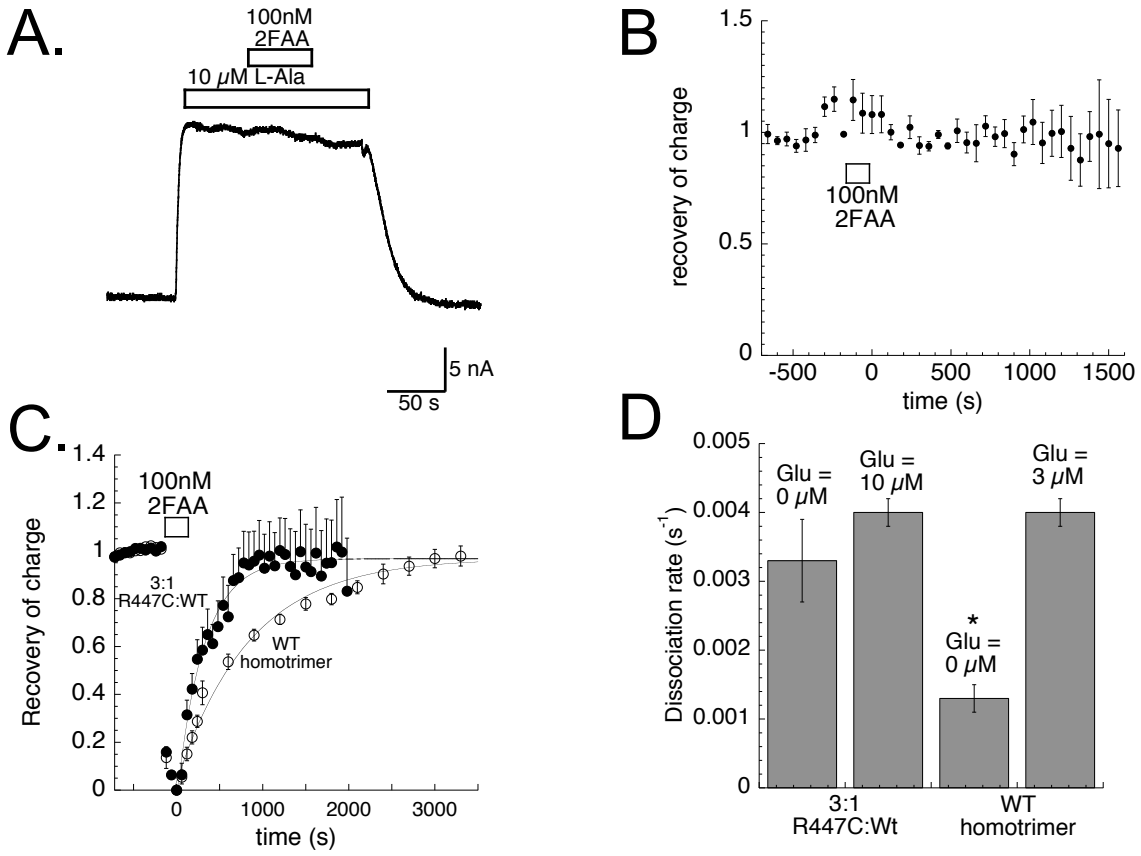

Figure 4.6: Removal of functional binding sites in a subset of subunits within the trimeric complex speeds the apparent off-rate of 2FAA. A. hEAAT3 R447C L-Ala current with 30mM SCN in the bath solution is not blocked by 100 nM 2FAA (-20 mV). **B.** No transient currents are blocked by 100 nM 2FAA in the mutant hEAAT3 R447C. **C.** The recovery from 2FAA (100 nM) block of the Na-dependent charge movements in oocytes co-injected with E3 (WT) and R447C at a ratio 1:3 (closed circles: k_{off} = 0.00327 +/- 0.0006 s^{-1}) compared to hEAAT3 WT (open circles, figure 5C). **D.** Summary of 2FAA recovery rates for WT and 3:1 R447C:WT in the presence and absence of L-Glu (*p < 0.01).

Discussion

It is critical to accurately estimate the block of an antagonist or nontransportable inhibitor. Experimentally, the K_i for an inhibitor is most commonly estimated using the Schild Analysis or derivation from the IC_{50} using the Cheng-Prusoff equation. However, for some very potent drugs, like 2-FAA, the extremely slow dissociation of the drug from the protein results in long periods of time for the system to reach a steady state. This makes accurate measurements at steady state, for either the Schild Analysis or the Cheng-

Prusoff conversion, difficult and possibly inaccurate due to experimental challenges associated with long drug application. For 2-FAA, we found long drug applications resulted in changes of the V_{max}, inward currents from high 2-FAA drug application (3-10 μM) in control and hEAAT 1, 2, or 3 injected oocytes, and longer dissociation rates for hEAAT3 and hEAAT1 with the higher concentrations, which could possibly be associated with 2-FAA depositing in the membrane or entering the cell allowing for a longer apparent k_{off}. We are confident that 2-FAA is still a competitive inhibitor because saturating concentrations of L-Glu can still recover the V_{max}.

An alternative approach to estimate the K_i, used in this paper, is to measure the kinetic blocking and recovery from block rates of 2-FAA. This method has been used previously to estimate the microscopic kinetics for very potent drugs such as ketamine at the NMDA receptor (Mayer et al., 1988), but never has been performed with as simple system as two-electrode voltage clamp of Xenopus oocytes. The advantages to using oocytes offer a simple, inexpensive experimental system with very robust current measurements in the nano-micro ampere range. This method is limited to measurements with very slow dissociation rates but has promising potential with the increasing development of high affinity molecules in the low nanomolar to picomolar range. Further, measuring the individual k_{on} and k_{off} offers information about the interactions between the protein and the molecule not obtainable from steady state measurements.

L-Glu has a k_{on} for the hEAAT2 of 6.8 x 10^6 $M^{-1}s^{-1}$ (Wadiche and Kavanaugh, 1998). For 2-FAA we detected a k_{on} an order of magnitude slower than from that of L-Glu (4.4 x 10^5 $M^{-1}s^{-1}$), which can possibly be reconciled by the large fluorine ring and its highly hydrophobic nature. The estimated on rate is similar for hEAAT1, hEAAT2, and hEAAT3, which supports the idea that the slower on-rate is less the interaction with the protein and more the properties of the molecule. As seen with the selectivity for many drugs at proteins, 2-FAA has a slower dissociation rate on hEAAT3 in comparison to hEAAT2 or hEAAT1; this accounts completely for the 10 fold higher affinity seen in the K_i.

Finally, the apparent dissociation rate for 2-FAA was about 3.3 times lower in the absence of L-Glu when we measured the Na-dependent charge movements. This demonstrates a mechanism that does not follow 1st order unbinding kinetics. When we

applied L-Glu in the washout of 2-FAA measuring the Na-dependent charge movements, the recovery from block was accelerated to rates seen in the presence of glutamate suggesting a competition for the binding site between glutamate and 2-FAA. Structurally, we can possibly consider the large basin as a "holding area" in addition to a "waiting area" that increases the capture efficiency of molecules. Supporting this view, removal of functional binding sites by coexpression of wt hEAAT3 in excess of R447C subunits, a mutant that renders the transporter insensitive to L-Glu binding, also accelerates the apparent off-rate of 2-FAA when measuring the Na-dependent transient currents. Considering that 2-FAA does not block R447C transient currents in oocytes that express R447C alone nor L-ala induce currents in these oocytes, it is likely that the rebinding of 2-FAA within the tirmeric complex accounts for the apparent change in the k_{off}. Physiologically, it is thought that glutamate transporters surrounding synapses buffer glutamate through binding, with a high probability of the molecule unbinding. This large aqueous basin could be a very important structural feature that allows the transporters to not only buffer but capture the L-Glu molecule and prevent it from escaping and activating NMDA or AMPA receptors.

References

Baburin I, Beyl S and Hering S (2006) Automated fast perfusion of Xenopus oocytes for drug screening. *Pflugers Arch* **453**(1):117-123.

Benveniste M, Mienville JM, Sernagor E and Mayer ML (1990) Concentration-jump experiments with NMDA antagonists in mouse cultured hippocampal neurons. *J Neurophysiol* **63**(6):1373-1384.

Bridges RJ, Kavanaugh MP and Chamberlin AR (1999) A pharmacological review of competitive inhibitors and substrates of high-affinity, sodium-dependent glutamate transport in the central nervous system. *Curr Pharm Des* **5**(5):363-379.

Dunlop J (2006) Glutamate-based therapeutic approaches: targeting the glutamate transport system. *Curr Opin Pharmacol* **6**(1):103-107.

Dunlop J and Butera JA (2006) Ligands targeting the excitatory amino acid transporters (EAATs). *Curr Top Med Chem* **6**(17):1897-1906.

Gouaux E and Mackinnon R (2005) Principles of selective ion transport in channels and pumps. *Science* **310**(5753):1461-1465.

Grewer C, Balani P, Weidenfeller C, Bartusel T, Tao Z and Rauen T (2005) Individual subunits of the glutamate transporter EAAC1 homotrimer function independently of each other. *Biochemistry* **44**(35):11913-11923.

Jones MV, Sahara Y, Dzubay JA and Westbrook GL (1998) Defining affinity with the GABAA receptor. *J Neurosci* **18**(21):8590-8604.

Kavanaugh MP (2004) Accessing a transporter structure. *Nature* **431**(7010):752-753.

Larsson HP, Tzingounis AV, Koch HP and Kavanaugh MP (2004) Fluorometric measurements of conformational changes in glutamate transporters. *Proc Natl Acad Sci U S A* **101**(11):3951-3956.

Leary GP, Stone EF, Holley DC and Kavanaugh MP (2007) The glutamate and chloride permeation pathways are colocalized in individual neuronal glutamate transporter subunits. *J Neurosci* **27**(11):2938-2942.

Levy LM, Warr O and Attwell D (1998) Stoichiometry of the glial glutamate transporter GLT-1 expressed inducibly in a Chinese hamster ovary cell line selected for low endogenous Na+-dependent glutamate uptake. *J Neurosci* **18**(23):9620-9628.

Mayer ML, Westbrook GL and Vyklicky L, Jr. (1988) Sites of antagonist action on N-methyl-D-aspartic acid receptors studied using fluctuation analysis and a rapid perfusion technique. *J Neurophysiol* **60**(2):645-663.

Otis TS and Kavanaugh MP (2000) Isolation of current components and partial reaction cycles in the glial glutamate transporter EAAT2. *J Neurosci* **20**(8):2749-2757.

Wadiche JI, Arriza JL, Amara SG and Kavanaugh MP (1995) Kinetics of a human glutamate transporter. *Neuron* **14**(5):1019-1027.

Wadiche JI and Kavanaugh MP (1998) Macroscopic and microscopic properties of a cloned glutamate transporter/chloride channel. *J Neurosci* **18**(19):7650-7661.

Watzke N, Bamberg E and Grewer C (2001) Early intermediates in the transport cycle of the neuronal excitatory amino acid carrier EAAC1. *J Gen Physiol* **117**(6):547-562.

Yernool D, Boudker O, Jin Y and Gouaux E (2004) Structure of a glutamate transporter homologue from Pyrococcus horikoshii. *Nature* **431**(7010):811-818.

Zerangue N and Kavanaugh MP (1996) Flux coupling in a neuronal glutamate transporter. *Nature* **383**(6601):634-637.

CHAPTER 5: DYNAMIC GATE MOTIONS OF HP2 IN THE NEURONAL GLUTAMATE TRANSPORTER EAAT3

G.P. Leary, D.C. Holley, R.C. Darlington, J.B.A. Ross, and M.P. Kavanaugh

Introduction

The human excitatory amino acid transporters (hEAAT1-5) are secondary active transporters that move L-Glutamate against its concentration gradient by stoichiometricly coupling L-Glu to 3 Na^+, H^+, and the countertransport of 1 K^+ (Zerangue and Kavanaugh, 1996). The transporters physiologically maintain a sub-micromole concentration of L-Glu in the extracellular space within the CNS (Herman and Jahr, 2007). An alternating access model of two gates has been a distinguishing feature of protein transport (Jardetzky, 1966; Kavanaugh, 1998; Lauger, 1980). The crystallization of a bacterial homolog (Glt_{ph}) of the hEAATs revealed two hairpin loops, one spanning half the membrane from the intracellular side (HP1) and the second, in close proximity to HP1, spanning half the bilayer from the extracellular face (Yernool et al., 2004). HP1 and HP2 give two physical structures in the glutamate transporter that could regulate this alternating access model.

Though it is suggested the gates for this model can be single amino acids (Miller, 2006), the potential motion of the HP2 loop as a gate was demonstrated in a crystal structure of Glt_{ph} with the competitive, non-transportable inhibitor TBOA bound, which forced HP2 10 Å toward the center of the trimeric complex relative to the 1st crystal structure (Boudker et al., 2007). Whether Glt_{ph} can act as a sufficient model for the hEAATs remains in question, though a FRET based analysis of hEAAT 3 suggested only small scale motions associated with L-Glu transport (Koch and Larsson, 2005). In contrast, recent molecular dynamics has shown substantial movement of HP2 in Glt_{ph} and hEAAT1 that differentially responds to the presence of substrates (Na^+ or L-Glu) and inhibitors (Huang and Tajkhorshid, 2008; Shrivastava et al., 2008). These dynamic motions of HP2 have been further demonstrated by cross-linking of HP2 to HP1, TMD8, TMD7, and TMD2 (Brocke et al., 2002; Leighton et al., 2006; Qu and Kanner, 2008; Ryan et al., 2004).

Cysteine modification of V417C hEAAT3 on HP2 allows for binding of L-Glu and activation of the anion conductance, but prevents substrate transport (Seal et al.,

2001). We defined distinct confirmations of HP2 based on unique accessibility in fluorophore labeling of V417C with TBOA, L-Glu, Na^+, or Choline present. Further, we used voltage clamp fluorometry, a method that takes advantage of the environmental sensitivity of a fluorescent probe, to identify conformational changes in the HP2 loop associated with binding of substrate (Tzingounis et al., 2002). Alexa Fluor 488 C_5 maleimide positioned on the modified V417C HP2 reported large increases in the fluorescence intensity upon binding of L-Glu, which is not observed with TBOA. The change in fluorescence ($\Delta F/F$) upon L-Glu binding increased when neighboring subunits contained a fluorophore, demonstrating the formation of dark fluorophore complexes at the center of the trimer. L-Glu binding relieves this quench by breaking the pi-pi bonds between fluorophores, suggesting the probes on HP2 physically separate and translate away from the central axis of the protein complex. This is in agreement with HP2 being the external gate, closing after L-Glu binds.

Experimental Procedures

Expression and Voltage Clamp Fluorometry with Xenopus laevis oocytes – Cysteine point mutagenesis of V417C was performed with QuikChange Site-Directed Mutagenesis Kit (Stratagene #200521). cRNA was microinjected in stage V-VI oocytes. hEAAT3 V417C mutant transporters were labeled with Alexa Fluor 488 C_5 maleimide (Molecular probes, A-10254). Currents and fluorescence were recorded 3-5 days later as previously described (Larsson et al., 2004; Wadiche et al., 1995b). Recording solution contained 96mM NaCl, 2mM KCl, 1mM $MgCl_2$, 1.8mM $CaCl_2$, and 5mM HEPES (pH7.4). Microelectrodes were filled with 3M KCl and had resistances from 1 to 3 MΩ. Two electrode voltage clamp recordings were performed at 22°-25°C with a Geneclamp 500 interfaced to an IBM-compatible PC using a Digidata 1320 A/D controlled with the pCLAMP 6.0 program suite (Molecular Devices). The currents were low-pass filtered at 1 kHz and digitized at 5 kHz. Data were analyzed offline; modeling and fitting of substrate concentration-dependence of the currents was performed with Kaleidagraph software (v 4.04).

Results

Specific labeling at V417C on HP2 of the neuronal excitatory amino acid transporter 3 (hEAAT3)

To examine possible dynamic gate motions of the HP2 loop, we engineered a cysteine point mutation in hEAAT3 at V417, a residue located at the tip of HP2 (Figure 5.1A). Cysteine modification of this mutant allows glutamate binding, activation of the uncoupled anion conductance, yet prevents transport of substrate (Seal et al., 2001). We repeated these measurements with our mutant to confirm the addition of Alexa Fluor 488 C_5 maleimide prevented radiolabeled uptake on the mutant (figure 5.1B). In addition, following labeling, the reversal potential of current/voltage (IV) relationship shifted near the chloride reversal potential (-12mV +/- Figure 5.1C) demonstrating the current is carried almost completely by the uncoupled anion conductance associated with the transporter (Wadiche et al., 1995a).

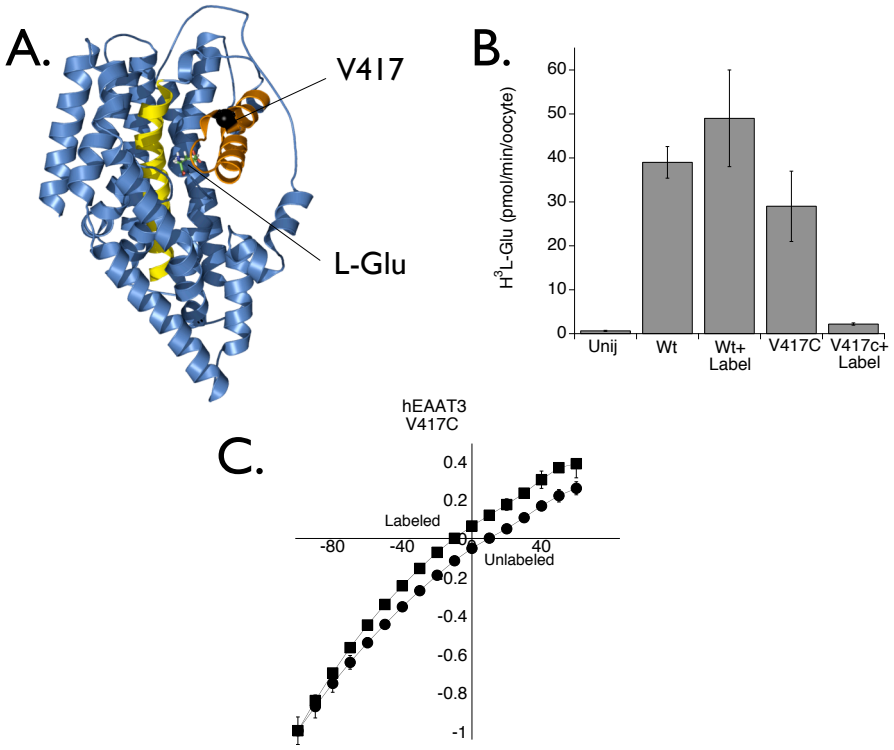

Figure 5.1: Cysteine modification of V417C hEAAT3 on HP2 allows glutamate binding but prevents L-Glu transport. A. An individual subunit of the hEAAT3 structural homology model threaded through the *Pyrococcus horikoshii* Glt_{ph} structure (Yernool et al., 2004) illustrating the location of the V417C point mutation (black sphere) on HP2. **B.** Radiolabel uptake of 10μM [^{3}H]L-Glu verifies modification of V417C with Alexa Fluor 488 C_5 maleimide prevented L-Glu transport (Seal et al., 2001). **C.** A left shift of the V417C current/voltage (IV) relationship following labeling (300μM*min) with Alexa Fluor 488 C_5 maleimide.

A compiled z-stack of confocal images (Figure 5.2A) shows Alexa Fluor 488 C_5 maleimide (300 μM*min) specifically labeled oocytes injected with hEAAT3 V417C and further confirms that the endogenous cysteine residues (C9, C100, C256, C343) in the wildtype (wt) hEAAT3 do not label with this thiol reactive dye. The labeling of V417C saturates and depends on the concentration of probe and time (figure 5.2B). In Figure 5.2C the sequence of hEAAT3 was threaded through the Glt_{ph} crystal structures (2NWX and 2NWW) showing HP2 in the proposed open conformation (Boudker et al., 2007) overlaid with HP2 from closed structure revealing a 10 Å shift of t the HP2 loop (Figure 5.1A) (Yernool et al., 2004). The Alexa Fluor 488 C_5-maleimide was attached *in silico* to V417C in either conformation illustrating the potential distance. The fluorophores chemical structure was minimized within its local environment using SYBYl 8.0.

We measured the accessibility kinetics for the fluorophore labeling at V417C when choline, Na^+, L-Glu, or TBOA were present (Figure 5.2C_choline is a cation replacement for Na that does not interact with the hEAATs). The half maximum labeling is about the same for Na or choline (Na_{50} = 31 μM*min and $Choline_{50}$ = 51 μM*min), suggesting the empty transporter is similar to the Na^+ bound state. When L-Glu or TBOA is present the half maximum labeling concentration decrease by 4 fold ($L\text{-}Glu_{50}$ = 9 μM*min and $TBOA_{50}$ = 11 μM*min). This change suggests dynamic motions of the HP2 loop associated with binding or unbinding of either molecule. This was unexpected considering the crystal structure shows TBOA locking the transporter in an open confirmation similar to the Na^+ bound transporter (Boudker et al., 2007).

Unique HP2 confirmations with L-Glu, Na^+, Choline, and TBOA deciphered with voltage clamp fluorometry

Using voltage clamp fluorometry, we simultaneously measured transporter currents and fluorescent intensity changes associated with HP2. Oocytes were labeled to saturation with Alexa Fluor 488 C_5 maleimide and voltage clamped at -60mV. Neither HP2 nor the transporter interacted with L-Glu in the presence of choline (Figure 5.3A). Transitioning from choline to Na^+ changes both the conductance and fluorescence; this small current change is observed also in uninjected oocytes, but the fluorescence change is unique to V417C hEAAT3 expressing oocytes and is directly a result of Na^+ binding to the transporter. A Hill relationship (n_{hill} = 1.8_-125 mV) describes the Na^+ dependence

of the fluorescence change from choline, supporting at least 2 Na^+ responsible for this motion or rearrangement in the HP2 loop. It is noted that both of these Na^+ atoms may not be the ones directly associated with the coupled conductance during glutamate transport (Koch et al., 2007; Zerangue and Kavanaugh, 1996).

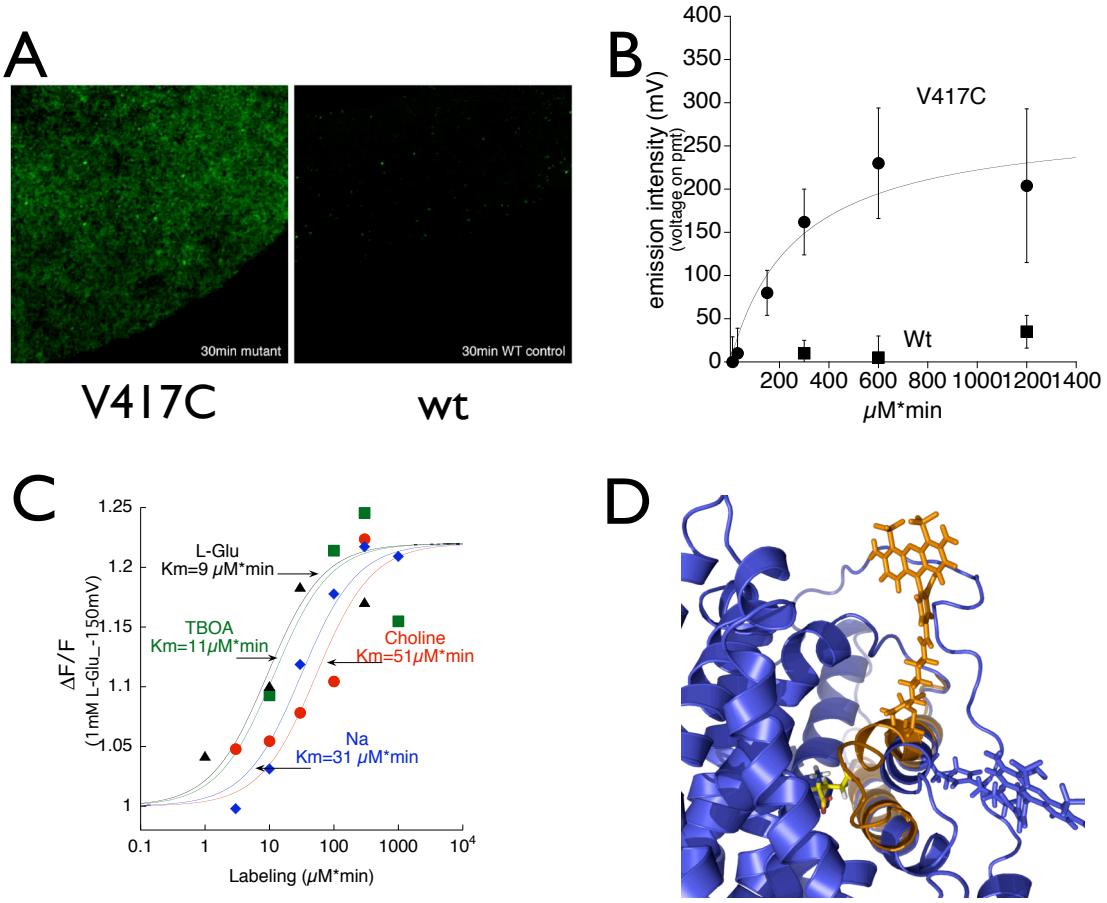

Figure 5.2: Specific labeling of V417C on HP2. **A.** A reconstruction of a z-stack series of confocal images (10x objective) for either V417C (left) or wt EAAT3 (right) labeled with Alexa Fluor 488 C_5 maleimide for 300 μM*min. **B.** Alexa Fluor 488 C_5 maleimide labeling kinetics for V417C compared to wt hEAAT3. **C.** Alexa Fluor 488 C_5 maleimide labeling kinetics for V417C in the presence of Na^+ (Km = 31 μM), choline(Km = 51 μM), Na^+ and 1mM L-Glu(Km = 9μM), or Na^+ and 200 μM TBOA(Km = 11μM). **D.** *In silico* attachment of Alexa Fluor 488 C_5 maleimide to V417C with HP2 in the proposed closed (orange) and open confirmations (blue).

L-Glu application in the presence of Na^+ resulted in a robust increase in fluorescence that directly correlates with the activation of the uncoupled anion conductance (Figure 5.3A). This large intensity change as well as conductance is not seen with the non-transported inhibitor TBOA (100 μM) (Figure 5.3A). The fluorescence intensity change

depended on the concentration L-Glu and has kinetics (Km = 26 µM) similar to the L-Glu activation of the anion conductance (Km= 33 µM) (Figure 5.3C).

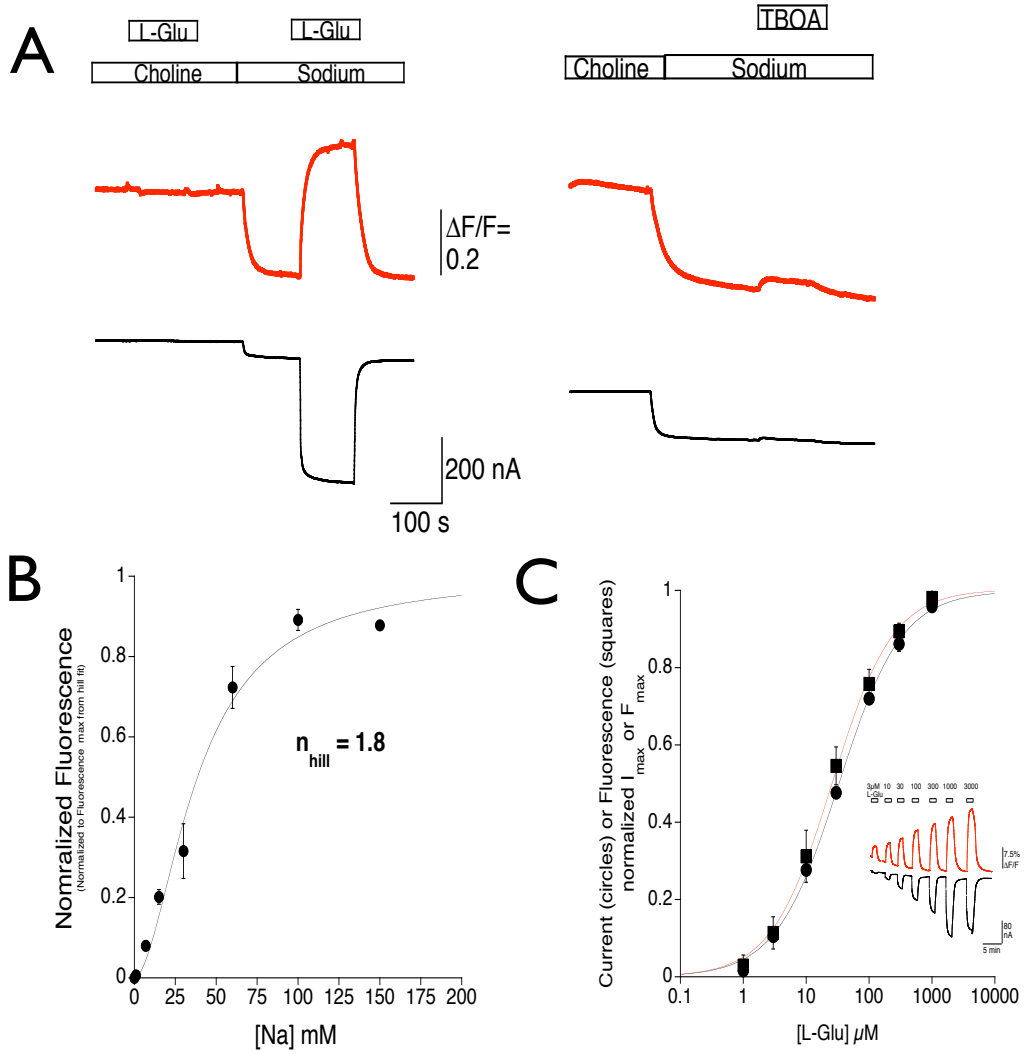

Figure 5.3: Fluorescence changes with external ions and substrate binding under voltage clamp fluorometry

A. Simultaneous fluorescence and current recording from oocytes injected with V417C hEAAT3 and labeled for 300 µM*min with Alexa Fluor 488 C_5 maleimide (-60 mV). **B.** The Na^+ dependence of the fluorescence intensity, from a solution change from choline to different Na^+ concentrations, fits well to a hill equation (Km = 39 mM_n_{hill} = 1.8). **C.** The L-Glu dose response for activation of the uncoupled anion conductance (circle_Km = 33 µM) and for fluorescence intensity change (square_Km = 26 µM). *Inset*: A representative recording showing the L-Glu dependence for the anion channel activation compared to the fluorescence intensity change. **D.** The ΔF/F plotted as a function of voltage with Na^+, 1mM L-Glu, Choline, or 100 µM TBOA present. The Na^+ ($V_{0.5}$ = -45 mV; zδ = 68.7) and choline relationships are fit with $\Delta F / F = \frac{F_{tot}}{1+e^{-z\delta(V-V_{0.5})/kT}} + F_{offset}$, and L-Glu ($V_{0.5}$ = 60 mV; zδ = 93.7) and TBOA ($V_{0.5}$ = 23 mV; zδ = 114.8) relationships are fit with $\Delta F / F = F_{tot} - \frac{F_{tot}}{1+e^{-z\delta(V-V_{0.5})/kT}} + F_{offset}$. Representative traces of the family of fluorescence voltage jumps in Na^+, L-Glu, choline, or TBOA are plotted above, respectively.

Voltage jumps with Na^+, L-Glu, or TBOA reveal fluorescence changes for HP2 that fit well to a Boltzmann distribution, suggesting two unique voltage dependent states assumed by HP2 with these substrates, while choline revealed no intensity changes with voltage (Figure 5.3D). At positive membrane potentials (150 mV or 200 mV), both the fluorescent intensities with Na^+ and L-Glu approached this choline state demonstrating a voltage dependent unbinding for Na^+ and L-Glu (Bergles et al., 2002; Wadiche et al., 1995b). With L-Glu or TBOA bound, the Boltzmann distribution is inverted demonstrating a reorientation of HP2 upon binding distinct from Na^+ bound. TBOA allows for small intensity changes in response to voltage that never approach a choline state; this corresponds with a voltage independent binding and unbinding of inhibitor even at very positive potentials (Wadiche et al., 1995b).

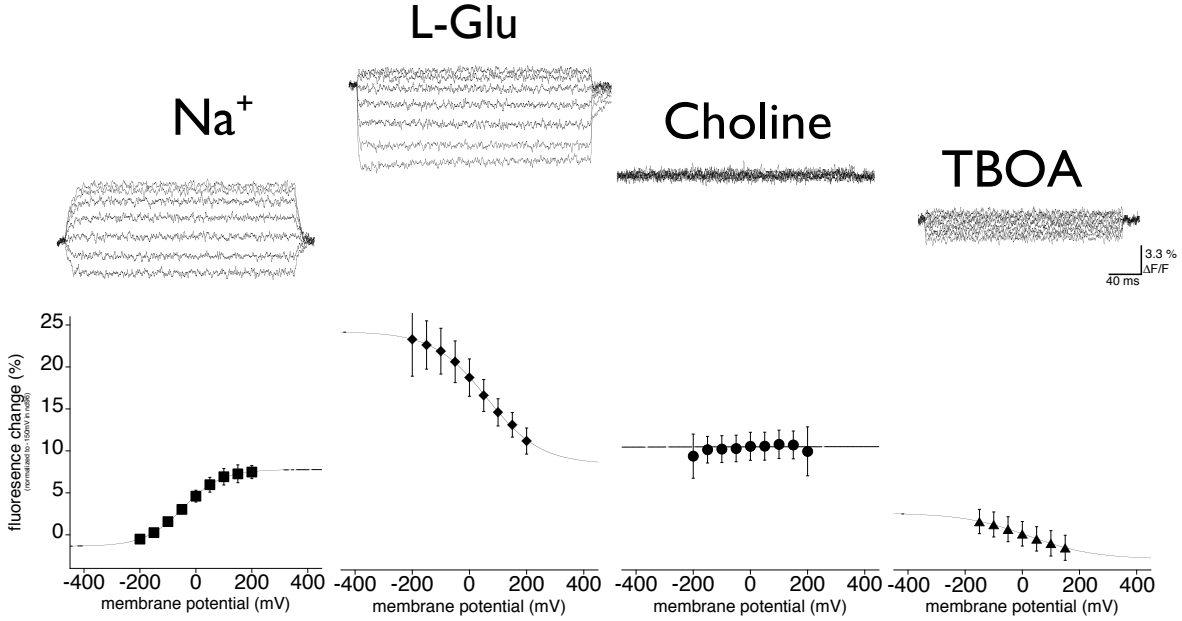

Figure 5.4: Rate analysis of the fluorescence recovery in L-Glu. **A.** A representative experiment showing [L-Glu] increases the fluorescence recovery time following a voltage jump to 150 mV. Fluorescence intensity is baselined at the last 5 ms of the 150 mV jump. **B.** A plot of the recovery rate (1/tau) as a function of the concentration of L-Glu in 100 mM Na^+ (circles) or 30mM Na^+ (squares). A linear regression on the limiting slope (10, 30, 100, and 300 µM L-Glu points) give a slope (k_{on}) = $3.2x10^4$ $M^{-1}s^{-1}$ and a y-intercept (k_{off}) = 2.7 s^{-1}. **C.** The fluorescence recovery time constant for 30, 100, and 1000 µM L-Glu does not depend on the return voltage (between 20 and -100mV) following a voltage jump to -150mV. *Inset:* Representative experiment in 1mM L-Glu showing the recovery from 150 mV voltage jump returning to either -100, -60, -20, or 20 mV.

With L-Glu present, a voltage jump to 150 mV reveals an exponential recovery of the fluorescence upon returning to -70mV. This recovery time constant decreases with

higher concentrations of L-Glu and is effected by the extracellular Na^+ concentration (Figure 5.4A). We consider this recovery to represents the rebinding of L-Glu and Na^+ to the transporter; we do not see these fluorescent tails for TBOA. By varying the holding potential, we demonstrated the binding of L-Glu for 30, 100, and 1000 µM is voltage independent from 20 mV to -100 mV (reference) (Figure 5.4C). Using a rate analysis and fitting a linear regression on the limiting slope (10, 30, 100, 300 µM L-Glu points) showed the microscopic on (slope) and off (y-intercept) rate constants are $k_{on} = 3.2x10^4$ and $k_{off} = 2.68\ s^{-1}$ (Figure 5.4B). This represents a minimum for the binding rate for L-Glu. Both rates are altered substantially compared to estimates for hEAAT3: $k_{on} = 6.8x10^6\ M^{-1}s^{-1}$ and $k_{off} = 300s^{-1}$ (Larsson et al., 2004). However, because both the off and on rate are slower, the K_d estimate, which is the $k_{off}/ k_{on} = 82$ µM, is not that different from the wt hEAAT3, 44 µM.

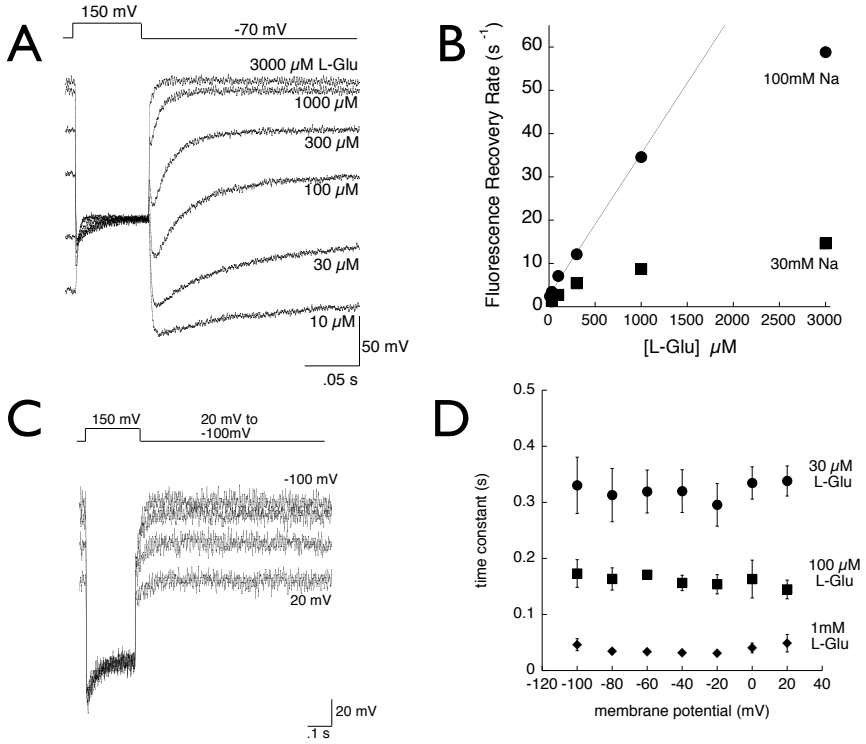

Figure 5.5: Rate analysis of the fluorescence recovery in L-Glu. **A.** A representative experiment showing [L-Glu] increases the fluorescence recovery time following a voltage jump to 150 mV. Fluorescence intensity is baselined at the last 5 ms of the 150 mV jump. **B.** A plot of the recovery rate (1/tau) as a function of the concentration of L-Glu in 100 mM Na^+ (circles) or 30mM Na^+ (squares). A linear regression on the limiting slope (10, 30, 100, and 300 µM L-Glu points) give a slope (k_{on}) = $3.2x10^4$ $M^{-1}s^{-1}$ and a y-intercept (k_{off}) = 2.7 s^{-1}. **C.** The fluorescence recovery time constant for 30, 100, and 1000 µM L-Glu does not depend on the return voltage (between 20 and -100mV) following a voltage jump to -150mV. *Inset:* Representative experiment in 1mM L-Glu showing the recovery from 150 mV voltage jump returning to either -100, -60, -20, or 20 mV.

Fluorescence reports on subunit interactions in hEAAT3 V417C

Unexpectedly, the ΔF/F for 1mM L-Glu increased with labeling (Figure 5.5A). When the V417C hEAAT3 mutant is expressed in excess of wildtype (1:5), the ΔF/F for 1mM L-Glu application does not increase with labeling time. V417C:wt (1:5) has about the same ΔF/F as is seen in the minimally labeled mutant expressed alone (5-10%) (Figure 5.5A_y-intercept). The V417C hEAAT3 mutant labeled to saturation has a large intensity change (25-35 %) upon L-Glu application that depends directly on the presence of fluorophores in neighboring subunits. The interaction of these fluorophores can further be seen by a left shift in the Boltzmann for 1mM L-Glu application with labeling time (Figure 5.5B); interestingly, the Boltzmann for Na^+ is not affected by the labeling time (Figure 5.5C). Figure 5.5D shows the lifetime in Na or Na^+ + L-Glu taken from an oocytes labeled to saturation revealing no change. If L-Glu binding was relieving some type of dynamic quench such as hetero Förster resonance energy transfer (hetero-FRET), a large change in the time constant of the lifetime would have been observed.

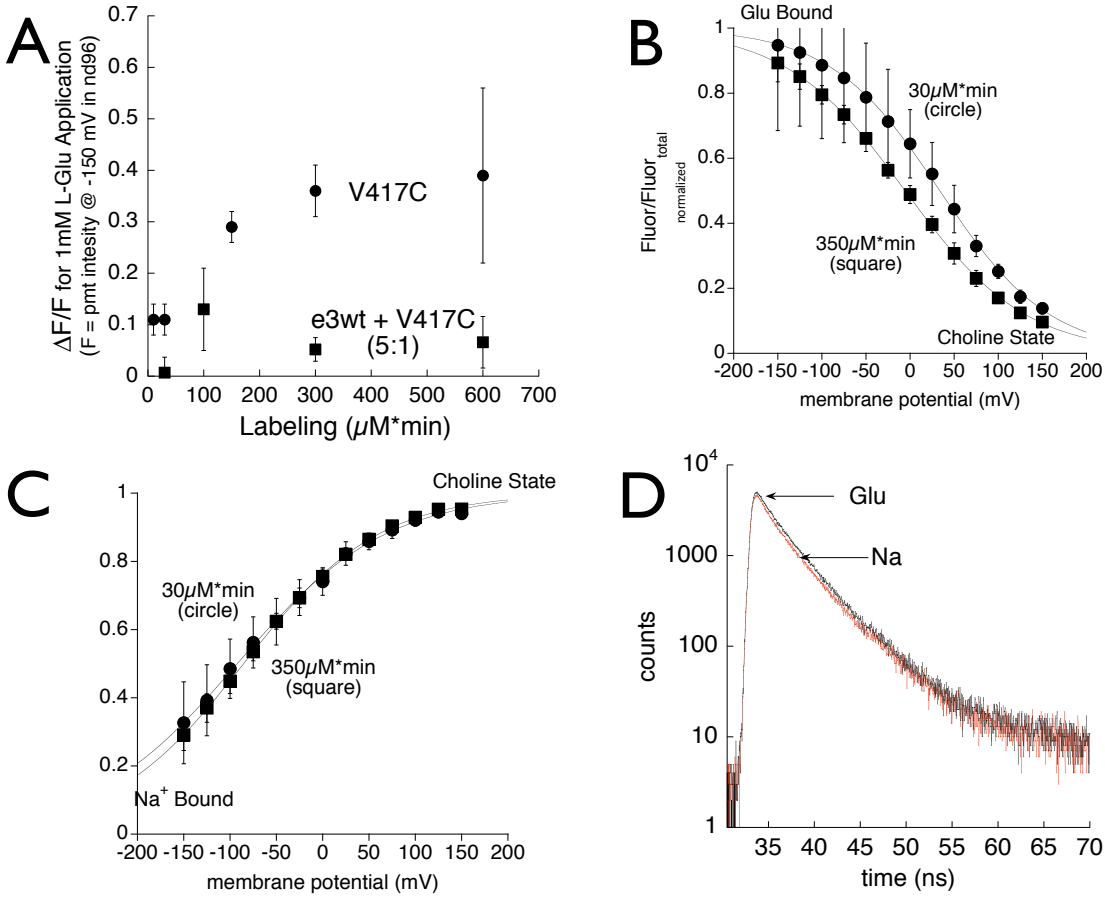

Figure 5.6: Fluorophore interaction from neighboring subunits accounts for increase in intensity upon L-Glu application. A. The ΔF/F for 1mM L-Glu increases with increased labeling for V417C hEAAT3 (circle) but not when V417C hEAAT3 is expressed in excess (1:5) of wt hEAAT3 (square). **B & C.** A left shift in the fluorescence/voltage relationship for 1mM L-Glu (left) but not Na^+ with either the 30 or 350 μM*min labeling. Both are fit with the same Boltzmann equations used in figure 3D. **D.** Representative trace for the fluorescence lifetime with and without L-Glu taken from a hEAAT3 V417C *Xenopus* oocycte labeled to saturation.

Discussion

From *Pyrococcus horikoshii,* a homologue of the glutamate transporters (Glt_{ph}), Yernool et al. (2004) provided a crystal structure with evidence that HP2 occluded a bound substrate molecule posing as theoretical external gate for the transporter. V417C hEAAT3 modified by Alexa Fluor 488 C_5 maleimide allowed us to observe unique motions of HP2 associated with binding and unbinding of substrates without the complication of transport (Figure 5.1B). Defining these fluorophores as forming dark complexes at the center of the trimer (Figure 5.6) allowed us a tool to observe motions of HP2 relative to the central axis. Because of the robust increase in fluorescence, L-Glu binding likely causes HP2 to physically break the hydrophobic pi-pi bonds and move the fluorophores away from the central axis, relieving a quench on the fluorophore. The left shift in the Boltzmann with increased labeling (Figure 5.6B) suggests more negative potentials are needed to allow binding of L-Glu supporting the fluorophores dimerization may constrain loop closing. This physical constraint from either dimerization or the extra mass placed on the loop is further supported by the slower microscopic on and off rates for L-Glu (Figure 5.4B). At very positive potentials, HP2 resembles the state with choline extracellular suggesting both Na and L-Glu have a voltage dependent unbinding (Figure 5.3C). This physical unbinding of L-Glu is further supported by the exponential fluorescence recovery following a voltage jump to 150 mV (Figure 5.5A), which we believe represent L-Glu rebinding. According to molecular dynamic simulations on Glt_{ph}, the closing of HP2 depends mostly on interactions with the substrate and is independent of interactions with Na^+ (Huang and Tajkhorshid, 2008). In contrast, we find that the large fluorescent changes thought to represent loop closure do not occur in the presence of Li^+ + L-Glu, though an inversion of the voltage dependence shows L-Glu still bind (data not shown). This suggests for hEAAT3 that the closing of the HP2 loop depends on the presence of both L-Glu and Na^+. These L-Glu and Na^+ induced motions

of HP2 in hEAAT3 directly correspond with and help validate predictions from Glt_{ph} that HP2 gates L-Glu.

A second crystal structure bound with the inhibitor TBOA maintains HP2 in a confirmation 10 Å toward the central axis of the trimer from its position with the substrate bound (Boudker et al., 2007). The small fluorescent intensity change upon TBOA application supports HP2 in a confirmation closer to the central axis in which the fluorophore dimers are still formed. The inverted Boltzmann fit seen with changes in voltage (Figure 5.3C) in addition to the increases in accessibility for TBOA (Figure 5.2C) demonstrate a distinct form of HP2 from Na^+ or L-Glu indicating complex interactions of HP2 with TBOA (Qu and Kanner, 2008). Even at very positive potentials with TBOA, the fluorescent intensity never resembles a choline state, supporting a voltage independent unbinding.

Low-resolution crystals with just Na^+ bound suggested HP2 assumed a similar open confirmation as with TBOA (Boudker et al., 2007). The accessibility of labeling V417C hEAAT3 as well as accessibility for residues on the loop shown by Qu and Kanner (2008) supports a very distinct HP2 conformation for Na^+ compared with the inhibitor bound. Using VCF, there was a robust decrease in the overall fluorescence transitioning from choline to Na^+, though little change in accessibility (Figure 5.3A, Figure 5.2C). This conformational change of HP2 directly correlates with the presence of at least 2 Na atoms (Figure 5.3B). Interestingly, with choline extracellular the transporter and HP2 seems like a social recluse. Measured by changes in conductance or fluorescence, the transporter is unwilling to respond or interact to high concentrations of L-Glu or inhibitor (Figure 5.3A) or to extreme changes in electrical potential between 200 and -200 mV. This is in contrast to large motions of HP2 expected from MD simulations (Huang and Tajkhorshid, 2008; Leighton et al., 2006). At the tip of the HP2 loop, it seems the accessibility for V417C is similar between Na^+ and choline; this result parallels MTSET labeling to the corresponding residue for M419 in Glt-1 (Qu and Kanner, 2008).

References

Bergles DE, Tzingounis AV and Jahr CE (2002) Comparison of coupled and uncoupled currents during glutamate uptake by GLT-1 transporters. *J Neurosci* **22**(23):10153-10162.

Boudker O, Ryan RM, Yernool D, Shimamoto K and Gouaux E (2007) Coupling substrate and ion binding to extracellular gate of a sodium-dependent aspartate transporter. *Nature* **445**(7126):387-393.

Brocke L, Bendahan A, Grunewald M and Kanner BI (2002) Proximity of two oppositely oriented reentrant loops in the glutamate transporter GLT-1 identified by paired cysteine mutagenesis. *J Biol Chem* **277**(6):3985-3992.

Herman MA and Jahr CE (2007) Extracellular glutamate concentration in hippocampal slice. *J Neurosci* **27**(36):9736-9741.

Huang Z and Tajkhorshid E (2008) Dynamics of the extracellular gate and ion-substrate coupling in the glutamate transporter. *Biophys J* **95**(5):2292-2300.

Jardetzky O (1966) Simple allosteric model for membrane pumps. *Nature* **211**(5052):969-970.

Kavanaugh MP (1998) Neurotransmitter transport: models in flux. *Proc Natl Acad Sci U S A* **95**(22):12737-12738.

Koch HP, Hubbard JM and Larsson HP (2007) Voltage-independent sodium-binding events reported by the 4B-4C loop in the human glutamate transporter excitatory amino acid transporter 3. *J Biol Chem* **282**(34):24547-24553.

Koch HP and Larsson HP (2005) Small-scale molecular motions accomplish glutamate uptake in human glutamate transporters. *J Neurosci* **25**(7):1730-1736.

Larsson HP, Tzingounis AV, Koch HP and Kavanaugh MP (2004) Fluorometric measurements of conformational changes in glutamate transporters. *Proc Natl Acad Sci U S A* **101**(11):3951-3956.

Lauger P (1980) Kinetic properties of ion carriers and channels. *J Membr Biol* **57**(3):163-178(-RETURN-).

Leighton BH, Seal RP, Watts SD, Skyba MO and Amara SG (2006) Structural rearrangements at the translocation pore of the human glutamate transporter, EAAT1. *J Biol Chem* **281**(40):29788-29796.

Miller C (2006) ClC chloride channels viewed through a transporter lens. *Nature* **440**(7083):484-489.

Qu S and Kanner BI (2008) Substrates and Non-transportable Analogues Induce Structural Rearrangements at the Extracellular Entrance of the Glial Glutamate Transporter GLT-1/EAAT2. *J Biol Chem* **283**(39):26391-26400.

Ryan RM, Mitrovic AD and Vandenberg RJ (2004) The chloride permeation pathway of a glutamate transporter and its proximity to the glutamate translocation pathway. *J Biol Chem* **279**(20):20742-20751.

Seal RP, Shigeri Y, Eliasof S, Leighton BH and Amara SG (2001) Sulfhydryl modification of V449C in the glutamate transporter EAAT1 abolishes substrate transport but not the substrate-gated anion conductance. *Proc Natl Acad Sci U S A* **98**(26):15324-15329.

Shrivastava IH, Jiang J, Amara SG and Bahar I (2008) Time-resolved mechanism of extracellular gate opening and substrate binding in glutamate transporter. *J Biol Chem*.

Tzingounis AV, Larsson HP and Kavanaugh MP (2002) Voltage clamp and fluoorometric techniques for studying glutamate transporter function. *in Transmembrane Transporters* ed. Quick, M. (Wiley-Liss, New York):203-215.

Wadiche JI, Amara SG and Kavanaugh MP (1995a) Ion fluxes associated with excitatory amino acid transport. *Neuron* **15**(3):721-728.

Wadiche JI, Arriza JL, Amara SG and Kavanaugh MP (1995b) Kinetics of a human glutamate transporter. *Neuron* **14**(5):1019-1027.

Yernool D, Boudker O, Jin Y and Gouaux E (2004) Structure of a glutamate transporter homologue from Pyrococcus horikoshii. *Nature* **431**(7010):811-818.

Zerangue N and Kavanaugh MP (1996) Flux coupling in a neuronal glutamate transporter. *Nature* **383**(6601):634-637.

CHAPTER 6: CONCLUSIONS

In mammals including humans, high affinity glutamate transporters are encoded by a group of five genes (EAAT 1-5; SLC1A1-A5) that are members of the dicarboxylate/amino acid:cation symporter family that also includes the neutral amino acid transporters, ASCT1 and ASCT2. This gene family is distinct from the family of genes encoding the transporters for neurotransmitters such as GABA, serotonin, dopamine, norepinephrine, glycine, and others. The excitatory amino acid transporters (EAATs) are found throughout the central nervous system and peripheral tissues. These glutamate transporters are the major routes for cellular uptake of synaptically released glutamate (Danbolt, 2001), and they maintain a low nanomolar extracellular glutamate concentration in the brain (Herman and Jahr, 2007). Many major neurological diseases like amyotrophic lateral sclerosis, epilepsy, Huntington's disease, Alzheimer's disease, or ischemic stroke have deficits in glutamate transporter expression (Beart and O'Shea, 2007)).

With the recent publication of two crystal structures of Glt_{Ph} an archaeal analog of the EAATs (Boudker et al., 2007; Yernool et al., 2004), many question have been raised about how these secondary active transporters can move glutamate against its own concentration gradient. The crystal structures of Glt_{Ph} revealed three identical subunits that cluster together to form a homotrimer. The interface of the subunits creates a large aqueous basin (~40,000 $Å^3$) that dips beyond the 1st leaflet of the bilayer, though there is no clear water filled pathway that extends completely through the protein like is seen in the K^+ channels (Doyle et al., 1998). In this dissertation we have explored what functional significance the bowl-shaped, homotrimeric complex has on both the coupled transport current as well as the uncoupled anion current associated with the transporter. In chapter 2 we concluded that both the glutamate and chloride permeation pathways reside in individual subunits, opposed to a pathway created by the interface of the subunits as is common in ionotropic receptors. This evidence supports the subunits essentially can function independently, a conclusion reached also by other labs (Grewer et al., 2005; Koch et al., 2007). This, however, highlights our lack of understanding for the purpose of the homotrimer.

In chapter 4, we studied the microscopic rates for block and recovery from block for a novel transporter inhibitor, 2-FAA, that has a K_i = 8 nM. The microscopic off-rate for 2-FAA was three times lower when no glutamate was present, which led to the conclusion that the quaternary structure of the transporter (the aqueous basin) effectively restricts diffusion of the blocker and increases the probability of rebinding of 2-FAA in a neighboring subunit. Extending these results to glutamate, we recently have shown that under conditions in which glutamate binding becomes rate limiting, at low concentrations (1 μM) or at very negative membrane potentials (-120 mV), the co-expression of functional and nonfunctional subunits reveals a deficit in the ability to sustain a glutamate inward current (unpublished observations). Similar to 2-FAA, this demonstrates that the bowl created by the homotrimer actually increases the capture efficiency for glutamate molecules by restricting the diffusion of the molecules upon unbinding, at physiological concentrations of substrate (1 μM).

Chapters 3 and 5 focus more on understanding the transport of glutamate and the gating of the anion channel within an individual subunit. For the past two decades, a two-gate, alternating access model has been proposed to explain how membrane proteins can transport substrates. In the crystal structure of Glt_{Ph}, two hairpin loops are apparent, one spanning half the distance of the plasma membrane from the extracellular space (HP2) and the other spanning half the distance of the membrane from the cytoplasm (HP1). These two loops have been proposed to act as the gates regulating transport, and both lie very close to amino acid residues known to be critical for transport (Yernool et al., 2004). Placing a thiol-reactive, fluorescent probes on HP2 resulted in fluorescence intensity changes that drastically report on the presence of glutamate binding to the transporter, but not TBOA. The intensity change depends on fluorophores present in neighboring subunits demonstrating that the fluorophores form quenched dimer complexes at the center of the bowl that break and fluoresce upon L-Glu binding and HP2 loop closure. This data offers some of the first real time measurements of HP2 loop closure. This HP2 loop motion is supported by crosslinking experiments between HP2 loop to TMD8 in the presence of L-Glu (Qu and Kanner, 2008).

The research in this dissertation begins to bridge the gap between our functional understandings of these transporters from the past thirty years and how this maps onto a

crystal structure at a resolution below 10 Å. Multiple lines of evidence, including this dissertation, have supported Glt_{Ph} as a good initial model for the EAATs structure (Qu and Kanner, 2008; Ryan and Mindell, 2007). Future research will attempt to elucidate the small differences in protein structure that confer the small functional differences between the EAAT 1-5, and further, it will work to map the 15 state reaction mechanism to unique structural conformations of the protein, providing a new understanding of secondary active transporters.

References

Beart PM and O'Shea RD (2007) Transporters for L-glutamate: an update on their molecular pharmacology and pathological involvement. *Br J Pharmacol* **150**(1):5-17.

Boudker O, Ryan RM, Yernool D, Shimamoto K and Gouaux E (2007) Coupling substrate and ion binding to extracellular gate of a sodium-dependent aspartate transporter. *Nature* **445**(7126):387-393.

Danbolt NC (2001) Glutamate uptake. *Prog Neurobiol* **65**(1):1-105.

Doyle DA, Morais Cabral J, Pfuetzner RA, Kuo A, Gulbis JM, Cohen SL, Chait BT and MacKinnon R (1998) The structure of the potassium channel: molecular basis of K+ conduction and selectivity. *Science* **280**(5360):69-77.

Grewer C, Balani P, Weidenfeller C, Bartusel T, Tao Z and Rauen T (2005) Individual subunits of the glutamate transporter EAAC1 homotrimer function independently of each other. *Biochemistry* **44**(35):11913-11923.

Herman MA and Jahr CE (2007) Extracellular glutamate concentration in hippocampal slice. *J Neurosci* **27**(36):9736-9741.

Koch HP, Brown RL and Larsson HP (2007) The glutamate-activated anion conductance in excitatory amino acid transporters is gated independently by the individual subunits. *J Neurosci* **27**(11):2943-2947.

Qu S and Kanner BI (2008) Substrates and Non-transportable Analogues Induce Structural Rearrangements at the Extracellular Entrance of the Glial Glutamate Transporter GLT-1/EAAT2. *J Biol Chem* **283**(39):26391-26400.

Ryan RM and Mindell JA (2007) The uncoupled chloride conductance of a bacterial glutamate transporter homolog. *Nat Struct Mol Biol* **14**(5):365-371.

Yernool D, Boudker O, Jin Y and Gouaux E (2004) Structure of a glutamate transporter homologue from Pyrococcus horikoshii. *Nature* **431**(7010):811-818.